

Elementary processes in alkane activation over zeolite catalysts

Carsten Sievers

Vollständiger Abdruck der vom Department Chemie
der Technischen Universität München zur Erlangung der akademischen Grades eines
Doktors der Naturwissenschaften (Dr. rer. nat.)
genehmigten Dissertation.

Vorsitzender: Univ. Prof. Dr. N. Rösch

Prüfer der Dissertation:

1. Univ. Prof. Dr. J. A. Lercher

2. Univ. Prof. Dr. Klaus Köhler

3. Univ. Prof. Dr. U. Heiz

Die Dissertation wurde am 31.10.2006 bei der Technischen Universität München eingereicht
und durch das Department Chemie am 22.11.2006 angenommen.

“The important thing is not to stop questioning. Curiosity has its own reason for existing. One cannot help but be in awe when he contemplates the mysteries of eternity, of life, of the marvelous structure of reality. It is enough if one tries merely to comprehend a little of this mystery every day. Never lose a holy curiosity.”

Albert Einstein

Acknowledgements

As my time at the TU München is coming to an end it is time to give a thought to the people who accompanied me on my way. Without you the work in this thesis would not have been possible.

Firstly, I would like to thank Prof. Johannes A. Lercher for accepting me in his group and assigning me to this interesting topic. Our scientific discussions were truly inspiring and you encouraged me to “develop” faster than I had imagined. I appreciate that I was given the academic freedom to participate in various other projects, which broadened my horizon significantly. Thank you for the chance of traveling to a number of international conferences, which were a great place for networking and input.

Thanks to Roberta Olindo for your advice and support. I want to express my gratitude to Andreas Jentys for his help, in particular for all things you taught me about spectroscopy. I appreciated being the “next one on the list” for the upgrades of computers and office space.

I would like to thank Thomas Müller for inspiration, guidance and the diversification of my research activities. I really enjoyed our project on supported ionic liquids, from which I learnt to understand new areas of research without working on them full time. You taught me a lot about writing publications and made me hunt for the last little mistakes in manuscripts.

Thanks to Xaver, Martin, and Andreas for technical support and measurements as well as to Heike and Helen for their help with paperwork.

In the last three and a half years I had the chance to work with a great number of nice colleagues. Among them I want to express my special gratitude to Florencia, Jan-Olaf, Hendrik, and Alex, for their enormous help and the knowledge, which they passed to me. Thanks to Jürgen, Christoph, Frederik, and Florian for a bit of distraction in the last year. I also would like to thank Hiroaki, Toshi, Adam, Andras F., Stefan, Iker, Renate, Qing, Xuebing, Christian, Maria, Phillip, Yongzhong, Anirban, Praveen, Aonsurang, Herui, Felix, Benjamin, Chintan, Lay-Hwa, Wolfgang, Rino, Elvira, Rino, Stephan, Virginia, Peter S., Andreas, Dechao, Manuela, Tobias, Rinchar, Peter H., Hitri, Prashant, Rahul, Chiraq, Oriol, Olga, Krishna, Matteo, Ana, and Sandra for being good colleagues.

One of the most enjoyable parts of my work at TC2 was the collaboration with guest researchers who joined my project and contributed the work in this thesis in a variety of different ways. Namely, I would like to thank Ayumu, Höpke, Mahdi, Bele, Julia, Manuel, Christiane, Qiang, Neeraj, Silvana, and Ilkka.

Solid state NMR spectroscopy was an important part of my work. This complex technique required a lot of external consulting and technical support. I would like to thank Gabi Raudaschl-Sieber, Anuji Abraham, Jeroen van Bokhoven, Stefan Steuernagel, Rainer Haeßner, and Gerd Gemecker for all the help I received from them.

Thanks to Evgeny A. Pidko and Prof. Rutger A. van Santen for the introduction into DFT calculations. My time at the TU Eindhoven was full of new inspiration.

Despite the great equipment at TC2, we sometimes depend on other groups for additional measurements. I would like to thank Prof. Dieter Freude and Dennis Schneider for the ^{27}Al DOR NMR measurements, Helmut Krause for GC/MS measurements and his support with MALDI-TOF mass spectroscopy, Herr Barth and Frau Ammari for HCN elemental analyses and Birgit Wierczinski and Xilei Lin for the neutron activation analyses.

I also want to express my gratitude to my parents Eva and Kurt Sievers who supported me in many ways throughout my studies and PhD program. Finally, I would like to thank Laura for being my favorite distraction, an intensive course on good Canadian English and all the nice moments in the last years.

Thank you for everything

Carsten

Table of Contents

1. General introduction.....	1
1.1. Catalytic conversions in refining.....	2
1.2. Alkane activation.....	4
1.2.1. Protolytic cracking	4
1.2.2. Hydride abstraction and hydride transfer	5
1.2.3. Formation of alkyl groups	6
1.3. Carbenium ion based reactions	7
1.3.1. Catalytic cracking.....	8
1.3.2. Isomerization.....	9
1.3.3. Isobutane alkylation	10
1.4. Zeolite catalysts.....	15
1.5. Scope of this thesis	18
1.6. References	20
2. Adsorption of branched alkanes of H-LaX	25
2.1. Introduction	26
2.2. Experimental	27
2.2.1. Catalyst preparation and reactants.....	27
2.2.2. Characterization	28
2.2.3. Adsorption of alkanes.....	29
2.3. Results	30
2.3.1. Characterization	30
2.3.2. Gravimetric and calorimetric measurements.....	33
2.3.3. In situ IR spectroscopic measurements	37
2.3.4. MAS-NMR measurements	42
2.4. Discussion	44
2.4.1. Types of the interaction.....	44
2.4.2. Influence of polarization	45
2.4.3. Localized interaction	47
2.4.4. Distortion of the zeolite framework	49
2.4.5. Influence of the activation temperature.....	49
2.5. Conclusions	50

2.6. Acknowledgements	51
2.7. References	51
3. Low temperature activation of branched octane isomers over lanthanum exchanged zeolite X catalysts	54
3.1. Introduction	55
3.2. Experimental	56
3.2.1. Catalyst preparation and reactants.....	56
3.2.2. General characterization.....	56
3.2.3. Adsorption and surface reaction.....	57
3.3. Results	58
3.3.1. Basic characterization of the materials.....	58
3.3.2. Adsorption of n-octane and 2-methylheptane	58
3.3.3. Adsorption and activation of di- and tri-branched alkanes	62
3.4. Discussion	68
3.4.1. Adsorption of alkanes.....	68
3.4.2. Activation of alkanes.....	71
3.4.3. Carbon-carbon bond related surface reactions	73
3.5. Conclusions	76
2.6. Acknowledgements	76
3.7. References	77
4. Comparison of zeolites H-LaX and H-LaY as catalysts for isobutane/ 2-butene alkylation.....	79
4.1. Introduction	80
4.2. Experimental	81
4.2.1. Catalyst preparation.....	81
4.2.2. Alkylation reaction.....	82
4.2.3. Physicochemical characterization	82
4.3. Results	84
4.3.1. Physicochemical characterization	84
4.3.2. Performance in alkylation	89
4.4. Discussion	93
4.4.1. Catalytic performance	93

4.4.2. Influence of physicochemical properties.....	96
4.4.3. Influence of lanthanum exchange	98
4.5. Conclusions	100
4.6. Acknowledgement.....	101
4.7. References	101
5. Stages of aging and deactivation of zeolite H-LaX in isobutane/2-butene alkylation.....	104
5.1. Introduction	105
5.2. Experimental	106
5.2.1. Catalyst preparation.....	106
5.2.2. Catalytic reactions	107
5.2.3. Catalyst characterization	107
5.3. Results	109
5.3.1. Characterization of the fresh catalyst.....	109
5.3.2. Catalytic experiments.....	110
5.3.3. Characterization of spent catalysts.....	112
5.4. Discussion	117
5.4.1. Modification of the catalytic properties	117
5.4.2. Nature of the deposits.....	119
5.5. Conclusions	122
5.6. Acknowledgements	123
5.7. References	123
6. Summary	126
6.1. Summary	127
6.2. Zusammenfassung.....	131
Curriculum vitae.....	135
List of publications.....	136

Chapter 1

General introduction

This chapter gives an introduction to the background of the thesis. The first section is a brief review of industrial refining. Then, mechanisms of alkane activation and carbenium ion based reactions are presented and zeolites are introduced. Finally, the scope of this thesis is presented.

1.1. Catalytic conversions in refining

Crude oil is a complex mixture of hydrocarbons. Its enormous importance for industrialized countries becomes evident from the impact of the oil price on the economical climate. In 2004, the worldwide consumption amounted to 83 million barrels/day. In modern refineries crude oil is converted into a variety of products to satisfy the needs in transportation and industry (Figure 1.1).

Industrial oil processing started in the 1860's. Initially, kerosene was the most important product with naphtha (gasoline) as a by-product. Early refining was essentially limited to distillation. Undesired products were often disposed in the nearest river. In the following decades the invention of the combustion engine shifted the demand to gasoline and diesel. The development of thermal cracking helped to satisfy these needs.

Catalysis in refining started in the 1920's when Eugene Houdry showed that acid treated natural clays could be used to convert heavy crude oil fractions into more valuable lighter ones by catalytic cracking. The first commercial unit was started by Sun Oil in 1936. The development of moving bed processes brought a significant improvement for catalyst regeneration. A major landmark was the introduction of zeolite based catalysts in 1962, which brought a remarkable improvement of fluid catalytic cracking units (FCC), because zeolites were an order of magnitude more active than the catalysts previously used. Zeolites catalysts led to a significant reduction of the hydrocarbon residence time in the reactor, while high conversion was maintained. In addition to the desired gasoline fraction, FCC units produce significant amounts of C₃-C₅ paraffins and olefins. Isopentane and isopentene were often left in the gasoline pool.

The surplus of light olefins and paraffins also led to the introduction of alkylation in refineries, which was pioneered by Vladimir Ipiateff. In this process, light olefins, mostly butenes, are alkylated with isobutane forming a mixture of high-octane paraffins. The first alkylation unit in 1938 used sulfuric acid as catalyst. Later a process using hydrofluoric acid was developed. Isobutane/n-butene alkylation will be described in more detail in section 1.3.3.

In the 1940's refineries started focusing on the production of high octane fuels, which gave a significant advantage to Allied airplanes in World War II. The new requirements were met by the introduction of catalytic reforming, which includes isomerization and the conversion of cycloparaffins (naphthenes) to higher-octane aromatics. Originally molybdenum catalysts were used in a technically demanding process. The introduction of Pt catalysts with up to a year of lifetime led to a significant simplification of reforming units.

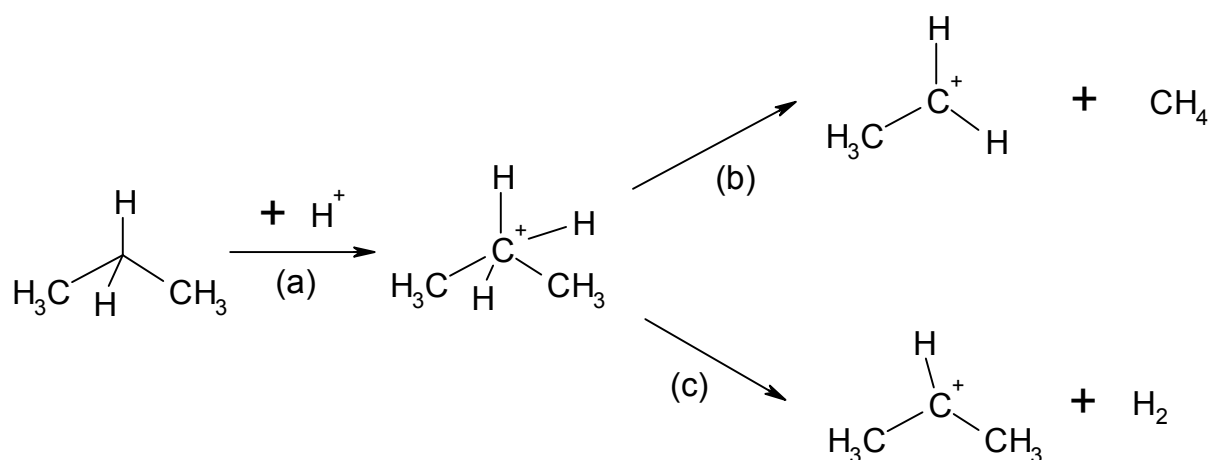
1.2. Alkane activation

Various initiation steps for carbenium ion based alkane conversions have been discussed in literature [4-8]. In addition to true alkane activation, olefin impurities in the feed, which are readily protonated by the Brønsted acid sites in zeolites, have frequently been proposed as the source of the first carbenium ions [9,10]. Note that at elevated temperature alkenes may also be formed by thermal cracking. In this section different possibilities of alkane activation by catalytic reactions will be discussed.

1.2.1. Protolytic cracking

In 1984 Haag and Dessau suggested a mechanism for the monomolecular conversion of alkanes [4], which was based on Olah's chemistry of superacids [11]. At high temperature (approximately 800 K) zeolites are capable of protonating alkanes forming highly unstable pentavalent carbonium ions (Scheme 1.1a). The carbonium ion rapidly decays into a carbenium ion and an alkane (protolytic cracking, Scheme 1.1b) or a carbenium ion and H₂ (protolytic dehydrogenation, Scheme 1.1c).

The intrinsic activation energy for protolysis of alkanes is approximately 200 kJ·mol⁻¹ independent of the zeolite structure and the size of the alkane [12]. This is in good agreement with theoretical calculations for cracking of ethane [13]. Due to the high energy of activation, protolytic cracking is favored at high temperature. Moreover, protolytic cracking is only kinetically relevant at low conversion [4], while β-scission dominates at high conversion (Section 1.3.1.). Consequently, it has been suggested that protolysis is the initiation step in industrial catalytic cracking [14].



Scheme 1.1: Protolytic activation of propane: (a) Formation of a carbonium ion by protonation of an alkane, (b) protolytic cracking, (c) protolytic dehydrogenation

Strong evidence for the protolytic mechanism was derived from the product distribution of the cracking of light alkanes [12,15]. If n-butane, for example, is converted by protolytic cracking, the product mixture will contain equimolar amounts of butene isomers and H₂, propene and methane as well as ethane and ethene.

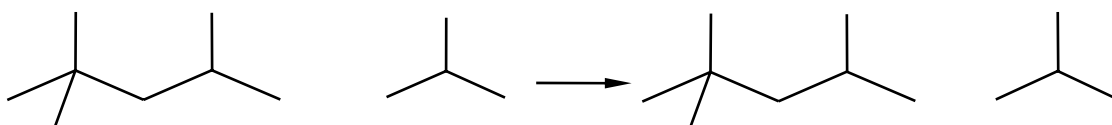
1.2.2. Hydride abstraction and hydride transfer

In addition to protolytic cracking, carbenium ions can be formed from alkanes by hydride abstraction. This reaction may occur in zeolites if sufficiently strong Lewis acid sites are present.

Marczewski *et al.* demonstrated that alkanes are activated over the solid Lewis acid Al₂O₃/AlCl₃ [16]. Based on these findings Schoofs *et al.* proposed hydride abstraction by extralattice aluminum species as activation step of H/D exchange of isobutane over deuterated MFI- and FAU-type zeolites [6]. They also suggested that the resulting carbenium ion is deprotonated forming an olefin. However, the lifetime of this olefin would be limited near a Brønsted acid site.

Theoretical studies of hydride abstraction from isobutane by extraframework aluminum cations [17] and Brønsted acid sites [18] gave activation energies of 193 kJ mol⁻¹ and 245 kJ mol⁻¹, respectively. These values are comparable to those found for protolytic activation.

In hydride transfer the hydride is abstracted by a carbenium ion, which is present on the catalyst surface (Scheme 1.2). This elementary reaction is the chain propagation step in carbenium ion based reaction, such as cracking, isomerization and alkylation. The specific relevance of hydride transfer for these reactions will be discussed in Section 1.3.



Scheme 1.2: Hydride transfer from an isobutane molecule to a 2,4,4-trimethyl-2-pentyl carbenium ion [3]

Hydride transfer has been subject of a number of theoretical studies [19-25]. However, experimental determinations of hydride transfer rates remain scarce. Lukyanov proposed that the formation of isobutane during n-hexane cracking at 673 K is a good indicator for the hydride transfer activity of the catalyst [26]. Platon and Thomson pointed out that the results from this methods may not be transferable to reactions at lower temperatures and suggested

the conversion of cyclohexene with isobutane as a low temperature test reaction for the assessment of hydride transfer activity [27,28].

The rate of hydride transfer is strongly influenced by the nature of the carbenium ions, which are involved in the reaction. Weitkamp *et al.* found that the stability of carbenium ions decreases in the order: tertiary > secondary > primary > methyl [29]. Cardona *et al.* demonstrated that hydride transfer to a secondary carbenium ion is much slower than to a tertiary one [30].

1.2.3. Formation of alkyl groups

In addition to protolysis and hydride abstraction, which result in the formation of carbocations, the formation of alkyl groups has been suggested as activation on Ga and Zn exchanged ZSM5 [31-33]. The transition states for ethane activation, which is claimed to follow this mechanism, have the composition $[\text{H-Ga-C}_2\text{H}_5]^+$ and $[\text{Zn-C}_2\text{H}_5]^+$, respectively. In a subsequent step they decompose forming an ethylene molecule [31].

Fărcașiu suggest that extraframework aluminum ions are capable of activating alkanes by insertion of Al^{3+} into a CH bond [5].

1.3. Carbenium ion based reactions

The intermediates of acid catalyzed alkane conversions are usually described as carbenium ions. In contrast to this, Kazansky *et al.* showed in theoretical studies that a description as alkoxy groups is more appropriate [34-36]. Figure 1.2 shows the energy diagram for the protonation of isobutene. Initially, a π -complex is formed in a reaction step, which does not require activation [34]. The protonation step has an intrinsic activation energy of $22.9 \text{ kcal}\cdot\text{mol}^{-1}$ and proceeds *via* a carbenium ion like transition state (TS) forming a *tert*-butoxy group on the zeolite surface. In agreement with Kazansky's results it was found that only sterically very demanding carbenium ions are stable in zeolite [37].

Despite the fact that carbenium ions hardly exist as stable species in zeolites, carbenium ion based mechanisms provide an appropriate description of the reactivity of alkoxy groups in zeolites indicating that the formation of a carbenium ion-like transition state is involved in these reactions.

In the following sections the most important carbenium ion based reaction in refining will be reviewed, namely catalytic cracking (1.3.1.), isomerization (1.3.2.), and isobutane/n-butene alkylation (1.3.3.).

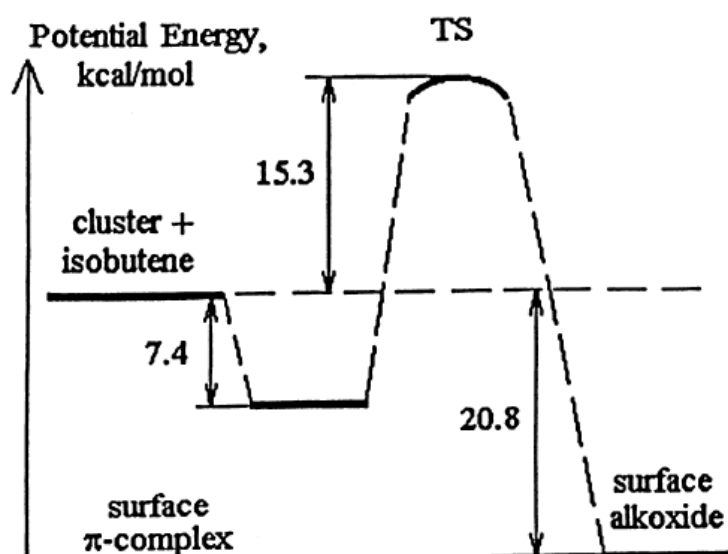


Figure 1.2: Protonation of isobutene on a Brønsted acid site (energies in $\text{kcal}\cdot\text{mol}^{-1}$) [34]

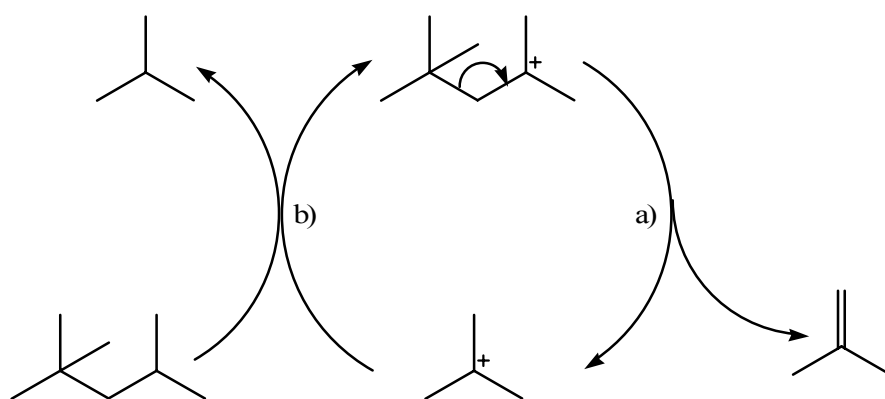
1.3.1. Catalytic cracking

Fluid catalytic cracking (FCC) is the largest heterogeneously catalyzed process in the world. It is an essential part of every refinery converting gas oil and heavy residue into lighter compounds, such as gasoline, distillate fuels and petrochemical feedstocks (Figure 1.1). Today, approximately 35 % of the US gasoline pool is produced by FCC [38]. Worldwide, more than 350 FCC units are operated in refineries processing ca. 1400 tons/day.

It is widely accepted that the key step in the mechanism of FCC (Scheme 1.3) is the cleavage of a C-C bond in β -position from the charged carbon atom [39]. This step results in the formation of an alkene molecule and a smaller carbenium ion, which remains on the catalyst. The rate of the β -scission is the faster the more stable the carbenium ions involved in the reaction are. Weitkamp *et al.* found that the stability decreases with decreasing degree of substitution: tertiary > secondary > primary > methyl [29]. If the carbenium ion is large enough multiple β -scission steps can occur. The chain propagates *via* hydride transfer.

Zeolite Y was introduced as FCC catalyst in the 1960's with a major impact on the economics of refining. Various modifications such as dealumination and incorporation of rare earth cations have since been introduced in order to increase the hydrothermal stability of the zeolite, which has to endure temperature of 800 K in the riser reactor and 1000 K in the regeneration unit. Modern catalysts contain aluminum oxide, clays or other inorganic materials as binders, in addition to zeolite Y.

In industrial unit FCC, catalysts deactivate within seconds due to the formation of heavy polyaromatic deposits, which are commonly referred to as coke [40]. Consequently, enormous efforts have been taken to understand and limit the processes leading to coking [40-49]. Coke is formed in a reaction sequence, which includes oligomerization, cyclization and



Scheme 1.3: Mechanism of catalytic cracking including β -scission (a) and hydride transfer (b)

dehydrogenation [43]. The cyclic ions resulting from this sequence have a long lifetime on the catalyst surface, which favors the growth of even larger molecules. Coke may deactivate the catalyst by either site poisoning or pore mouth plugging [50-53]. Note that in pore mouth plugging one coke molecule can block the access to more than one active site. Prior to complete pore mouth plugging, coke molecules may decrease to diameter of the zeolite pores, increasing diffusion resistance [47,54].

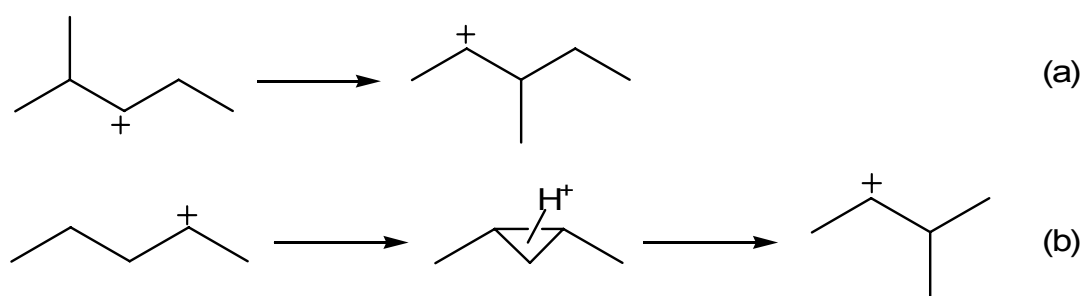
1.3.2. Isomerization

Isomerization is an important process for increasing the octane number of gasoline blends, because the octane numbers of branched or cyclic hydrocarbons exceed those of n-alkanes significantly (Table 1.1). There are two types of isomerization reaction: (1) Type A isomerization proceeds *via* alkyl or hydride shift (Scheme 1.4a). Due to its low activation energy this reaction is relatively fast. Hence, it is observed under rather mild conditions, for example as side reaction during isobutane/n-butene alkylation (Section 1.3.3). (2) In type B isomerization the skeleton of the alkane molecule is modified (Scheme 1.4b). In other words branchings are added or removed. Skeleton-isomerization proceeds *via* a protonated cyclopropane transition state [55-58]. As the formation of this transition state has a high energy of activation, type B isomerization is always slower than type A isomerization [59].

Table 1.1: Octane numbers of C₅ and C₆ hydrocarbons [60]

Hydrocarbon	RON-0 ^a	MON-0 ^b
n-Pentane	62	61
Isopentane	93	90
Cyclopentane	102	85
n-Hexane	31	30
2-Methylpentane	74	75
3-Methylpentane	75	76
2,2-Dimethylbutane	94	95
2,3-Dimethylbutane	105	104
Cyclohexane	84	77
Methylcyclopentane	96	85
Benzene	>100	>100

^a RON-0 = clear research octane number, ^b MON-0 = clear motor octane number



Scheme 1.4: Isomerization mechanisms: (a) type A isomerization: hydride or alkyl group shift (b) type B isomerization: skeleton isomerization

1.3.3. Isobutane alkylation

The isobutane/n-butene alkylation unit in refineries is located downstream from the FCC unit (Figure 1.1). Alkylation produces a mixture of branched octane isomers, which are an ideal blending component for high-octane fuels. In 2005, the worldwide alkylation capacity amounted to approximately 2 million barrels per day and it is expected to grow further (Figure 1.3).

Currently, only liquid acid-catalyzed processes are operated on an industrial scale with approximately equal market shares for processes using sulfuric and hydrofluoric acid. Both of these catalysts suffer from serious disadvantages.

Anhydrous HF is a corrosive and highly toxic liquid with a boiling point close to room temperature. Therefore, refineries with HF alkylation plants are under pressure to install expensive mitigation systems minimizing the dangers of HF leaks. Moreover, authorities in many industrialized countries have ceased to license new HF alkylation plants.

Sulfuric acid is also a corrosive liquid, but not volatile, making its handling easier. Its major disadvantage is the high acid consumption in the alkylation process, which can be as much as 70–100 kg of acid/ton of alkylate. The spent acid contains water and heavy hydrocarbons and has to be regenerated, usually by burning. The cost of such a regenerated acid is about 2–3 times the market price for freshly produced sulfuric acid [61].

Therefore, many researchers have investigated solid acids, which may substitute hydrofluoric and sulfuric acid in industrial processes. Among those, zeolites have received the most attention. Particularly promising candidates are the large pore zeolites Beta [62-64], X [65,66] and Y [30,63,67-74].

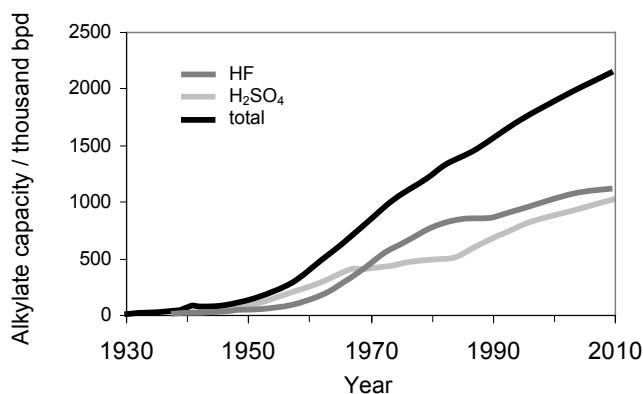
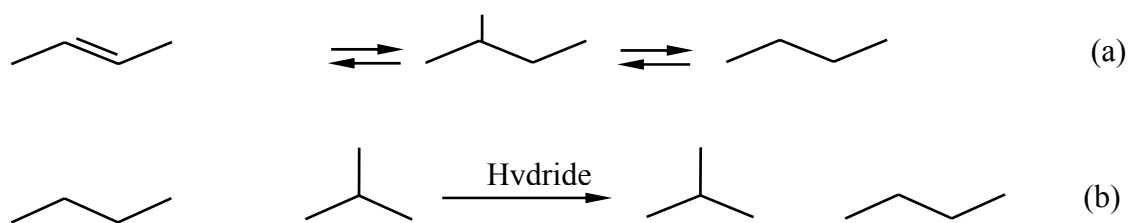


Figure 1.3: Worldwide capacity of alkylation processes using HF and H₂SO₄ as catalysts (bpd = barrels per day) [75]

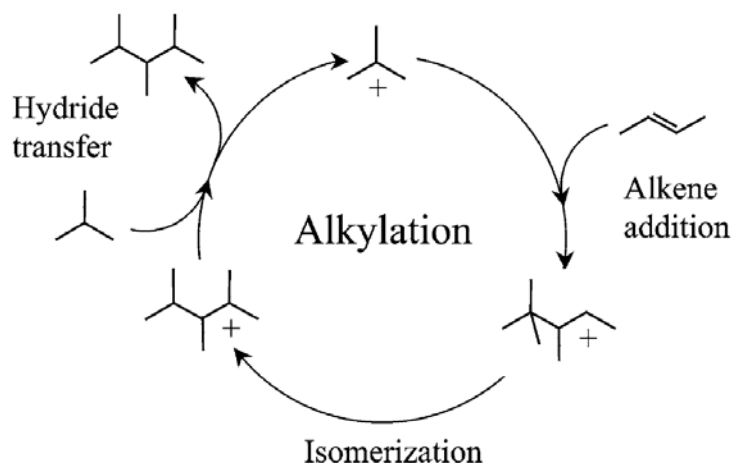
1.3.3.1. Mechanistic details

In isobutane/n-butene alkylation the first carbenium ions are formed by protonation of butene molecules (Scheme 1.5a). The *sec*-butyl carbenium formed in this step abstracts a hydride from an isobutane molecule forming a *tert*-butyl carbenium ion and n-butane (Scheme 1.5b). Direct activation of isobutane by protonation is only observed at temperatures significantly higher than those used in typical alkylation reactions [76].

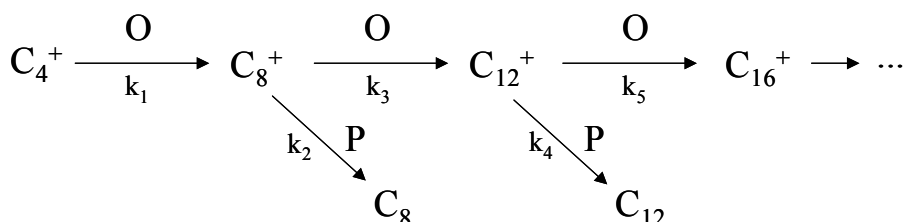
The catalytic cycle of isobutane/n-butene alkylation is shown in Scheme 1.6. In the first step, a 2-butene molecule is added to the *tert*-butyl carbenium ion forming a 2,2,3-trimethyl-3-pentyl carbenium ion, which may isomerize into another trimethylpentyl carbenium ion. The cycle is closed by hydride transfer from an isobutane molecule to the octyl carbenium, which is released as trimethylpentane (TMP) molecule.



Scheme 1.5: Initiation steps in isobutane/2-butene alkylation: (a) protonation of 2-butene, (b) hydride transfer from isobutane to a *sec*-butyl carbenium ion



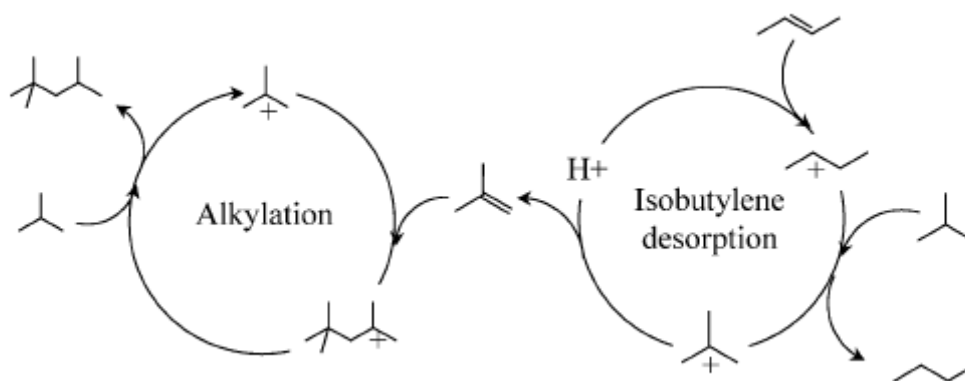
Scheme 1.6: Mechanism of isobutane/2-butene alkylation including the key reaction steps alkene addition, isomerization and hydride transfer [65]



Scheme 1.7: Pathway to oligomerization products with O = olefin and P = paraffin [77]

The selectivity to octane isomers is controlled by the ratio of the rates of hydride transfer and alkene addition (Scheme 1.7). A high rate of alkene addition leads to the formation of large carbenium ions and, thus, heavy end products. In zeolite catalyzed alkylation the intrinsic rate of alkene addition is two to three orders of magnitude higher than that of hydride transfer [63,77]. Therefore, it is important to conduct the reaction under conditions, which favor hydride transfer over alkene addition.

Within the octane fraction the relative rates of hydride transfer and isomerization determine the selectivity. The primary product of the addition of 2-butene to isobutane is 2,2,3-TMP. However, with most catalysts only minor concentration of 2,2,3-TMP are observed, while 2,3,3-, 2,3,4-, and 2,2,4-TMP dominate the octane fraction [3]. This observation shows that isomerization by hydride- or methyl shift is fast compared to hydride transfer. Feller *et al.* even observed that alkylation over H-LaX yields less 2,2,3-TMP than in thermodynamic equilibrium, while surprisingly high concentrations of 2,2,4-TMP were found [65]. The authors explained this by the fact that hydride transfer to a 2,2,3-trimethyl-3-pentyl carbenium ion suffers from particularly strong steric hindrance.



Scheme 1.8: Mechanism of self-alkylation including desorption of isobutene and addition of the isobutene molecule to a *tert*-butyl carbenium ion [65]

An alternative pathway, which explains the preferred formation of 2,2,4-TMP over some catalysts, is self-alkylation [65,73,77]. This reaction sequence includes deprotonation of a *tert*-butyl carbenium ion, which leads to the formation of an isobutene molecule and frees a Brønsted acid site (Scheme 1.8). On the free Brønsted acid site a butene molecule is protonated as in the initiation step. The isobutene molecule adds to a *tert*-butyl carbenium ion forming a 2,4,4-trimethyl-2-pentyl carbenium ion, which forms a 2,2,4-TMP molecule if it abstracts a hydride before isomerization occurs.

1.3.3.2. Deactivation and regeneration

Despite their advantages in handling rapid deactivation has prevented the implementation of zeolites in commercial alkylation plants. The formation of heavy products in the zeolite pores plays a key role for deactivation. Therefore, many groups have investigated spent deactivation catalysts by IR [66,73,78], UV/Vis [69,79-81], ^{13}C -NMR [69,70,82], temperature programmed oxidation [67] and matrix assisted laser desorption ionization-time of flight mass spectrometry (MALDI-TOF MS) [78]. Moreover, extracted deposits were investigated after dissolution of the zeolite in HF using ^1H -NMR and GC/MS [73]. It was found that the deposits consist of partly unsaturated cycles with highly branched side chains [73,78,79]. Moreover, the formation of aromatic compounds was proposed [78].

Poisoning of active sites [69] and pore mouth plugging [67,83] have been proposed as deactivation pathways. It has also been suggested that a combination of both mechanisms is responsible for deactivation [78,79,84]. According to this theory, deposits adsorb irreversibly on Brønsted acid sites and, thus, decrease the number of active sites for alkylation, which

increases the rate of polymerization relative to alkylation. Therefore, more deposits are formed and the pores of the zeolite are blocked.

Several methods have been developed for the regeneration of solid alkylation catalysts. The most commonly discussed ones are oxidative removal of the deposits [85] extraction with supercritical hydrocarbons [74,86-90] and hydrocracking [66,79,91].

Combustion of carbonaceous deposits at high temperature (ca. 850 K) is commonly applied to catalysts in FCC units (Section 3.1.). However, zeolites with a low Si/Al ratio, which are commonly used as alkylation catalysts, have a lower thermal stability. Therefore, high temperatures will induce dealumination and degradation of the catalyst. Deposits on alkylation catalysts have H/C ratios between 1.6 and 1.8 [73,78,79]. Therefore, they should be combusted at moderate temperatures, but the heat released in this process leads to the formation of hard coke by dehydrogenation and aromatization, in particular when the deposits are cyclic molecules [85].

It has been shown that the formation of deposits and, therefore, deactivation is reduced when the reaction is conducted under supercritical conditions, which should allow continuous extraction of the deposits [87,88]. The most straightforward approach is conducting the reaction in supercritical isobutane ($p_{\text{crit}} = 36.5$ bar, $T_{\text{crit}} = 681$ K). However, under these conditions side reactions, such as cracking, lower the octane number and, thus, the alkylate quality. For this reason, various groups have investigated the use of inert solvents, which reach supercritical conditions at lower temperatures and pressures [86]. Among the inert solvents, carbon dioxide received the most attention [88,89]. Ginosar *et al.* compared various solvents under supercritical condition and concluded that light hydrocarbons are superior to carbon dioxide for isobutane/butene alkylation [90]. Note that in heavily deactivated catalysts, extraction with supercritical hydrocarbons does not lead to complete removal of the deposits [74].

Hydrogenative regeneration requires the addition of a noble metal to the acidic zeolite catalyst [66,79]. Recently, it was shown that the activity of Pt-LaX is completely restored even after several repetitions of the alkylation-regeneration cycle [79]. Pichler *et al.* demonstrated that hydrocracking of dodecane over Pt-CaY starts 523 K [91]. This indicates that hydrocracking is a much milder method than combustion and, hence, avoids the disadvantages outlined previously.

1.4. Zeolite catalysts

Zeolites are crystalline aluminosilicates with a micropore network. Figure 1.4 illustrates the structures of selected zeolites. The primary building blocks of all zeolites are SiO_4 and AlO_4 tetrahedra, which are linked to each other by sharing an oxygen atom at their corners. This occurs in a way that periodic three dimensional framework structures are formed. Tetrahedra with an aluminum atom in the centre have the net formula AlO_2^- . The negative framework charge is compensated by cation (often Na^+). Al-O-Al bonds in zeolites are very instable. Therefore, the maximum amount of aluminum, which can be incorporated in a zeolite framework, corresponds to 50 % of the tetrahedra ($\text{Si}/\text{Al} = 1$). This finding is expressed in Löwenstein's rule [92].

The secondary building blocks differ between different types of zeolites. In the top line of Figure 1.4 the structure of a faujasite type zeolite is shown. The secondary building block of this zeolite is a sodalite cage, which consists of 24 tetrahedra in the geometrical form of a cubo-octahedron. The sodalite cages are linked to each other *via* a hexagonal prism. A faujasite type zeolite with a Si/Al ratio between 1.0 and 1.5 is referred to as zeolite X, while one with a higher Si/Al ratio is called zeolite Y.

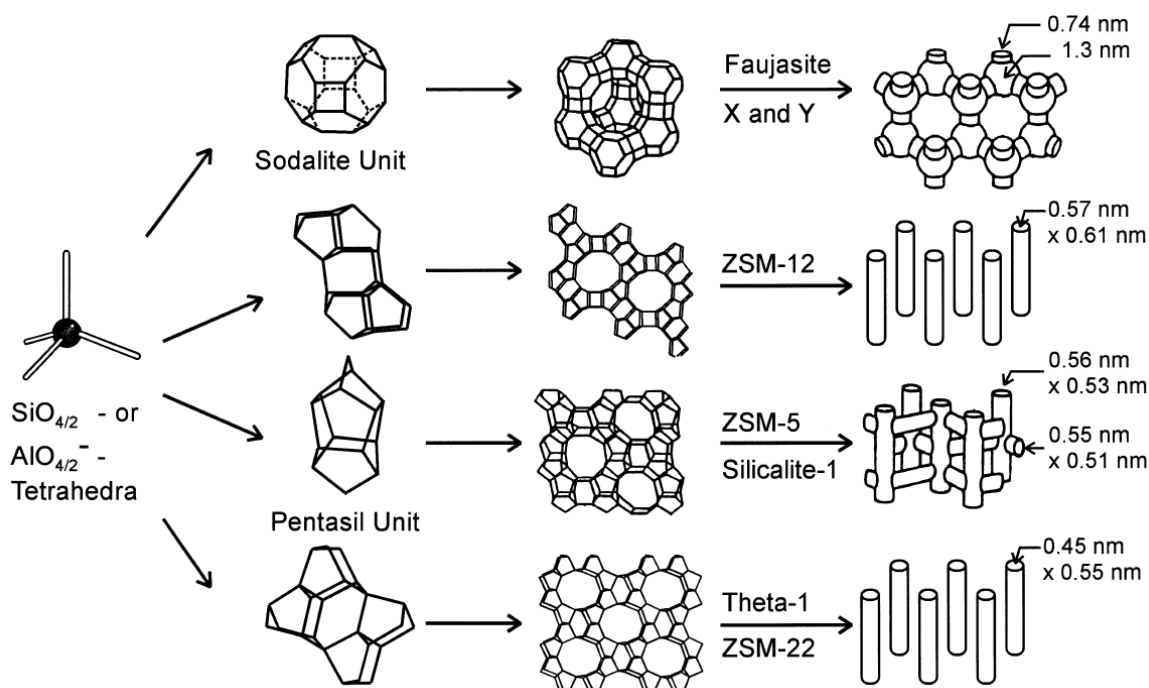


Figure 1.4: Structures and dimensions of faujasite, ZSM-12, ZSM-5 and ZSM-22 [93]

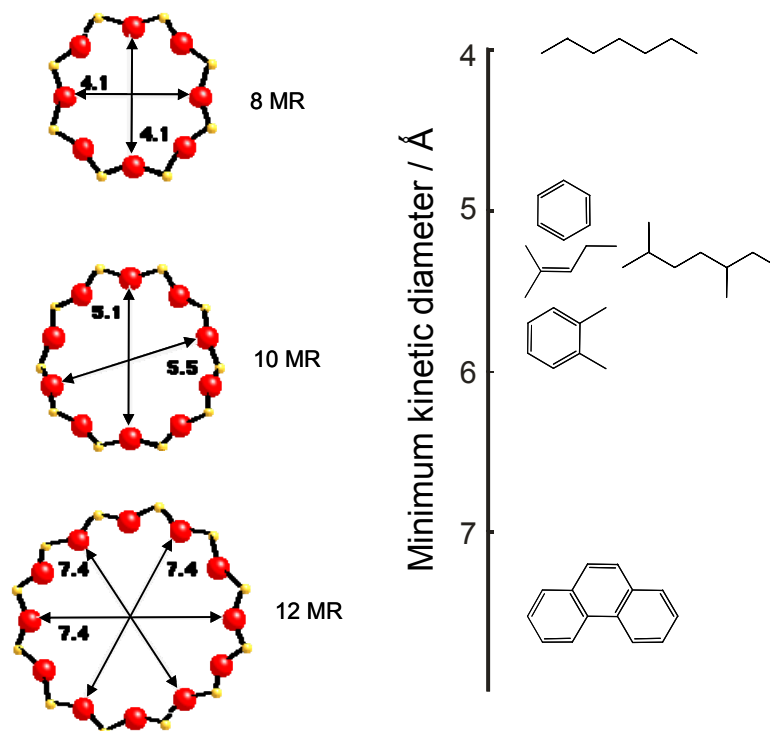


Figure 1.5: Comparison of the dimensions of pore openings in zeolites and the kinetic diameters of selected hydrocarbons [94]

A variety of zeolite structures, e.g. faujasite and mordenite, are found in nature. The first synthetic zeolites were produced in the late 1940's [95]. In contrast to natural zeolites, synthetic ones have a reproducible quality and contain only few impurities. Nowadays, ca. 140 zeolite structures are known. An overview of zeolite structure has been published in ref. [96].

Large quantities of zeolites are produced as sorbents and water softeners in laundry detergents. However, the biggest scientific challenge remains tailoring the properties of zeolites for a wide range of applications in heterogeneous catalysis.

The pore sizes of zeolites are in the same order of magnitude as the kinetic diameters of hydrocarbon molecules. Therefore, shape selectivity can be obtained for reactions, which take place inside the zeolite framework. Shape selectivity can affect the reactants (selective diffusion into the pores), the products (selective diffusion out of the pores) or the transition states (selection of reaction pathways inside the pores). In Figure 1.5 the dimensions of the pore openings in zeolites are compared to the kinetic diameters of hydrocarbon molecules. The pores of zeolite A can only be accessed through an 8 membered ring, while ZSM5 contains 10 membered rings. In large pore zeolites, such as beta, faujasite, and mordenite 12 membered rings are found as the largest pore openings.

Ion exchange of the charge compensating cations into the zeolite is a powerful tool for the modification of the properties of the material. Zeolites, which contain protons, are solid Brønsted acids with a wide range of industrial application, e.g. fluid catalytic cracking (*vide supra*). In the absence of other cations, the concentration of Brønsted acid sites is proportional to the aluminum concentration in the framework. However, the strength of an individual site decreases with increasing aluminum concentration, because the electronegativity of aluminum is lower than that of silicon.

Incorporation of metal cations gives rise to Lewis acidity. There are also many examples of application of metal cation exchanged zeolites, e.g. Ga-ZSM5 for aromatization of small alkanes [97], Pt-BEA and Pd-BEA for hydroisomerization [57,98] and Cu, Co and Fe exchanged ZSM5 for the reduction of NO_x with hydrocarbons [99]. The properties and catalytic applications of zeolites have been the subject of various review articles [93,94].

1.5. Scope of this thesis

Rare earth exchanged faujasite type zeolites are of great interest as catalysts for fluid catalytic cracking in refineries. Moreover, it was shown in recent literature that H-LaX is a promising candidate for solid acid catalyzed isobutane/n-butene alkylation. Incorporation of lanthanum cations primarily serves the purpose of increasing the hydrothermal stability of the zeolites. However, it has also been proposed that lanthanum cations influence the acidity of the zeolite.

In catalytic cracking and isobutane alkylation, the formation of carbonaceous deposits leads to premature deactivation of the catalysts. As a result cracking catalysts have to be regenerated frequently, and the industrial implementation of zeolite catalyzed alkylation processes has been prevented by the regeneration costs. Understanding the reactions, which lead to deactivation is of great interest in order to improve the physicochemical properties of the catalysts to suit the requirements for industrial applications.

In this thesis, the conversion of alkanes over lanthanum exchanged faujasites was investigated. The focus was on obtaining a profound understanding of the elementary processes, which determine the catalytic performance of these materials. Detailed characterization of the catalysts was conducted by a variety of physicochemical techniques. Based on these results, conclusion of the reactivity and catalytic stability of LaFAU catalysts are drawn.

In the first part the interaction of alkanes with H-LaX was investigated. In chapter 2, sorption of alkanes with four to seven carbon atoms on H-LaX was studied by gravimetry, calorimetry as well as IR and NMR spectroscopy. Particular emphasis was put on the polarization, which is induced on the sorbed molecules. In chapter 3, sorption, activation and surface chemistry of octane isomers on H-LaX is described. Unlike smaller alkanes, octane isomers are activated even at low temperatures (303 – 373 K).

The second part of this thesis is focused on the use of lanthanum exchanged faujasites as catalysts for isobutane/2-butene alkylation. In chapter 4, the performance of H-LaX (Si/Al = 1:1) and H-LaY (Si/Al = 2.4) in alkylation is compared. It is shown that the differences of the catalytic performance are due different concentration of strong acid sites. The creation of strong acid sites in both materials is discussed.

The formation of carbonaceous deposits and their impact on deactivation of H-LaX in isobutane/2-butene are described in chapter 5. For this purpose the reaction was stopped after different times on stream and the spent catalyst was characterized by a variety of

physicochemical techniques. This approach provided a detailed understanding of the processes, which eventually lead to deactivation of the catalyst.

Chapter 6 gives a summary of the most important results and conclusions.

1.6. References

- [1] R.P. Silvy, *Appl. Catal. A-Gen.* 261 (2004) 247.
- [2] J.E. Naber, K.P. de Jong, W.H.J. Stork, H.P.C.E. Kuipers, M.F.M. Post, *Stud. Surf. Sci. Catal.* 84 (1994) 2197.
- [3] A. Feller, J.A. Lercher, *Adv. Catal.* 48 (2004) 229.
- [4] W.O. Haag, R.M. Dessau, *Duality of Mechanism for Acid-Catalyzed Paraffin Cracking*; 8th Int. Congress on Catalysis, 1984, Berlin, Vol. 2, p. 305.
- [5] D. Fărcașiu, P. Lukinskas, *J. Phys. Chem. A* 106 (2002) 1619.
- [6] B. Schoofs, J. Schuermans, R.A. Schoonheydt, *Micropor. Mesopor. Mater.* 35-36 (2000) 99.
- [7] T.F. Narbeshuber, A. Brait, K. Seshan, J.A. Lercher, *Appl. Catal. A-Gen.* 146 (1996) 119.
- [8] T.F. Narbeshuber, A. Brait, K. Seshan, J.A. Lercher, *J. Catal.* 172 (1997) 127.
- [9] J. Scherzer, R.E. Ritter, *IEC Prod. Res. Dev.* 17 (1978) 219.
- [10] W.F. Pansing, *J. Phys. Chem.* 69 (1965) 392.
- [11] G.A. Olah, G. Klopman, Schlosbe.Rh, *J. Am. Chem. Soc.* 91 (1969) 3261.
- [12] T.F. Narbeshuber, H. Vinek, J.A. Lercher, *J. Catal.* 157 (1995) 388.
- [13] S.A. Zygmunt, L.A. Curtiss, P. Zapol, L.E. Iton, *J. Phys. Chem. B* 104 (2000) 1944.
- [14] G. de la Puente, U.A. Sedran, *J. Catal.* 179 (1998) 36.
- [15] M. Guisnet, N.S. Gnep, D. Aittaleb, Y.J. Doyemet, *Appl. Catal. A-Gen.* 87 (1992) 255.
- [16] M. Marczewski, *J. Chem. Soc.-Faraday Trans.* 82 (1986) 1687.
- [17] C.J.A. Mota, D.L. Bhering, A. Ramirez-Solis, *Int. J. Quantum Chem.* 105 (2005) 174.
- [18] X.B. Zheng, P. Blowers, *J. Phys. Chem. A* 110 (2006) 2455.
- [19] M. Boronat, C.M. Zicovich-Wilson, A. Corma, P. Viruelab, *Phys. Chem. Chem. Phys.* 1 (1999) 537.
- [20] M. Boronat, P. Viruelab, A. Corma, *Phys. Chem. Chem. Phys.* 2 (2000) 3327.
- [21] V.B. Kazansky, M.V. Frash, R.A. van Santen, *Catal. Lett.* 48 (1997) 61.
- [22] M. Boronat, P. Viruela, A. Corma, *J. Phys. Chem. B* 103 (1999) 7809.
- [23] M. Boronat, P. Viruela, A. Corma, *J. Phys. Chem. B* 101 (1997) 10069.
- [24] M.V. Frash, V.N. Solkan, V.B. Kazansky, *J. Chem. Soc.-Faraday Trans.* 93 (1997) 515.
- [25] C.J.A. Mota, P.M. Esteves, M.B. deAmorim, *J. Phys. Chem.* 100 (1996) 12418.

-
- [26] D.B. Lukyanov, *J. Catal.* 145 (1994) 54.
- [27] A. Platon, W.J. Thomson, *Catal. Lett.* 101 (2005) 15.
- [28] A. Platon, W.J. Thomson, *Appl. Catal. A-Gen.* 282 (2005) 93.
- [29] J. Weitkamp, P.A. Jacobs, J.A. Martens, *Appl. Catal.* 8 (1983) 123.
- [30] F. Cardona, N.S. Gnep, M. Guisnet, G. Szabo, P. Nascimento, *Appl. Catal. A-Gen.* 128 (1995) 243.
- [31] V.B. Kazansky, I.R. Subbotina, N. Rane, R.A. van Santen, E.J.M. Hensen, *Phys. Chem. Chem. Phys.* 7 (2005) 3088.
- [32] N. Rane, A.R. Overweg, V.B. Kazansky, R.A. van Santen, E.J.M. Hensen, *J. Catal.* 239 (2006) 478.
- [33] E.A. Pidko, V.B. Kazansky, E.J.M. Hensen, R.A. van Santen, *J. Catal.* 240 (2006) 73.
- [34] V.B. Kazansky, *Catal. Today* 51 (1999) 419.
- [35] I.N. Senchenya, V.B. Kazansky, *Catal. Lett.* 8 (1991) 317.
- [36] V.B. Kazansky, I.N. Senchenya, *J. Catal.* 119 (1989) 108.
- [37] J.F. Haw, J.B. Nicholas, T. Xu, L. Beck, D.B. Ferguson, *Accounts Chem. Res.* 29 (1996) 259.
- [38] W.C. Cheng, G. Kim, A.W. Peters, X. Zhao, K. Rajagopalan, M.S. Ziebarth, C.J. Pereira, *Catal. Rev.-Sci. Eng.* 40 (1998) 39.
- [39] B.S. Greensfelder, H.H. Voge, G.M. Good, *Ind. Eng. Chem.* 41 (1949) 2573.
- [40] R.W. Coughlin, A. Hasan, K. Kawakami, *J. Catal.* 88 (1984) 163.
- [41] H.S. Cerqueira, P. Ayrault, J. Datka, M. Guisnet, *Micropor. Mesopor. Mater.* 38 (2000) 197.
- [42] H.S. Cerqueira, C. Sievers, G. Joly, P. Magnoux, J.A. Lercher, *Ind. Eng. Chem. Res.* 44 (2005) 2069.
- [43] K.A. Cumming, B.W. Wojciechowski, *Catalysis Reviews - Science and Engineering* 38 (1996) 101.
- [44] C.E. Snape, B.J. McGhee, J.M. Andresen, R. Hughes, C.L. Koon, G. Hutchings, *Appl. Catal. A-Gen.* 129 (1995) 125.
- [45] K. Qian, D.C. Tomczak, E.F. Rakiewicz, R.H. Harding, G. Yaluris, W.-C. Cheng, X. Zhao, A.W. Peters, *Energy & Fuels* 11 (1997) 596.
- [46] E. Furimsky, *Fuel Process. Technol.* 67 (2000) 205.
- [47] P.D. Hopkins, J.T. Miller, B.L. Meyers, G.J. Ray, R.T. Roginski, M.A. Kuehne, H.H. Kung, *Appl. Catal. A-Gen.* 136 (1996) 29.
- [48] M. Guisnet, P. Magnoux, *Catal. Today* 36 (1997) 477.

-
- [49] M. Guisnet, P. Magnoux, *Appl. Catal. A-Gen.* 212 (2001) 83.
- [50] G.F. Froment, *Stud. Surf. Sci. Catal.* 6 (1980) 1.
- [51] M.-F. Reyniers, H. Beirnaert, G.B. Marin, *Appl. Catal. A-Gen.* 202 (2000) 49.
- [52] M.-F. Reyniers, Y. Tang, G.B. Marin, *Appl. Catal. A-Gen.* 2 (2000) 65.
- [53] M. Guisnet, P. Magnoux, D. Martin, *Stud. Surf. Sci. Catal.* 111 (1997) 1.
- [54] B.A. Williams, S.M. Babitz, J.T. Miller, R.Q. Snurr, H.H. Kung, *Appl. Catal. A-Gen.* 177 (1999) 161.
- [55] A. Sassi, J. Sommer, *Appl. Catal. A-Gen.* 188 (1999) 155.
- [56] H. Vansina, M. Baltanas, G.F. Froment, *IEC Prod. Res. Dev.* 22 (1983) 526.
- [57] E. Blomsma, J.A. Martens, P.A. Jacobs, *J. Catal.* 159 (1996) 323.
- [58] M. Boronat, P. Viruela, A. Corma, *Appl. Catal. A-Gen.* 146 (1996) 207.
- [59] M. Saunders, S.P. Budiansky, *Tetrahedron* 35 (1979) 929.
- [60] S.T. Sie, in: G. Ertl, H. Knözinger, J. Weitkamp (Eds.), *Handbook of Heterogeneous Catalysis*, VCH Verlagsgesellschaft mbH, Weinheim, 1997, Vol. 4, p. 1998.
- [61] E. Furimsky, *Catal. Today* 30 (1996) 223.
- [62] K. Yoo, P.G. Smirniotis, *Appl. Catal. A-Gen.* 227 (2002) 171.
- [63] K.P. de Jong, C.M.A.M. Mesters, D.G.R. Peferoen, P.T.M. van Brugge, C. de Groot, *Chem. Eng. Sci.* 51 (1996) 2053.
- [64] A. Corma, A. Martínez, P.A. Arroyo, J.L.F. Monteiro, E.F. Sousa-Aguiar, *Appl. Catal. A-Gen.* 142 (1996) 139.
- [65] A. Feller, A. Guzman, I. Zuazo, J.A. Lercher, *J. Catal.* 224 (2004) 80.
- [66] R. Josl, R. Klingmann, Y. Traa, R. Gläser, J. Weitkamp, *Catal. Commun.* 5 (2004) 239.
- [67] C.A. Querini, E. Roa, *Appl. Catal. A-Gen.* 163 (1997) 199.
- [68] A. Corma, A. Martínez, C. Martínez, *J. Catal.* 146 (1994) 185.
- [69] C. Flego, I. Kiricsi, J. Parker, W. O., M.G. Clerici, *Appl. Catal. A-Gen.* 124 (1995) 107.
- [70] M. Stöcker, H. Mostad, T. Rørvik, *Catal. Lett.* 28 (1994) 203.
- [71] T. Rørvik, H. Mostad, O.H. Ellestad, M. Stocker, *Appl. Catal. A-Gen.* 137 (1996) 235.
- [72] K.S. Yoo, P.G. Smirniotis, *Catal. Lett.* 103 (2005) 249.
- [73] J. Pater, F. Cardona, C. Canaff, N.S. Gnep, G. Szabo, M. Guisnet, *Ind. Eng. Chem. Res.* 38 (1999) 3822.
- [74] D.M. Ginosar, D.N. Thompson, K.C. Burch, *Appl. Catal. A-Gen.* 262 (2004) 223.
- [75] P.S. Pryor, *PTQ Winter 2004* (2004) 69.

-
- [76] M.A. Sanchez-Castillo, N. Agarwal, C. Miller, R.D. Cortright, R.J. Madon, J.A. Dumesic, *J. Catal.* 205 (2002) 67.
- [77] M.F. Simpson, J. Wei, S. Sundaresan, *Ind. Eng. Chem. Res.* 35 (1996) 3861.
- [78] A. Feller, J.-O. Barth, A. Guzman, I. Zuazo, J.A. Lercher, *J. Catal.* 220 (2003) 192.
- [79] R. Klingmann, R. Josl, Y. Traa, R. Gläser, J. Weitkamp, *Appl. Catal. A-Gen.* 281 (2005) 215.
- [80] I. Kiricsi, C. Flego, G. Bellussi, *Appl. Catal. A-Gen.* 126 (1995) 401.
- [81] K. Yoo, E. Burckle, P. Smirniotis, *Catal. Lett.* 74 (2001) 85.
- [82] J. Weitkamp, S. Maixner, *Zeolites* 7 (1987) 6.
- [83] S. Sahebdehfar, M. Kazemeini, F. Khorasheh, A. Badakhshan, *Chem. Eng. Sci.* 57 (2002) 3611.
- [84] F.A. Diaz-Mendoza, L. Pernet-Bolano, N. Cardona-Martínez, *Thermochim. Acta* 312 (1998) 47.
- [85] C.A. Querini, *Catal. Today* 62 (2000) 135.
- [86] D.M. Ginosar, R.V. Fox, P.C. Kong, US Patent 6,103,948 (2000), to Bechtel BWXT Idaho, LLC
- [87] A. Husain, US patent 5,304,698 (1994), to Mobil Oil Corporation
- [88] C.J. Lyon, V.S.R. Sarsani, B. Subramaniam, *Ind. Eng. Chem. Res.* 43 (2004) 4809.
- [89] G.M. Santana, A. Akgerman, *Ind. Eng. Chem. Res.* 40 (2001) 3879.
- [90] D.M. Ginosar, D.N. Thompson, K. Coates, D.J. Zalewski, *Ind. Eng. Chem. Res.* 41 (2002) 2864.
- [91] H. Pichler, J. Weitkamp, H. Schulz, H.O. Reitemeyer, *Erdöl, Kohle, Erdgas, Petrochem.* 25 (1972) 494.
- [92] W. Löwenstein, *Am. Mineral.* 39 (1954) 92.
- [93] J. Weitkamp, *Solid State Ion.* 131 (2000) 175.
- [94] J.A. Lercher, A. Jentys, in: J.A. Schwarz, C.I. Contescu, K. Putyera (Eds.), *Encyclopedia of Nanoscience and Nanotechnology*, Marcel Dekker, Inc., New York, 2004.
- [95] R.M. Barrer, *Nature* 164 (1949) 112.
- [96] W.M. Meier, D.H. Olson, C. Baerlocher, *Atlas of Zeolite Structure Types*, 4th ed., Elsevier, London, 1996.
- [97] G.L. Price, V. Kanazirev, *J. Catal.* 126 (1990) 267.
- [98] M. Tromp, J.A. van Bokhoven, M.T. Garriga Oostenbrink, J.H. Bitter, K.P. de Jong, D.C. Koningsberger, *J. Catal.* 190 (2000) 209.

- [99] Z. Sobalik, J. Dedecek, I. Ikonnikov, B. Wichterlova, *Micropor. Mesopor. Mater.* 21 (1998) 525.

Chapter 2

Adsorption of branched alkanes on H-LaX

The interaction of light alkane isomers with zeolite H-LaX was investigated under mild conditions similar to those used by processes such as alkylation. The presence of La^{3+} cations increases the heat of adsorption compared to HY zeolites and induces a strong polarization on the adsorbed alkanes. The polarization is particularly strong for molecules with a single branching in the 2 position. At high uptake, sorbate-sorbate interactions lead to a further increase of the heat of adsorption. Due to a high loss of entropy these interactions were only observed when complete pore filling was approached. The specific interaction of different parts of the sorbate molecule was investigated by ^{13}C MAS NMR. It was shown that a positive partial charge is induced on secondary and tertiary carbon atoms. This polarization may be seen as intermediate to hydride abstraction. When molecular water is present on the activated catalyst, it blocks the strongest adsorption sites, but it also contributes to the heat of adsorption of alkanes and surprisingly enhances their polarization.

2.1. Introduction

Acidic zeolites are important catalyst for a wide range of petrochemical processes such as catalytic cracking [1], alkylation [2,3] and isomerization [4]. The properties of zeolites can be modified by methods like steaming and ion exchange in order to fulfill the requirements as catalysts for specific reactions.

However, zeolites are thermally metastable. The structural stability of zeolites is increased by the introduction of rare-earth cations, with lanthanum being exceptionally suitable. During calcination, La^{3+} cations migrate into the sodalite cages [5]. In addition to this, Brønsted acid sites are formed by hydrolysis when the zeolite is exposed to water [6-8]. Van Bokhoven *et al.* showed that the effect of La^{3+} cations in H-USY is similar to that of well dispersed extraframework aluminum [9]. As a result of its presence the Si-O-Al and Si-O-Si angles increase. In addition to this, a withdrawal of electron density from the zeolite framework has been claimed to be induced by La^{3+} [9]. In this context, Carvajal *et al.* reported that La^{3+} exchange leads to an increase of the hexane cracking activity of various zeolite Y samples [10]. In contrast, Ivanov *et al.* reported that the incorporation of 5 wt.% La into zeolite ZSM-5 only has a small effect on the adsorption of propane, butane and propene [11].

Adsorption is one of the key steps in catalytic conversions, because it determines the way, in which molecules interact with the catalyst. A variety of techniques was used to investigate alkane adsorption on zeolites including gravimetry [12-19], calorimetry [14-17,19,20], chromatography [21,22], IR spectroscopy [14-17], ^{13}C NMR spectroscopy [19] and theoretical methods such as Monte Carlo simulations [23-25].

Three kinds of interactions are observed when alkanes are adsorbed on zeolites: (i) interaction with the zeolite lattice *via* dispersive van-der-Waals forces, (ii) interaction with the Brønsted acid sites and (iii) intermolecular interactions of the adsorbed molecules. The strongest interaction is the one with the zeolite lattice [16]. When n-alkanes are adsorbed in faujasite type zeolites the heat of adsorption increases by 7 kJ mol^{-1} for each additional CH_2 group. In contrast to this, the contribution from the interaction of alkanes with Brønsted acid sites in zeolites with a Si/Al ratio lower than 5 amounts to 6 kJ mol^{-1} independent of the size of the alkane molecule [15]. The contribution of intermolecular interaction increases with increasing coverage. Eder *et al.* reported that the heat of adsorption of n-hexane in FAU had increased by 15 kJ mol^{-1} when the zeolite was saturated [15]. In the absence of such intermolecular interaction, the influence of the different contributions to the heat of adsorption

largely depends on pore structure of the zeolite. As long as the sorbate molecule fits into the zeolite pores a higher heat of adsorption is observed for small pore zeolites [16].

Despite their low contribution to the heat of adsorption directed interactions may lead to polarization of sorbed hydrocarbons. Kazansky and Pidko demonstrated that molar extinction coefficient is a good measure for polarization of sorbed hydrocarbons [26]. In Chapter 3, it will be shown that strong polarization of alkanes in H-LaX induces hydride abstraction and, thus, activation of the sorbed alkanes.

So far, only a quite limited number of studies addressed the adsorption of branched alkanes on zeolites [12,13,17,22]. In addition, alkane adsorption was mostly studied on aluminum free zeolites [12,13,15,18,20] or zeolites in the H-form [14-17,19,21,22]. As a result, the effects of modifications such as steaming in the presence of multivalent exchanged cations on the sorption properties are still ambiguous.

In this chapter, the adsorption of butane, pentane, hexane and heptane isomers on zeolite H-LaX was chosen, because the material shows a high potential as a solid acid catalyst for isobutane/2-butene alkylation [27,28]. The activation temperature was chosen so that the catalyst contained small amounts of residual water, which were shown to be important for the interactions with alkanes [29]. The results of different physicochemical techniques provide an in depth understanding of the interaction of alkanes with the zeolite.

2.2. Experimental

2.2.1. Catalyst preparation and reactants

The parent NaX zeolite was obtained from Chemische Werke Bad Köstritz (Si/Al = 1.2). In a first step, the parent material was exchanged two times with 0.2 M lanthanum nitrate solution using a liquid-to-solid ratio of 11 ml·g⁻¹. The zeolite was stirred in this solution for 2 h at 343 K. After washing the resulting material with doubly distilled water to remove nitrate, it was dried first at room temperature and then at 393 K. Subsequently, it was calcined in dry air. The temperature was slowly increased to 723 K and maintained at that level for 1 h. The ion-exchange step, including washing and drying at room temperature, was repeated three times. Finally, the catalyst was calcined again using the same procedure as for the first calcination. n-Butane (99.5%) and isobutane (99.95%) were obtained from Messer. n-Pentane (99.8%), 2-methylbutane (99.7%), n-hexane (99.7%), 2-methylpentane (99.5%), 3-methylpentane (99.5%), 2,2-dimethylbutane (99.5%), 2,3-dimethylbutane (99.5%), n-heptane

(99.8%), 2-methylhexane (99%), 2,2-dimethylpentane (99%) and 2,4-dimethylpentane (99%) were purchased from Sigma-Aldrich.

2.2.2. Characterization

IR spectra of adsorbed pyridine were recorded on a Perkin Elmer 2000 spectrometer between 4000 and 1000 cm^{-1} at a resolution of 4 cm^{-1} . For activation, the zeolite was pressed into a self-supporting wafer and heated to 393 K with a rate of 5 $\text{K}\cdot\text{min}^{-1}$ at 10^{-6} mbar. After 4 h the temperature was increased to 453 K using the same heating rate and kept at 453 K for 8 h. Pyridine was adsorbed at 423 K with an equilibrium pressure of 0.1 mbar. After outgassing for 1 h, a spectrum was recorded. The samples were then heated to 723 K for 1 h to remove pyridine adsorbed on weak acid sites. A spectrum was taken after reducing the temperature to 423 K. After the experiment, a weighing disc of standardized size was punched out from the wafer to determine the density. The concentrations of Lewis and Brønsted acid sites were determined using the extinction coefficients published by Emeis [30].

For the determination of the Al, Si and Na concentration by AAS (UNICAM 939 atomic absorption spectrometer) 20-40 mg the catalyst were dissolved in a mixture of 0.5 ml of hydrofluoric acid (48%) and 0.1 ml of nitro hydrochloric acid and heated to the boiling point of the mixture. The lanthanum content was determined by EDX (Jeol JSM-5900 LV spectrometer). For the latter measurements, the sample was placed on a conductive carbon target. The spectrometer was operated at a voltage of 25 kV.

For pore volume determination by adsorption of nitrogen, approximately 150 mg were activated in vacuum at 523 K for 2 h. Subsequently, the dehydrated sample was weighed. The adsorption isotherms were measured at 77.4 K using a PMI automated BET sorptometer.

For ^{27}Al - and ^{29}Si -MAS-NMR H-LaX was fully hydrated in a desiccator and subsequently packed into a 4 mm ZrO_2 rotor (hydrated sample). For comparison with the sample after adsorption (*vide infra*), an additional sample of H-LaX was also investigated after activation at 453 K for 8 h. The measurements were performed on a Bruker AV500 spectrometer ($B_0 = 11.7$ T) at a rotation speed of 15 kHz. The chemical shifts are reported relative to an external standards of solid $\text{Al}(\text{NO}_3)_3$ ($\delta = -0.5427$ ppm) and tetrakis-trimethylsilyl-silane ($\delta = -9.843$ ppm for the left peak). For ^{27}Al -MAS-NMR 2400 scans were recorded for the single pulse experiment. A recycle time of 0.25 s was used. The RF field was 61 kHz. The excitation pulse had a length of 0.46 μs , which corresponds to a $\pi/12$ -pulse. The ^{29}Si spectrum was recorded as the sum of 40000 scans with a recycle time of 5 sec. The excitation pulse had a length of 1.5 μs .

The ^{27}Al DOR-NMR measurements were performed on a Bruker AV750 with an outer spinning rate of 1300 Hz and an inner spinning rate of approximately 6 kHz. The resonance frequency for ^{27}Al was 195.5 MHz.

2.2.3. Adsorption of alkanes

The gravimetric and calorimetric measurements were performed in a modified SETARAM TG-DSC 111 instrument with a BARATRON 122A pressure transducer. The samples were pressed into platelets and 10-15 mg were placed in a quartz crucible. For activation, the samples were heated in vacuum ($p < 10^{-6}$ mbar) to 393 K at $5 \text{ K}\cdot\text{min}^{-1}$. After 4 h at 393 K, the temperature was increased to 453 K at $5 \text{ K}\cdot\text{min}^{-1}$ and maintained for 8 h. After activation, the temperature was reduced to 348 K. The influence of the activation temperature was investigated by activating several samples at 723 K for 1 h after the drying at 393 K for 4 h. The sorbates were added in pulses and after each pulse the system was equilibrated. This was monitored by observation of the sample weight, heat flow, and pressure. The system was regarded to be in steady state or equilibrium, when changes in any of the three parameters were not observed for 15 minutes.

For the IR measurements, the samples were pressed into self-supporting wafers and activated in vacuum using the same temperature program as for the gravimetric experiments. The measurements were performed on a Bruker IF 66v/S spectrometer in absorption transmission mode. 60 scans were co-added within 6 sec to obtain one spectrum with a resolution of 4 cm^{-1} . Spectra were recorded every 30 sec. The sorbates were added in pulses at 348 K and the system was regarded to be equilibrated, when variations were not observed in three consecutive spectra. The spectra were normalized by comparison of the zeolite lattice vibrations ($1530\text{-}1740 \text{ cm}^{-1}$).

For ^{13}C CP- and ^{27}Al -MAS NMR measurements the samples were activated using the same procedure as for the gravimetric measurements. Alkanes were adsorbed at an equilibrium pressure of 0.5 mbar. Then, the sample were packed into ZrO_2 rotors and spun at 15 kHz. The samples were measured on a Bruker AV500 spectrometer with a resonance frequency of 125.8 MHz for ^{13}C . The sensitivity was enhanced by applying cross polarization [31]. The contact time was 5 ms. At least 40000 scans were recorded for a spectrum.

2.3. Results

2.3.1. Characterization

Elemental analysis by AAS gave concentration of 10.8, 13.6 and 0.04 wt.% for Al, Si and Na, respectively. This shows that an ion exchange degree of 99.6% was reached and that the Si/Al ratio was 1.21. A lanthanum content of 24.3 wt.% was measured by EDX. The micropore volume was $0.19 \text{ cm}^3 \cdot \text{g}^{-1}$.

The nature and concentration of acid sites were determined using IR spectra of adsorbed pyridine. The concentrations of Brønsted and Lewis acid site were 0.40 and $0.14 \text{ mmol} \cdot \text{g}^{-1}$, respectively. The concentration of strong acid sites, which retain pyridine at 723 K , was determined to be 0.12 and $0.09 \text{ mmol} \cdot \text{g}^{-1}$ for Brønsted and Lewis acid sites, respectively.

Figure 2.1a shows the ^{27}Al MAS NMR spectrum of hydrated H-LaX. The overlapping peaks at 55 and 46 ppm are attributed to tetrahedrally coordinated aluminum in the zeolite framework positions with protons and La^{3+} cations as charge compensating cations, respectively [9]. The peak at 3 ppm is assigned to octahedrally coordinated aluminum, which is present as extraframework species. The nature of extraframework aluminum in zeolites is still subject of discussion. It has been proposed to be present as charge compensating ions in extra-framework positions or in a separate phase outside the zeolite pores [9,32].

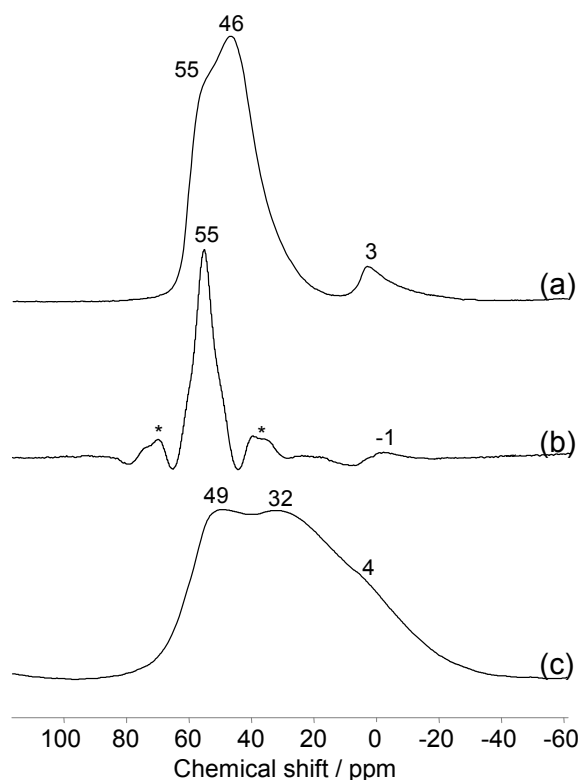


Figure 2.1: ^{27}Al NMR spectra of H-LaX: (a) MAS spectrum of hydrated H-LaX, (b) DOR spectrum of hydrated H-LaX, (c) MAS spectrum H-LaX after activation at 453 K

Table 2.1: Spectral parameters of the simulated ^{27}Al MAS NMR spectrum

δ_{iso} (ppm)	QCC (MHz)	Relative area (%)	Assignment	Concentration ($\text{mmol}\cdot\text{g}^{-1}$) ^a
59.3	2.7	8	Td Al^{3+} close to H^+	0.38
57.1	5.1	87	Td Al^{3+} close to La^{3+}	4.25
4.7	2.0	1	Flexible EFAl	0.06
3.3	3.8	4	Separate EFAl phase	0.17

^a Based on the total Al concentration as determined by AAS.

Double rotation (DOR) NMR is a technique, which eliminates the second-order quadrupolar coupling [33,34]. The peak positions in the resulting spectrum is exclusively determined by the isotropic chemical shift δ_{iso} . The DOR spectrum only showed one peak for tetrahedrally coordinated Al at 55 ppm (Figure 2.1b). This shows that the isotropic shift of both tetrahedral species is similar. Therefore, the species corresponding to the peak at 46 ppm must experience a strongly distorted environment, which is responsible for a quadrupolar induced shift. This shows that charge compensation by La^{3+} cations does not alter the partial charge of the adjacent Al atoms significantly, but changes the geometry of their coordination. As in the MAS spectrum, the peak corresponding to octahedral aluminum was observed at -1 ppm. The MAS and DOR spectra have approximately the same line shape indicating that a variety Al species with different isotropic shifts was present in H-LaX.

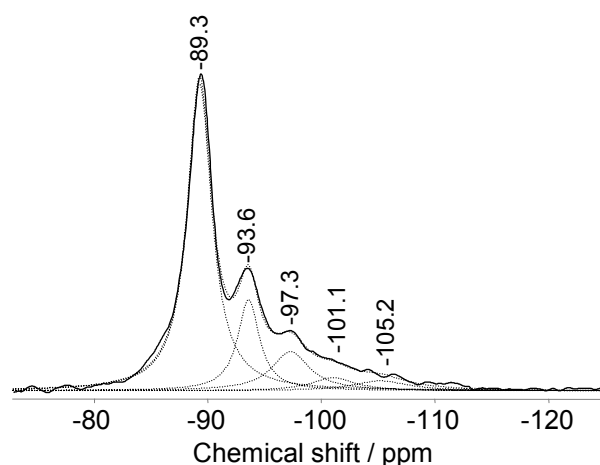


Figure 2.2: ^{29}Si MAS NMR spectrum of hydrated H-LaX: experimental spectra (—) and simulation (···)

Table 2.2: Chemical shifts, line widths and areas of the simulated peaks in the ^{29}Si MAS NMR spectrum of H-LaX

Si(nAl)	Chemical shift (ppm)	Line width (ppm)	Relative area (%)
n = 4	-89.3	2.6	63
n = 3	-93.6	2.3	17
n = 2	-97.3	4.0	12
n = 1	-101.1	4.5	5
n = 0	-105.2	5.8	4

Based on the additional information from the DOR NMR spectrum the MAS NMR spectrum was simulated. The results of the simulation are compiled in Table 2.1. The presence of octahedral aluminum indicates that dealumination has occurred to a moderate extent during the calcination after ion exchange. The concentration of aluminum close to protons was in good agreement with the acid site concentration measured by IR spectroscopy of adsorbed pyridine.

The ^{27}Al MAS NMR spectrum of H-LaX after activation at 453 K is shown in Figure 2.1c. The removal of water during activation leads to strong broadening of the peaks, due to quadrupolar interactions, which result from distortion of the local environment of the aluminum nuclei. Moreover, the peaks corresponding to tetrahedrally coordinated aluminum species shifted to 49 and 32 ppm, respectively. The peak of octahedral Al was only observed as a weak shoulder at 3 ppm. Due to the large line width of the peaks the spectrum could not be quantified. However, it was used as reference for spectra after adsorption of alkanes (*vide infra*).

The ^{29}Si -MAS-NMR spectrum of H-LaX is shown in Figure 2.2 along with the simulated spectrum (simulation parameters compiled in Table 2.2). Based on Löwenstein's rule a Si/Al ratio of 1.21 was calculated. Comparison to the AAS results indicates that only 5 % of the aluminum was present in extra framework species.

In comparison to NaX, a high field shift of approximately 4 ppm was observed for H-LaX. Klein *et al.* explained this with an increasing strain of the Si-O-T bonds (T being Al or Si) in the six ring window close to the La^{3+} cation in the sodalite cage [35]. The line width decreased as a function of the number of next nearest Al neighbors. Gaare and Akporiaye reported that the preferred position of La^{3+} ions in a faujasite type zeolite is close to $\text{Si}(\text{OAl})_4$ sites [5]. Based on this, the broad lines of silicon atoms with fewer Al atoms in the vicinity are explained with an overlap of two species. These differ by the counter ion for the charge

compensation. While the charge of one species is compensated by La^{3+} cations, protons compensate the charge of the other one.

2.3.2. Gravimetric and calorimetric measurements

The adsorption isotherms of n-alkanes on H-LaX are shown in Figure 2.3. The isotherms were simulated based on the assumption that two adsorption regimes are present. In the first regime alkanes only interact with the zeolite. Sorbate-sorbate interactions dominate in the second regime, in which a stronger interaction is observed. Eder *et al.* referred to this regime as accumulative adsorption, which must be described by a modified Langmuir term, in which the number of sorption sites depends on the coverage of the sites from the first regime [15]. Following this approach the exponent was determined from double logarithmic plot of the heat of adsorption over the uptake [15]. In the present study, a value close to 1 was found for all sorbates.

Based on these considerations the isotherms were simulated using the formula:

$$\sigma = \frac{K_{ads1} \cdot p \cdot \sigma_1}{1 + K_{ads1} \cdot p} + \frac{n \cdot \left(\frac{K_{ads1} \cdot p \cdot \sigma_1}{1 + K_{ads1} \cdot p} \right)^1 \cdot K_{ads2} \cdot p}{1 + K_{ads2} \cdot p} \quad (1)$$

Where K_{ads1} and K_{ads2} are the adsorption constants, σ_1 the number of sorption sites without sorbate-sorbate interactions and n a scaling parameter for the number of sites for accumulative adsorption. The isotherms were fitted by varying the adsorption constants, the number of sorption sites and the scaling parameter n . The fitting parameters for the isotherm are compiled in Table 2.3.

The initial adsorption constants increased exponentially with increasing size of the sorbate molecule. Only the increase from hexane to heptane was somewhat smaller. For 2-methylpentane and 2,3-dimethylbutane a slightly larger value was found compared to the linear isomers, while the initial adsorption constant of molecules containing quaternary carbon atoms was significantly lower. The adsorption constants in the regime of accumulative adsorption also increased with increasing molecular size. For most alkanes the adsorption constant decreased with the degree of branching in this regime. Only for pentane isomers similar values were found. It was observed that the first points of the fitted isotherms were consistently lower than the measured values.

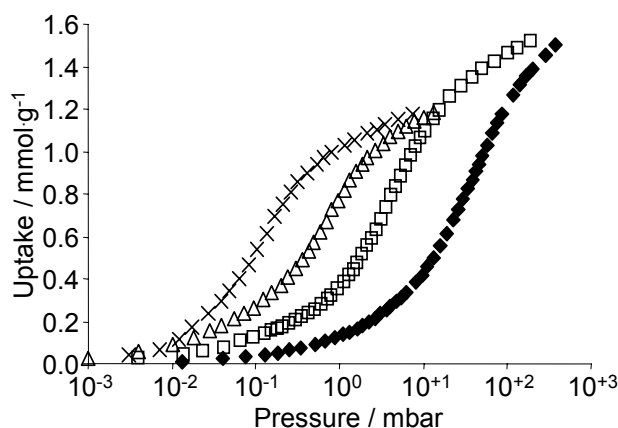


Figure 2.3: Adsorption isotherms on H-LaX: n-butane (\blacklozenge), n-pentane (\square), n-hexane (Δ), n-heptane (\times)

Table 2.3: Adsorption constants and concentration of sorption sites (σ_m) for strong initial interaction (1), moderate uptake (2) and adsorption including sorbate-sorbate interactions (3)

Sorbate	K_{ads0}	K_{ads1}	K_{ads2}	σ_0 (mmol.g)	σ_1 (mmol/g)	σ_2 (mmol/g)	σ_{tot} (mmol/g)	$c(C)_{max}^a$ (mmol/g)
Activated at 453 K								
n-Butane		$1.1 \cdot 10^2$	$1.2 \cdot 10^1$		0.92	0.95	1.87	7.7
Isobutane		$9.2 \cdot 10^1$	$6.8 \cdot 10^0$		0.96	0.72	1.68	6.6
n-Pentane		$7.8 \cdot 10^2$	$9.5 \cdot 10^1$		0.83	0.71	1.54	7.5
2-Methylbutane		$7.2 \cdot 10^2$	$1.1 \cdot 10^2$		0.83	0.70	1.53	7.7
n-Hexane		$7.6 \cdot 10^3$	$7.5 \cdot 10^3$		0.65	0.64	1.29	7.6
2-Methylpentane		$8.4 \cdot 10^3$	$5.9 \cdot 10^2$		0.58	0.73	1.31	7.7
3-Methylpentane		$6.8 \cdot 10^3$	$5.8 \cdot 10^2$		0.63	0.67	1.30	7.6
2,2-Dimethylbutane		$4.6 \cdot 10^3$	$5.2 \cdot 10^2$		0.61	0.59	1.20	7.0
2,3-Dimethylbutane		$8.2 \cdot 10^3$	$5.4 \cdot 10^2$		0.58	0.66	1.24	7.3
n-Heptane		$2.4 \cdot 10^4$	$8.6 \cdot 10^3$		0.64	0.52	1.16	8.4
2-Methylhexane		$2.2 \cdot 10^4$	$6.4 \cdot 10^3$		0.53	0.64	1.17	8.3
2,2-Dimethylpentane		$1.4 \cdot 10^4$	$5.8 \cdot 10^3$		0.52	0.63	1.14	8.3
Activated at 723 K								
n-Hexane	$5.5 \cdot 10^4$	$2.2 \cdot 10^3$	$1.3 \cdot 10^3$	0.22	0.53	0.75	1.50	9.0
2-Methylpentane	$5.6 \cdot 10^4$	$1.8 \cdot 10^3$	$1.2 \cdot 10^3$	0.25	0.48	0.73	1.46	8.7
2,2-Dimethylbutane	$4.7 \cdot 10^4$	$1.5 \cdot 10^3$	$1.0 \cdot 10^3$	0.21	0.43	0.63	1.27	7.6

^a $c(C)_{max}$ - concentration of carbon atoms at maximum uptake

The concentration of sorption sites in both regimes decreased with increasing size of the molecule. It was, however, comparable for n-alkanes and alkanes with a single branching. The presence of multiple branching and, in particular, of quaternary carbon atoms led to a decrease of the maximum coverage. The same was observed for isobutane indicating that isobutane cannot be packed as tightly as n-butane. Note that the maximum concentration of

carbon atoms was identical for n-butane, n-pentane and n-hexane, while a higher concentration was found for n-heptane. This shows that the required space per carbon atom is constant. The increased carbon concentration for n-heptane is likely to be due to condensation of the sorbate outside the micropores.

The heat of adsorption was determined as a function of the hydrocarbon uptake by calorimetry (Figure 2.4). All sorbates had a constant heat of adsorption at low uptake. For molecules with five or more carbon atoms an increase of the heat of adsorption was observed when the coverage of catalyst exceeded a certain level. The molar uptake, at which this increase was observed, decreased with increasing size of the sorbate molecule. In the second regime the heat of adsorption was 10-16 kJ mol⁻¹ higher than in the first one. Note that the concentration of sorption sites in the first regime coincided with the loading, at which the heat of adsorption started increasing. Table 2.4 compiles the values of the heat of adsorption (H_{ads}) in both adsorption regimes. For butane isomers the increase of the heat of adsorption was not reached under the conditions that could be applied in the setup.

In agreement with previous studies, a linear increase of the initial heat of adsorption with increasing chain length was observed for n-alkanes (Figure 2.5) [15,16]. The same trend is also found for single branched 2-methylalkanes. The heat of adsorption of branched alkanes was 3-4 kJ mol⁻¹ lower than that of the corresponding n-isomers. A second branching at a different carbon atom did not lead to a further reduction of the heat of adsorption. However, molecules with quaternary carbon atoms had a head of adsorption, which was reduced by additional 2 kJ mol⁻¹.

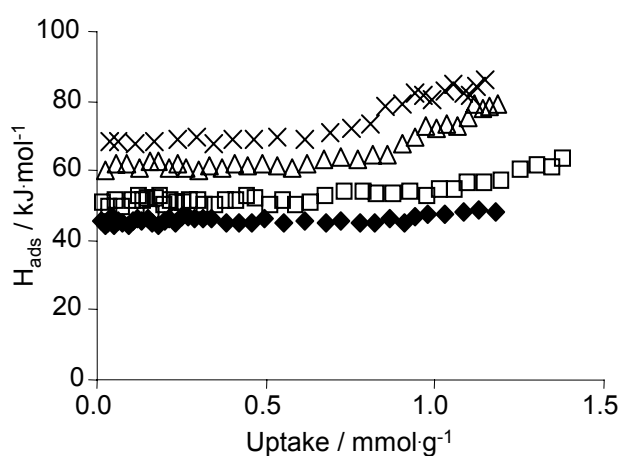


Figure 2.4: Development of the heat of adsorption with the sorbate uptake: n-butane (◆), n-pentane (□), n-hexane (Δ), n-heptane (x)

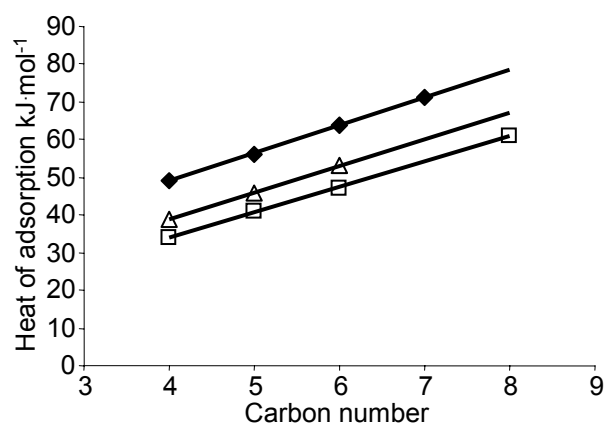


Figure 2.5: Heat of adsorption of n-alkanes: H-LaX (◆), H-Y (Δ) [15], Y (□) [15]

Table 2.4: Initial heat of adsorption (H_{ads}) of alkanes on H-LaX

Sorbate	H_{ads1} (kJ/mol)	H_{ads2} (kJ/mol)	H_{ads3} (kJ/mol)
Activated at 453 K			
n-Butane	49	49	-
Isobutane	45	45	-
n-Pentane	56	56	66
2-Methylbutane	51	51	61
n-Hexane	-	64	76
2-Methylpentane	-	61	72
3-Methylpentane	-	61	73
2,2-Dimethylbutane	-	59	67
2,3-Dimethylbutane	-	61	70
n-Heptane	-	71	87
2-Methylhexane	-	68	82
2,2-Dimethylpentane	-	66	77
2,4-Dimethylpentane	-	67	-
Activated at 723 K			
n-Hexane	66	62	74
2-Methylpentane	65	60	73
2,2-Dimethylbutane	60	56	65

Note that only the initial heat of adsorption is reported for 2,4-dimethylpentane. When the loading of this molecule reached $0.45 \text{ mmol} \cdot \text{g}^{-1}$ cracking of the sorbate was observed. Similar reactivity will be described in Chapter 3 for octane isomers with multiple branchings.

Adsorption of n-hexane, 2-methylpentane and 2,2-dimethylbutane was also investigated on H-LaX, which had been activated at 723 K for 1 h. This activation procedure decreased the sample weight by 1.8 wt.%. IR spectroscopy showed that this activation procedure completely

removes residual molecular water from the zeolite. In contrast to the samples activated at 453 K, three adsorption regimes were observed. At low coverage an additional adsorption regime was found (labeled as regime 0), in which the heat of adsorption was higher. When these adsorption sites are saturated the heat of adsorption decreased by kJ mol^{-1} . Note that after this decrease of the heat of adsorption was 1-3 kJ mol^{-1} lower than the corresponding values after adsorption on samples activated at 453 K. Parallel trends were observed for the adsorption constants. Note that the changes of the adsorption constant between the last two regimes were much less pronounced than in the case of the sample after activation at 453 K. In addition to this, the maximum uptake increased showing that the available volume in the zeolite pores increased when water was completely removed (Table 2.3). The number of additional adsorption sites followed the order n-hexane > 2-methylpentane > 2,2-dimethylbutane.

2.3.3. In situ IR spectroscopic measurements

The IR spectrum zeolite H-LaX contains a relatively broad band between 3760 and 2620 cm^{-1} , which is assigned to the stretching vibrations residual water [36] remaining on the zeolite after mild activation at 453 K (Figure 2.6a) [27,29]. The band of the deformation vibration of water was observed at 1630 cm^{-1} . The bands of zeolitic OH groups were observed at 3730 cm^{-1} (silanol groups), 3608 and 3652 cm^{-1} (bridging hydroxyl groups) and 3533 cm^{-1} (LaOH groups) [36].

When alkanes are adsorbed on the zeolite, IR bands corresponding to CH stretching vibrations (3000 to 2750 cm^{-1}) and CH deformation vibrations (1500 to 1350 cm^{-1}) were observed. Figure 2.6b shows the spectrum of 2-methylpentane on H-LaX as an example. With increasing uptake the bands of the CH vibrations increased, while the band of the free bridging hydroxyl groups and silanol groups decreased. At the same time a broad peak appeared at 3528 cm^{-1} , which is assigned to the stretching vibration of perturbed bridging OH groups (Figure 2.6b). Note that the band of the LaOH stretching vibrations remained unchanged.

The concentration of interacting Brønsted acid sites was determined from the decrease of the IR band at 3608 cm^{-1} using concentration of Brønsted acid site concentration determined by IR spectroscopy of adsorbed pyridine for quantification. The resulting values were

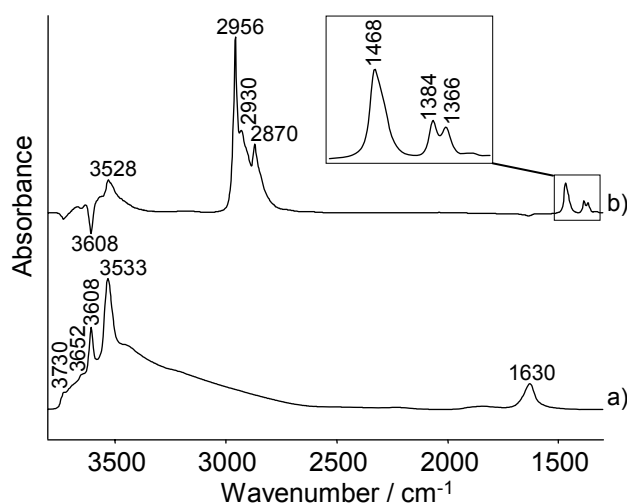


Figure 2.6: IR spectra: a) H-LaX after activation at 453 K, b) difference spectrum after adsorption of 2-methylpentane at 348 K at a pressure of 0.1 mbar

correlated to the gravimetrically measured alkane uptake of the zeolite at the same pressure (Figure 2.7). In all cases regimes with a constant stoichiometry were identified, in which a linear correlation between the interacting Brønsted acid sites and the amount of adsorbed alkane exists. The stoichiometric ratios are compiled in Table 2.5. Note that a value smaller than 1 means that not all sorbed molecules interact with a Brønsted acid site.

In the initial part, each molecule of sorbed n-butane and isobutane interacted on average with 1.2 and 0.8 Brønsted acid sites, respectively. When an uptake of approximately 0.05 mmol g^{-1} was reached, a distinct change of the stoichiometry occurred. At this point approximately 6 % of the Brønsted acid sites are interacting with alkanes. In the second regime the average number of interaction decreased to 0.38 and 0.24 for n-butane and isobutane, respectively. A similar behavior was observed for n-pentane. It has to be mentioned that complete saturation of the Brønsted acid sites was not achieved for butane and pentane isomers within the available pressure range.

The initial regime was not found during the adsorption of 2-methylbutane and hexane and heptane isomers. Instead, linear correlations were observed until at least half of the concentration of Brønsted acid sites interacted with adsorbed molecules. When the uptake increased further, the number of interactions with Brønsted acid sites decreased as saturation was approached. The number of interactions with Brønsted acid sites increased with increasing size of the molecule Except for the low uptake regime.

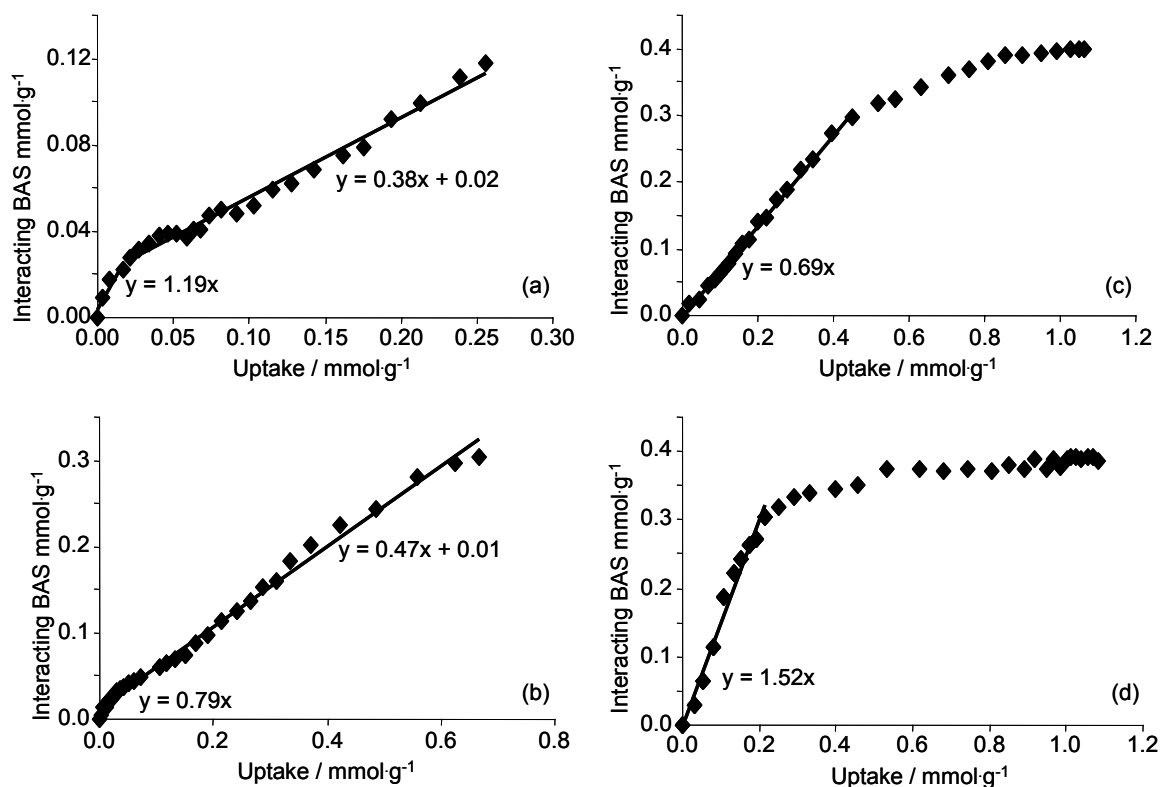


Figure 2.7: Interaction of adsorbed alkanes with Brønsted acid sites: (a) n-butane, (b) n-pentane, (c) n-hexane, (d) n-heptane

Table 2.5: Average number of Brønsted acid sites interacting with one sorbed molecule

Sorbate	Low uptake (SiOHAl/ alkane)	Before BAS ^a saturation (SiOHAl/ alkane)
n-Butane	1.19	0.38
Isobutane	0.84	0.24
n-Pentane	0.79	0.47
2-Methylbutane	-	0.41
n-Hexane	-	0.69
2-Methylpentane	-	0.72
3-Methylpentane	-	0.65
2,2-Dimethylbutane	-	0.88
2,3-Dimethylbutane	-	0.52
n-Heptane	-	1.52
2-Methylhexane	-	2.27
2,2-Dimethylpentane	-	2.05

^a BAS – Brønsted acid site

Let us now compare the absorbance in the region of the CH stretching vibrations to the gravimetric uptake (Figure 2.8). Up to four regimes were identified, in which the absorbance increases linearly with increasing uptake. They will be referred to as: (1) “low uptake” (only

for butane isomers and n-pentane), (2) “before Brønsted acid site saturation”, (3) “after Brønsted acid site saturation” and (4) “near complete pore filling”. The apparent extinction coefficients were determined from the slopes within these regimes (Table 2.6). Kanzansky *et al.* showed that the extinction coefficient of adsorbed alkanes is a measure for their polarization [26,37].

In general, heptane and hexane isomers followed the trends, as octane isomers (Chapter 3). Initially, a steep increase of the absorbance with increasing uptake was observed. When the Brønsted acid sites were saturated, the apparent extinction coefficient decreased. Note that the apparent extinction coefficient increased again when complete pore filling was approached. However, this stage was only reached for the heptane isomers.

In the regime before Brønsted acid site saturation, the apparent extinction coefficients increased with increasing carbon number of the sorbate molecule. However, the opposite trend was observed after saturation of Brønsted acid sites.

It is interesting to note the 2-methylpentane and 2-methylhexane initially had significantly higher apparent extinction coefficients than the other isomers. This indicates a particularly strong interaction of the tertiary CH bond. Interestingly, this effect was not observed for 3-methylpentane and 2,3-dimethylbutane, in which the tertiary carbon atom is in a sterically more demanding position so that they cannot approach the polarization sites as easily. The variations in the molar extinction coefficient were somewhat higher for hexane isomers than for structurally related heptane isomers.

The curves for butane and pentane isomers show some distinct differences. A linear correlation between the uptake and the absorbance was found for n-pentane and 2-methylbutane over the entire range measured. However, a complete saturation of the Brønsted acid sites was not observed under these conditions. In contrast to the observation for all other alkanes, an additional regime with a low extinction coefficient was found for the butane isomers at low uptake. Note that only 0.05 mmol g^{-1} of adsorbed molecules interacted in this way.

After activation at 723 K the apparent molar extinction coefficients were significantly lower. As long as free Brønsted acid sites were present the apparent molar extinction coefficient decreased with increasing branching of the sorbate molecule. After saturation of the Brønsted acid sites the same value was found for all isomers.

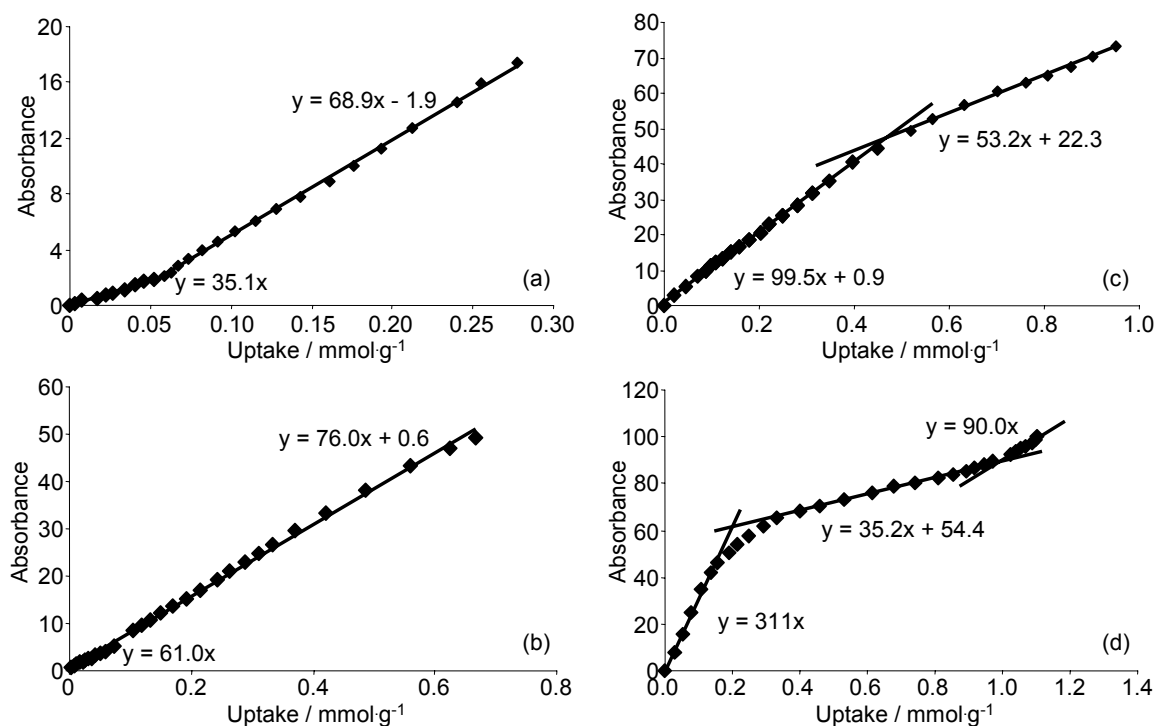


Figure 2.8: Absorbance at 2900 cm^{-1} at different uptakes: a) n-butane, b) n-pentane, c) n-hexane, d) n-heptane

Table 2.6: Apparent extinction coefficients of alkanes adsorbed on H-LaX

Sorbate	Low uptake	Before BAS saturation ^a	After BAS saturation ^a	Near complete pore filling
<i>Activated at 348 K</i>				
n-Butane	35.1	68.9	-	-
Isobutane	23.7	53.8	-	-
n-Pentane	61.0	76.0	-	-
2-Methylbutane		64.5	-	-
n-Hexane		99.5	53.2	-
2-Methylpentane		182	36.0	-
3-Methylpentane		107	61.6	-
2,2-Dimethylbutane		123	41.8	-
2,3-Dimethylbutane		81.8	41.9	-
n-Heptane		311	35.2	90.0
2-Methylhexane		419	34.9	79.9
2,2-Dimethylpentane		288	22.2	53.6
<i>Activated at 723 K</i>				
n-Hexane		67.1	24.4	-
2-Methylpentane		62.2	24.5	-
2,2-Dimethylbutane		56.2	24.0	-

^a BAS – Brønsted acid site

2.3.4. MAS-NMR measurements

The precise coordination of adsorbed hexane isomers was investigated by ^{13}C CP MAS NMR spectroscopy (Figure 2.9). Compared to the chemical shift of the sorbates in CDCl_3 the peaks of the primary carbon atoms were shifted upfield by 0.4 to 1.0 ppm upon adsorption while the peaks of secondary and tertiary carbon atoms were shifted downfield (Table 2.7). Only a very small downfield shift was observed for the quaternary carbon atom in 2,2-dimethylbutane.

The spectra were recorded using a cross polarization (CP) pulse sequence, in which the relative intensities of different carbon nuclei depends the magnetization transfer from protons to the probed nuclei (*vide infra*). In general, the sensitivity of secondary and tertiary carbon atoms was higher than the sensitivity of primary carbon atoms (Table 2.7). The spectrum of adsorbed 2,2-dimethylbutane showed a different behavior. The strongest relative intensity was

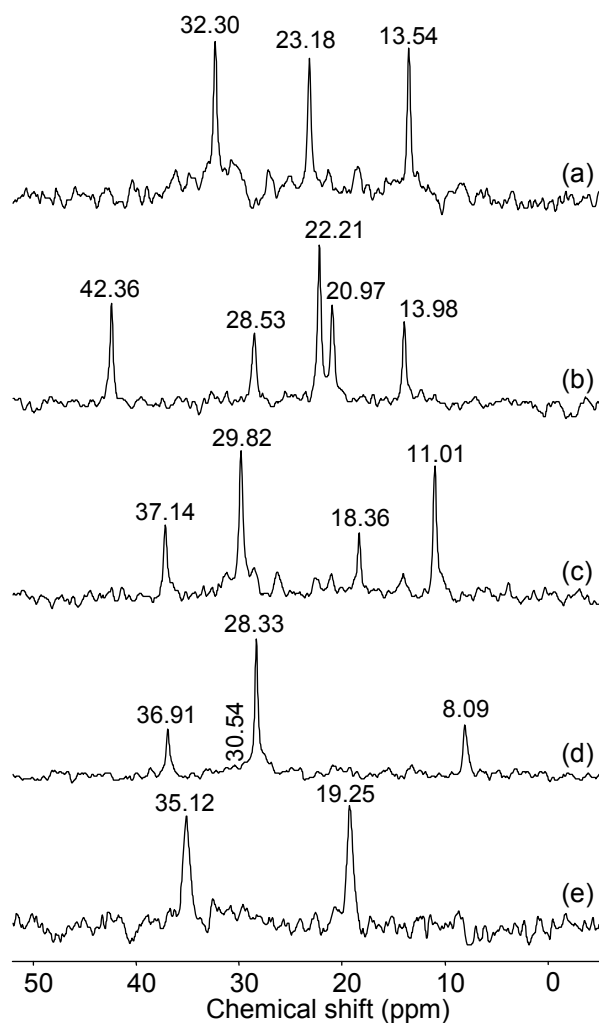
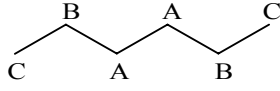
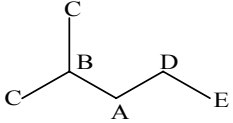
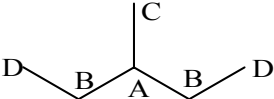
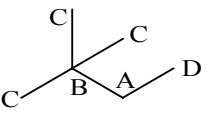
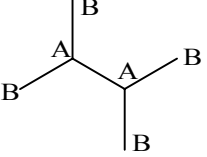


Figure 2.9: ^{13}C CP-MAS-NMR spectra of hexane isomers adsorbed on H-LaX: (a) n-hexane, (b) 2-methylpentane, (c) 3-methylpentane, (d) 2,2-dimethylbutane, (e) 2,3-dimethylbutane

Table 2.7: Chemical shift of hexane isomers in CDCl₃ and adsorbed on H-LaX

Molecule		δ_{ads} (ppm)	δ_{liquid} (ppm)	$\Delta\delta$ (ppm)	Intensity (a.u.) ^a	Assignment
n-Hexane	A	32.30	31.84	0.46	1.00	
	B	23.18	22.90	0.28	0.68	
	C	13.54	14.30	-0.76	0.65	
2-Methylpentane	A	42.36	41.65	0.71	0.85	
	B	28.53	27.95	0.58	0.82	
	C	22.21	22.83	-0.62	0.70	
	D	20.97	20.71	0.26	1.00	
	E	13.98	14.52	-0.54	0.78	
3-Methylpentane	A	37.14	36.41	0.73	0.71	
	B	29.82	29.36	0.46	1.00	
	C	18.36	18.97	-0.61	0.74	
	D	11.01	11.62	-0.61	0.63	
2,2-Dimethylbutane	A	36.91	36.70	0.21	0.82	
	B	30.54	30.61	-0.07	0.16	
	C	28.33	29.16	-0.83	0.81	
	D	8.09	9.07	-0.98	1.00	
2,3-Dimethylbutane	A	35.12	34.03	1.09	1.00	
	B	19.25	19.66	-0.41	0.44	

^a Relative intensities normalized by the number of equivalent carbon atoms.

observed for the methyl group D. A very low relative intensity was observed for the quaternary carbon atom, which is not bound to a proton and, thus, cannot be excited by direct magnetization transfer.

The interaction of adsorbed alkanes with zeolite H-LaX was also investigated by ²⁷Al MAS NMR spectroscopy (Figure 2.10). The difference spectrum of sorbed n-hexane on H-LaX showed a negative peak at 62 ppm and a positive peak between 20 and 0 ppm (similar spectra were obtained for all other isomers). The shift in the ²⁷Al MAS NMR spectra is

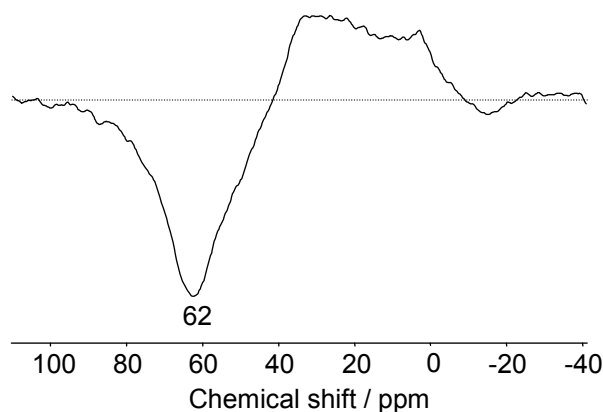


Figure 2.10: ^{27}Al MAS NMR difference spectrum of n-hexane adsorbed on H-LaX

assigned to a strong distortion of the local environment of the framework aluminum atoms, which have protons as charge compensating cations. The integral of these peaks amounted to 2-4 % of the total integral in the ^{27}Al NMR spectrum.

2.4. Discussion

2.4.1. Types of the interaction

At low coverage alkanes adsorb on the zeolite walls with van der Waals forces [14-16]. IR spectroscopy shows that sorbed alkane molecules also interact with Brønsted acid sites. The interaction between an alkane and a Brønsted acid site in a faujasite type zeolite provides additional 6 kJ mol^{-1} to the dominating van-der-Waals forces [15]. The number of molecules interacting with Brønsted acid site increased with increasing size of the sorbate molecules. Note that the sorption stoichiometry, however, did not change until at least half of the Brønsted acid sites were interacting with sorbate molecules. Only heptane isomers interact with more than one Brønsted acid site on average. Therefore, non Brønsted acidic sorption sites must exist, which are able to adsorb smaller alkanes with a similar heat of adsorption as Brønsted acid sites. Under the conditions chosen, equilibrium is speculated to be established between the sorption sites with and without interaction with Brønsted acid sites. We speculate that these sites are Lewis acid sites.

During the adsorption of butane isomers and n-pentane the first molecules ($\text{ca. } 0.05 \text{ mmol g}^{-1}$) had a ratio of approximately one interacting Brønsted acid site per adsorbed molecule. This observation indicates that a small number of Brønsted acid sites exists in a sterically constraint environment, which is unfavorable for the adsorption of molecules with more than 5 carbon atoms. When the uptake increased the preference towards adsorption on Brønsted acid sites was much less pronounced.

The influence of sorbate-sorbate interaction varies depending on the zeolite used. Eder *et al.* observed for H-FAU that the heat of adsorption starts increasing once the amount of adsorbed molecules exceeds 5% of the maximum uptake [16]. For alkane adsorption on zeolite H-LaX the heat of adsorption remained constant until at least 50% of the maximum uptake was reached. Note that the saturation of the Brønsted acid sites did not affect on the heat of adsorption. Therefore, we conclude that at moderate uptake the contribution of the sorbate-sorbate interactions is comparable to the contribution from the directed interaction with Brønsted acid sites. When the loading is increased further, sorbate-sorbate interaction becomes more pronounced leading to an increase of the heat of adsorption. Despite the additional contribution of sorbate-sorbate interactions to the heat of adsorption these sites are not occupied at low uptake, because adsorption on these sites decreases the flexibility of the adsorbed molecules [38]. This decrease does not only affect the newly adsorbed, but also those molecules, which are already present in the environment.

In agreement with previous studies the heat of adsorption increased linearly with increasing number of carbon atoms [15,16]. The increment was approximately 7 kJ mol^{-1} , which is identical with the value found by Eder *et al.* for the adsorption of n-alkanes on faujasites [15,16]. However, the heat of adsorption was 10 kJ mol^{-1} higher than reported for adsorption of n-alkane on H-FAU with a Si/Al ratio of 2.7 [16]. The major differences between the materials are the Si/Al ratio (H-LaX: 1.21, H-LaY: 2.7) and the presence of polyvalent cations in H-LaX. Eder *et al.* suggested that the increase of the aluminum concentration in the zeolite lattice increases the polarity of the zeolite, so the interaction with an apolar alkane is weakened [15]. Polyvalent cations, such as extraframework aluminum and La^{3+} cations, are also polar sites. However, if these cations are present in the supercages of the zeolite, the cage volume will be decreased increasing so the non-directed interactions and in consequence the heat of adsorption [14].

2.4.2. Influence of polarization

Although the contribution of directed interactions to the heat of adsorption is relatively small, Brønsted acid and metal sites are capable of strongly polarizing sorbed alkanes [16,26,39]. Metal cations such as Zn^{2+} , Ga^{+} , Ca^{2+} and Mg^{2+} even exceed the proton in polarization power [26,37,40,41]. Kazansky *et al.* proposed that the molar extinction coefficient of sorbed hydrocarbons can be used as an indicator for polarization [26,37].

In the H-LaX material discussed here ^{27}Al MAS NMR indicates that extraframework aluminum exists. In additions to this, La^{3+} cations are present as charge compensating cations.

Although most of the La^{3+} cations migrate into the sodalite cages during calcination, a considerable amount remains in the super cages [42]. Both cations act as Lewis acid sites and affect the properties for acid catalyzed reactions in a similar way. Thus, we speculate that the interaction of sorbed alkanes with La^{3+} cation and/or extraframework aluminum sites must play a significant role for adsorption and polarization [9].

As long as Brønsted acid sites are available they will contribute to the polarization of alkane molecules that adsorb on them. The strength of the interaction with a Brønsted acid site is characterized by a red shift of the bridging hydroxyl groups upon adsorption of the alkane [43]. Eder *et al.* reported a red shift of 103 cm^{-1} for the adsorption of n-pentane on H-FAU (Si/Al = 2.7) [16]. In the present study a shift of 80 cm^{-1} was found for the adsorption of alkanes on H-LaX independent of the sorbed alkane and the uptake. This indicates that the interaction of sorbed alkanes with the Brønsted acid site of H-LaX is weaker than in the case of H-FAU. This interpretation is supported by the fact that only a part of the alkanes with six or less carbon atoms interact with a Brønsted acid site (*vide supra*). Therefore, the strong polarization cannot be caused by interaction with Brønsted acid site alone. This conclusion is supported by the fact that at low uptake a reduced extinction coefficient was found for butane isomers and n-pentane, while an extraordinarily high number of interactions with Brønsted acid sites was observed in this regime.

We conclude that the strong polarization of hexane and heptane isomers is induced by a synergetic effect of metal cations and Brønsted acid sites in the zeolite. Butane and pentane isomers are too small to interact with both sites at the same time. Therefore, butane isomers and n-pentane are only polarized by Brønsted acid sites when they adsorb on sterically constraint Brønsted acid site. When the uptake exceeds 0.05 mmol g^{-1} , polarization by cations becomes predominant. For isopentane only polarization by $\text{La}^{3+}/\text{Al}^{3+}$ sites was observed.

The extent of the polarization also depends on the structure of the sorbate molecule. At low uptake particularly strong polarization was observed for 2-methylpentane and 2-methylhexane. This may result either from a strong polarization of the additional methyl group in the branched molecule or from a polarization induced indirectly *via* the methine group. If the polarization was due to an interaction of methyl groups 2,2-dimethylbutane and 2,2-dimethylpentane would also have a high apparent extinction coefficient at low uptake. However, the values measured were comparable to the corresponding n-alkanes. Therefore, it is likely that the high initial apparent extinction coefficients of 2-methylpentane and 2-methylhexane are due to a polarization of the methine group.

Although 3-methylpentane contains the same number of methyl, methylene and methine groups as 2-methylpentane, the apparent extinction coefficient in the initial regime was significantly lower. The difference between these molecules lies in the sterically more demanding location of the methine group in 3-methylpentane. This indicates that the polarization is sterically demanding even in a zeolite with as wide pores as the faujasite structure.

The extinction coefficients increase only slightly with increasing molecular size. Saturation of the Brønsted acid sites led to further decrease of the apparent extinction coefficient. This decrease was particularly pronounced for heptane isomers, which had lower extinction coefficients than hexane isomers with the same structural features.

This shows that the enhancement of the extinction coefficient by polarization is much higher than the differences that derive from the fact that larger molecules contain more atoms, which give rise to IR bands.

Note that changes of the polarization did not lead to a difference in the heat of adsorption indicating that the different adsorption sites are energetically similar. Therefore, equilibrium of molecules adsorbed on different sites is established and the changes of the polarization are due to saturation of one kind of adsorption sites. This interpretation is supported by the fact that alkanes with six or less carbon atoms interact in average with less than one Brønsted acid site (*vide supra*).

The regime of almost complete pore filling was only reached for the heptane isomers. In agreement with the results for the adsorption of octane isomers an increase of the apparent extinction coefficient was found (see Chapter 3). We tentatively assign this increase to the formation of supramolecular structures within the zeolite pores, in which a polarized molecule is capable of inducing polarization to an adjacent molecule.

2.4.3. Localized interaction

Solid state NMR spectroscopy is a very powerful tool to selectively probe the chemical shift of individual carbon atoms in adsorbed alkanes, which are, however, influenced by medium effects and the conformational equilibrium of the alkanes [19]. Medium effects lead to deshielding (increase of the chemical shift) due to the larger dielectric constant of the zeolite compared to the alkanes [44,45], while an increasing contribution of gauche conformers shields the ^{13}C nuclear spin [44]. Based on these considerations van Well *et al.* demonstrated that it is possible to differentiate between adsorption sites in the 8-ring cages and 10 ring channels in zeolite H-FER [19].

It has been suggested that medium effects affect methyl groups stronger than methylene groups [44]. In contrast, we observe here that in H-LaX the peak of methyl carbon atoms is shifted upfield (lower chemical shift) upon adsorption, while a downfield shift was observed for methylene and methine carbon atoms. This suggests that in H-LaX the medium effects are overcompensated by a strong polarization of the adsorbed alkane. The polarization is concluded to occur in such a way that a stronger positive partial charge is induced to secondary and tertiary carbon atoms, while primary carbon are less polarized. This state of polarization may be seen as a transition state towards the abstraction of a hydride ion from a tertiary carbon atom, which will be discussed in Chapter 3 as a pathway for alkane activation over H-LaX under very mild conditions. Moreover, hydride transfer to a carbenium ion/alkoxy group is facilitated for a sorbed alkane, which is polarized in this way.

The intensities in the ^{13}C CP NMR spectrum provide additional information about the interaction of different parts of the alkane. In the cross polarization experiment the molecule is excited by a pulse on protons [46]. Then, the magnetization is transferred to a ^{13}C atom and a ^{13}C spectrum is obtained. The efficiency of the magnetization transfer depends on a variety of factors so that the spectrum is not quantitative [31]. Strong signals are obtained for carbon atoms, which are close to a large number of protons. On the other hand a static orientation of the two nuclei enhances the efficiency of the magnetization transfer. Therefore, lower intensities are observed for carbon atoms in a highly flexible environment.

Despite the fact that primary carbon atoms are bound to the largest number of hydrogen atoms, it was found that they are underrepresented in the cross polarized spectrum compared to secondary and tertiary carbon atoms (Table 2.7). In the ^{13}C CP NMR spectrum of adsorbed 2,3-dimethylbutane the relative intensity of a methyl group was only half as much as of a methine group. This shows that methyl groups lose magnetization more quickly than methine groups [46]. In ^{13}C CP MAS investigations of polymers fast relaxation is observed for regions with a high flexibility [47]. Therefore, we assign the relatively low intensity of methyl carbon atoms to the fact that methyl groups of adsorbed alkanes are able to rotate to some extent freely. In contrast to the flexibility of methylene and methine groups is much more restricted. In 2,2-dimethylbutane the sensitivity of the methyl group peaks was significantly larger indicating that the rotation of the methyl groups in this bulky molecule is more restricted.

A very low relative intensity was found for the quaternary carbon atom in 2,2-dimethylbutane indicating that magnetization transfer over more than one bond has a minor influence with the experimental parameters of these spectra.

2.4.4. Distortion of the zeolite framework

The coordination number and degree of distortion of aluminum atoms in zeolites can be efficiently probed by solid state ^{27}Al MAS NMR. The presence of lanthanum species leads to a distortion of the local environment of framework aluminum atoms (*vide supra*) [9]. An even stronger distortion is observed when the zeolite is activated prior to measurement (Figure 2.1). However, the features of two different tetrahedrally coordinated aluminum species are still observable. Adsorption of hexane isomers led to an upfield shift of the peak corresponding to framework aluminum atoms with protons as charge compensating cations. This shows that the environment of framework aluminum atoms next to a Brønsted acid site is distorted upon interaction with a sorbed alkane molecule. Similar distortion has been described for H-Y after coke deposition [48]. In contrast to this, surface methoxy groups were found to decrease the distortion of the framework [48,49]. No effect was observed on aluminum atoms with lanthanum as charge compensating cations. However, these species are already heavily distorted. Therefore, it is not surprising that further distortion is not observed when an alkane molecule interacts with these sites. Overall, these observations show that the zeolite framework is not static during adsorption of the alkanes.

2.4.5. Influence of the activation temperature

The presence of water has a marked influence on the catalytic properties of H-LaX for isobutane/2-butene alkylation. Feller *et al.* proposed an optimum activation temperature of 443 K [27]. After this activation procedure approximately 1.8 wt.% of water are present on the catalyst. It was shown that water reduces the selectivity towards oligomerization and, hence, increases the catalyst lifetime [29]. When the activation temperature exceeds 573 K physisorbed water is removed completely from the zeolite. Moreover, dehydroxylation may occur to a certain extent reducing the concentration of Brønsted acid site [50]. However, in case of H-LaX the extent of dehydroxylation seems to be limited [29].

In the present study the influence of water on the sorption properties was investigated by comparing the adsorption of three hexane isomers on H-LaX after activation at 453 and 723 K, respectively. After activation at 723 K additional strong sorption sites become available for the alkane molecules. This shows that residual water selectively block the strongest sites for alkane adsorption in H-LaX.

Once the strong adsorption sites are saturated, the heat of adsorption decreased by 4-5 $\text{kJ}\cdot\text{mol}^{-1}$. The resulting heat of adsorption was lower than after activation at 453 K. Therefore, the interaction between water and sorbed alkane molecules must provide a small contribution

to the heat of adsorption. As expected, the contribution of sorbate-sorbate interaction was comparable for both activation methods.

The apparent extinction coefficient of sorbed alkanes was reduced significantly after activation at 723 K. Our results show that the presence of polar water molecules has a significant influence on the polarization of sorbed alkanes. It was demonstrated that physisorbed water is not located near Brønsted acid sites, but interacts strongly with the zeolite lattice [29]. This is likely to occur *via* hydrogen bonding between a hydrogen atom from the water molecule and a basic framework oxygen atom. As a result the oxygen atom of the water molecule points into the cavity of the zeolite or coordinates to a Lewis acid site. Due to its partial negative charge it is able to act as a base. Consequently, very high polarization may be achieved for if an alkane is located between a Lewis acid site and an adsorbed water molecule. This enhancement is particularly strong for alkanes with a single branching in the 2 position, because a positive partial charge is the most stable on a tertiary carbon atom and a branching in this position leads to the smallest steric constraint possible.

The number of additional sorption sites, which become available when water is removed was significantly higher for n-hexane and to a certain extent for 2-methylpentane than for 2,2-dimethylbutane. This shows that the sites are located in a sterically constrained environment, which can hardly be accessed by alkanes with quaternary carbon atoms. On the other hand small molecules, e.g., water, are able to strongly interact with these sites due to their significantly smaller size.

2.5. Conclusions

Alkane adsorption on zeolite H-LaX is dominated by dispersive van der Waals forces with an additional contribution of 6 kJ mol^{-1} from the interaction with Brønsted acid sites. Incorporation of La^{3+} cations increased the heat of adsorption by an additional 10 kJ mol^{-1} . Interaction with other alkane molecules also contributes to the heat of adsorption. However, this contribution is only observed, when the uptake is sufficiently high. It should be noted that at low coverage the larger loss of entropy would offset the higher enthalpy. Each additional CH_2 group in the sorbate molecule increased the heat of adsorption by 7 kJ mol^{-1} . The strongest adsorption was observed for n-alkanes, which obtain the best fit with the zeolite structure due to their structural flexibility. Alkanes with quaternary carbon atoms interacted weaker than their isomers.

At low coverage extraordinarily high apparent extinction coefficients indicate strong polarization of the sorbate molecules, in particular, for 2-methylpentane and 2-methylhexane. This effect was much stronger for molecules with at least 6 carbon atoms indicating that simultaneous interaction with different sites is required. Polarization decreased when the loading increased, but when complete pore filling was approached, ordering of the sorbate molecules in the pores enhanced polarization again.

A positive partial charge was induced on secondary and tertiary carbon atoms upon adsorption. This charge is likely to facilitate alkane activation by hydride abstraction and hydride transfer reactions. Methyl groups maintain a certain degree of structural flexibility.

Physisorbed water leads to blockage of additional sorption sites, on which the heat of adsorption of alkanes is 4-5 kJ mol⁻¹ higher than on the majority of sites. On the other hand coordination to physisorbed water also increases the heat of adsorption of alkanes slightly and drastically enhances the polarization of sorbed alkanes.

2.6. Acknowledgements

The author thanks Prof. Freude and Dennis Schneider for the ²⁷Al DOR-NMR and Martin Neukam for the AAS and BET measurements. Partial financial support by the European Union in the framework of NMP3-CT-2005-011730 IDECAT WP5 is gratefully acknowledged.

2.7. References

- [1] A. Corma, A.V. Orchilles, *Micropor. Mesopor. Mater.* 35-36 (2000) 21.
- [2] A. Feller, J.A. Lercher, *Adv. Catal.* 48 (2004) 229.
- [3] J. Weitkamp, Y. Traa, *Catal. Today* 49 (1999) 193.
- [4] A.C. Butler, C.P. Nicolaidis, *Catal. Today* 18 (1993) 443.
- [5] K. Gaare, D. Akporiaye, *J. Phys. Chem. B* 101 (1997) 48.
- [6] M. Hunger, D. Freude, H. Pfeifer, D. Prager, W. Reschetilowski, *Chem. Phys. Lett.* 163 (1989) 221.
- [7] P.B. Venuto, L.A. Hamilton, P.S. Landis, *J. Catal.* 5 (1966) 484.
- [8] A. Guzman, I. Zuazo, A. Feller, R. Olindo, C. Sievers, J.A. Lercher, *Micropor. Mesopor. Mater.* 83 (2005) 309.
- [9] J.A. van Bokhoven, A.L. Roest, D.C. Konigsberger, J.T. Miller, G.H. Nachttegaal, A.P.M. Kentgens, *J. Phys. Chem. B* 104 (2000) 6743.

-
- [10] R. Carvajal, P.-J. Chu, J.H. Lunsford, *J. Catal.* 125 (1990) 123.
- [11] A.V. Ivanov, G.W. Graham, M. Shelef, *Appl. Catal. B-Environ.* 21 (1999) 243.
- [12] C.L. Cavalcante, Jr., D.M. Ruthven, *Ind. Eng. Chem. Res.* 34 (1995) 177.
- [13] C.L. Cavalcante, Jr., D.M. Ruthven, *Ind. Eng. Chem. Res.* 34 (1995) 185.
- [14] F. Eder, J.A. Lercher, *J. Phys. Chem. B* 101 (1997) 1273.
- [15] F. Eder, J.A. Lercher, *Zeolites* 18 (1997) 75.
- [16] F. Eder, M. Stockenhuber, J.A. Lercher, *J. Phys. Chem. B* 101 (1997) 5414.
- [17] J.A.Z. Pieterse, S. Veefkind-Reyes, K. Seshan, J.A. Lercher, *J. Phys. Chem. B* 104 (2000) 5715.
- [18] M.S. Sun, O. Talu, D.B. Shah, *J. Phys. Chem.* 100 (1996) 17276.
- [19] W.J.M. van Well, X. Cottin, J.W. de Haan, B. Smit, G. Nivarthi, J.A. Lercher, J.H.C. van Hoff, R.A. van Santen, *J. Phys. Chem. B* 102 (1998) 3945.
- [20] S. Savitz, F. Siperstein, R.J. Gorte, A.L. Myers, *J. Phys. Chem. B* 102 (1998) 6865.
- [21] J.F. Denayer, G.V. Baron, J.A. Martens, P.A. Jacobs, *J. Phys. Chem. B* 102 (1998) 3077.
- [22] J.F. Denayer, W. Souverijns, P.A. Jacobs, J.A. Martens, G.V. Baron, *J. Phys. Chem. B* 102 (1998) 4588.
- [23] W.J.M. van Well, X. Cottin, B. Smit, J.H.C. van Hoff, R.A. van Santen, *J. Phys. Chem. B* 102 (1998) 3952.
- [24] S.P. Bates, W.J.M. van Well, R.A. van Santen, B. Smit, *J. Am. Chem. Soc.* 118 (1996) 6753.
- [25] B. Smid, *J. Phys. Chem.* 99 (1995) 5597.
- [26] V.B. Kazansky, E.A. Pidko, *J. Phys. Chem. B* 109 (2005) 2103.
- [27] A. Feller, A. Guzman, I. Zuazo, J.A. Lercher, *J. Catal.* 224 (2004) 80.
- [28] R. Josl, R. Klingmann, Y. Traa, R. Gläser, J. Weitkamp, *Catal. Commun.* 5 (2004) 239.
- [29] A. Guzman, I. Zuazo, A. Feller, R. Olindo, C. Sievers, J.A. Lercher, *Micropor. Mesopor. Mater.* (2006) accepted for publication.
- [30] C.A. Emeis, *J. Catal.* 141 (1993) 347.
- [31] C.E. Snape, B.J. McGhee, J.M. Andresen, R. Hughes, C.L. Koon, G. Hutchings, *Appl. Catal. A-Gen.* 129 (1995) 125.
- [32] S.M.C. Menezes, V.L. Camorim, Y.L. Lam, R.A.S. San Gil, A. Bailly, J.P. Amoureux, *Appl. Catal. A-Gen.* 207 (2001) 367.
- [33] A. Llor, J. Virlet, *Chem. Phys. Lett.* 152 (1988) 248.

-
- [34] A. Samoson, E. Lippmaa, *J. Magn. Reson.* 79 (1988) 255.
- [35] H. Klein, H. Fuess, M. Hunger, *J. Chem. Soc.-Faraday Trans.* 91 (1995) 1813.
- [36] J.W. Ward, *J. Phys. Chem.* 72 (1968) 4211.
- [37] V.B. Kazansky, I.R. Subbotina, F.C. Jentoft, R. Schlögl, *J. Phys. Chem. B* 110 (2006) 17468.
- [38] B. Smit, T.L.M. Maesen, *Nature* 374 (1995) 42.
- [39] J. Datka, M. Boczar, *React. Kinet. Catal. Lett.* 51 (1993) 161.
- [40] V.B. Kazansky, I.R. Subbotina, N. Rane, R.A. van Santen, E.J.M. Hensen, *Phys. Chem. Chem. Phys.* 7 (2005) 3088.
- [41] V.B. Kazansky, A.I. Serykh, E.A. Pidko, *J. Catal.* 225 (2004) 369.
- [42] M. Weihe, M. Hunger, M. Breuninger, H.G. Karge, J. Weitkamp, *J. Catal.* 198 (2001) 256.
- [43] M.L. Hair, W. Hertl, *J. Phys. Chem.* 74 (1970) 91.
- [44] L.J.M. van de Ven, J.W. de Haan, A. Bucinska, *J. Phys. Chem.* 86 (1982) 2516.
- [45] G. Boxhoorn, R.A. van Santen, W.A. van Erp, G.R. Hays, R. Huis, D. Clague, *J. Chem. Soc.-Chem. Commun.* (1982) 264.
- [46] D.D. Laws, H.-M.L. Bitter, A. Jerschow, *Angew. Chem. Int. Ed.* 41 (2002) 3096.
- [47] M. Geppi, F. Ciardelli, C.A. Veracini, C. Forte, G. Cecchin, P. Ferrari, *Polymer* 38 (1997) 5713.
- [48] J.A. van Bokhoven, A.M.J. van der Erden, R. Prins, *J. Am. Chem. Soc.* 126 (2004) 4506.
- [49] W. Wang, A. Buchholz, A. Arnold, M.C. Xu, M. Hunger, *Chem. Phys. Lett.* 370 (2003) 88.
- [50] A.P. Bolton, *J. Catal.* 22 (1971) 9.

Chapter 3

Low temperature activation of branched octane isomers over lanthanum exchanged zeolite X catalysts

Adsorption and surface chemistry of octane isomers on La-exchanged zeolite X were explored under near ambient conditions. At low coverage, the sorption constants depend mainly on dispersion forces. However, very strong polarization of the C-H bonds is indicated by an unusually high extinction coefficient of the C-H vibrations. Bi- and tri-branched alkanes react under these conditions and the reactivity increases with the degree of branching. The activation proceeds *via* hydride abstraction forming alkoxy groups, which subsequently isomerize, and crack. Cracking products desorb primarily *via* hydride transfer from mobile alkanes leading predominantly to isobutane and isopentane. The surface chemistry and alkanes produced show that adsorption and desorption, cracking and alkylation as well as hydride transfer reactions already occur at near ambient conditions in these zeolites.

3.1. Introduction

Acidic zeolite catalysts have a wide range of applications for reactions such as catalytic cracking [1], isomerization [2], and alkylation [3,4]. The tetrahedrally coordinated aluminum in the zeolite (causing its Brønsted acidity) is hydrothermally labile. The introduction of rare-earth elements, especially La^{3+} , into zeolite structures is used to structurally stabilize zeolites with faujasite structure.

In zeolite X La^{3+} cations preferentially occupy the sodalite cages after calcination [5]. Van Bokhoven *et al.* showed that La^{3+} cations act similar to well dispersed extra-framework octahedral aluminum in H-USY [6]. With increasing La^{3+} content also the Si-O-Al and Si-O-Si angles increase. Like other multivalent cations, La^{3+} cation hydrolyze water leading to the formation of LaOH groups and Brønsted acid sites.

The overall impact on acid base properties is discussed controversially. The introduction of such highly charged cations has been claimed to lead to electron density withdrawal from the framework making it more acidic [6]. In contrast, Ivanov *et al.* reported that the addition of 5 wt.% La^{3+} hardly influences the acid-base properties of ZSM-5 with regard to sorption of light alkanes and alkenes [7]. Carvajal *et al.* found a maximum activity for hexane cracking with zeolite Y, in which the La^{3+} content was ca. 20% of the Al content [8].

Adsorption of alkanes on zeolites has been investigated by a wide variety of physicochemical methods including IR-spectroscopy [9-12], gravimetry [9-16], calorimetry [9-12,16,17], chromatography [18,19], ^{13}C MAS NMR spectroscopy [16] and Monte Carlo simulations [20,21]. It has been shown that the sorption is dominated by van-der-Waals-forces. The directed interaction with Brønsted acid sites only accounts for 6-10 $\text{kJ}\cdot\text{mol}^{-1}$ depending on the zeolite structure [10]. It is interesting to note that only few publications address branched isomers [12-14,18,19].

At elevated temperature, direct activation of adsorbed alkanes by zeolites is claimed to occur *via* protolytic cracking [22]. The alkane is activated *via* a carbonium ion in the transition state decaying into dihydrogen or a small alkane and a carbenium ion. The true activation energy for this route is approximately 200 $\text{kJ}\cdot\text{mol}^{-1}$ independent of the zeolite structure and the size of the alkane [23]. This is in good agreement with theoretical calculations for ethane cracking [24]. It has also been suggested that strong Lewis acid sites in MFI and FAU catalyze alkane dehydrogenation [25,26], including even activation of the CH bond by oxidative addition to extra-framework aluminum [27].

All reaction routes lead to the formation of alkoxy groups in the presence of strong Brønsted acid sites. Once these are formed, reactions such as β -scission [28] or alkylation [3]

can easily take place. It has been the consensus that these reactions need elevated temperatures [22,29] or a super-acidic environment [30]. Here, we report for the first time unequivocal evidence that branched octanes react in a bimolecular mechanism also close to ambient temperatures on La-X zeolite opening potential new synthesis routes with zeolites at very mild conditions.

3.2. Experimental

3.2.1. Catalyst preparation and reactants

The parent Na-X zeolite was obtained from Chemische Werke Bad Köstritz (Si/Al = 1.2). In a first step, the parent material was exchanged two times with 0.2 M lanthanum nitrate solution using a liquid-to-solid ratio of 11 ml·g⁻¹. The mixture was stirred for 2 h at 343 K. After washing the resulting material with doubly distilled water to remove nitrate, it was dried first at room temperature and then at 393 K. Subsequently, it was calcined in flowing air at 723 K for 1 h (heating rate 1 K·min⁻¹). The ion-exchange step, including washing and drying at room temperature, was repeated another three times. Finally, the catalyst was calcined using the same procedure as for the first calcination.

n-Octane (99.8%), 2-methylheptane (99%), 3,4-dimethylhexane (99.5%), 2,2,4-trimethylpentane (99.8%), 2,3,3-trimethylpentane (99%) and 2,3,4-trimethylpentane (98%) were received from Sigma Aldrich and used without purification. Minor impurities (alkane isomers), were detected by gas chromatography.

3.2.2. General characterization

IR spectra of adsorbed pyridine were recorded on a Perkin Elmer 2000 spectrometer between 4000 and 1000 cm⁻¹ at a resolution of 4 cm⁻¹. For activation, the zeolite was pressed into a self-supporting wafer (10 mg·cm⁻²) and heated to 393 K with a rate of 5 K·min⁻¹ at 10⁻⁶ mbar. After 4 hours, the temperature was increased to 453 K with 5 K·min⁻¹ and maintained constant for 8 h. Pyridine was adsorbed at 423 K with an equilibrium pressure of 0.1 mbar. After outgassing for 1 h, a spectrum was recorded. The samples were then heated to 723 K for 1 h to remove pyridine adsorbed on weak acid sites. A spectrum was taken after reducing the temperature to 423 K. The concentrations of Lewis and Brønsted acid sites were determined from the IR spectra of adsorbed pyridine by integration of the bands at 1450 cm⁻¹ (pyridine on Lewis acid sites) and 1540 cm⁻¹ (pyridine on Brønsted acid sites) using the extinction coefficients published by Emeis [31].

For AAS (UNICAM 939 atomic absorption spectrometer) 20-40 mg of each sample were dissolved in 0.5 ml of hydrofluoric acid (48%) and heated to 343 K until the entire liquid had evaporated.

For the determination of the pore volume approximately 150 mg were activated in vacuum at 673 K for 2 h. Subsequently, the dehydrated sample was weighed. The adsorption isotherms were measured at 77.4 K using a PMI automated BET sorptometer.

3.2.3. Adsorption and surface reaction

A modified SETARAM TG-DSC 111 instrument with a BARATRON 122A pressure transducer was used for the gravimetric and calorimetric measurements. 10-15 mg of the sample, pressed into platelets, was activated in vacuum ($p < 10^{-6}$ mbar) by heating to 393 K with $5 \text{ K} \cdot \text{min}^{-1}$. After 4 h at 393 K, the temperature was increased to 453 K with $5 \text{ K} \cdot \text{min}^{-1}$ and kept for 8 h. After cooling to 348 K, the sorbates were added in pulses. After each pulse the system was equilibrated as monitored by observation of the sample weight, heat flow, and pressure. After experiments, in which a reaction was observed, the products were collected in a quartz flask, which was cooled in liquid nitrogen. When the pressure stopped decreasing, the system including the flask was filled with He to 1 bar.

The products were analyzed by injecting 0.2 ml of the gaseous product-helium mixture into an HP 6890 GC equipped with a 50 m DB-1 column. Detailed chromatograms of the C_3 - C_5 fraction were recorded using an HP 5890 GC with a 50 m Plot Al_2O_3 column. The results from both methods were normalized based on the isobutane peak.

In order to characterize the residue on the catalyst, the gravimetric experiment was repeated with 0.2 g of the zeolite. Following the procedure of ref. [32] after reaction, the samples were treated with aqueous hydrofluoric acid (48%) at 323 K for 1 day. The residue was dissolved in CH_2Cl_2 and analyzed by GC/MS using a Finnigan MAT 8200-GC-MS with an apolar OV1 methylpolysiloxane column.

For the IR measurements, the samples were pressed into self-supporting wafers and activated in vacuum using the same temperature program as for the gravimetric experiments for the isotherm measurement. For *in situ* IR spectroscopy, the samples were activated at 723 K for 1 h in order to completely remove water from the catalyst. This activation procedure does not lead to qualitative changes of the onset and the reaction, but improves the spectral resolution. The sorbates were added in pulses at 348 K. The system was regarded to be equilibrated, when variations were not observed in three consecutive spectra. The start of the cracking reaction was observed by an increase of the pressure and a decrease of the CH

stretching bands. The spectra were normalized by comparison of the overtone of the zeolite framework vibrations (1960-1730 cm^{-1}). The deformation vibrations were deconvoluted using a mixture of Gaussian and Lorentzian functions (1:1) applying a least squares fit method (Grams/AI (7.02)).

3.3. Results

3.3.1. Basic characterization of the materials

The concentrations of aluminum and silicon were 13.0 and 16.2 wt.%, respectively, leading to a Si/Al ratio of 1.2. The residual sodium concentration was 0.07 wt.% corresponding to an ion exchange degree of 99.4 %. The (apparent) BET specific surface area was $502 \text{ m}^2\text{g}^{-1}$ and the micropore volume $0.13 \text{ cm}^3\text{g}^{-1}$. 0.29 and 0.10 mmol g^{-1} of Brønsted and Lewis acid sites were determined by IR spectra of adsorbed pyridine, out of which 0.09 and 0.07 mmol g^{-1} were able to retain pyridine after outgassing at 723 K for 1 hour (strong acids sites). Note that the fraction of strong sites was much higher for the Lewis (70%) than for Brønsted acid sites (31%).

3.3.2. Adsorption of n-octane and 2-methylheptane

3.3.2.1. Gravimetric and calorimetric measurements

The adsorption isotherms of n-octane or 2-methylheptane (2-MHp) (see Figure 3.1 and Table 3.1) were fitted using the model described in Chapter 2. Only minor differences were observed for the maximum loading σ_m of the two sorbates indicating that the same concentration of adsorption sites is accessible for both isomers. Therefore, the branching in 2-MHp was concluded not to impede sorption in any parts of the zeolite pores. A higher initial heat of adsorption and a higher loss of entropy were observed for n-octane indicating a stronger interaction for the more flexible molecule.

The heat of adsorption of n-octane and 2-MHp remained unchanged up to an uptake of 0.8 mmol g^{-1} (Figure 3.2) and increased at higher uptakes. At an uptake of ca. 0.95 mmol g^{-1} it reached 104 kJ mol^{-1} for both sorbates and remained constant when the uptake increased further. The additional heat of adsorption is attributed to sorbate-sorbate interaction of the newly adsorbed molecules with molecules that are already present in the pores [9,10].

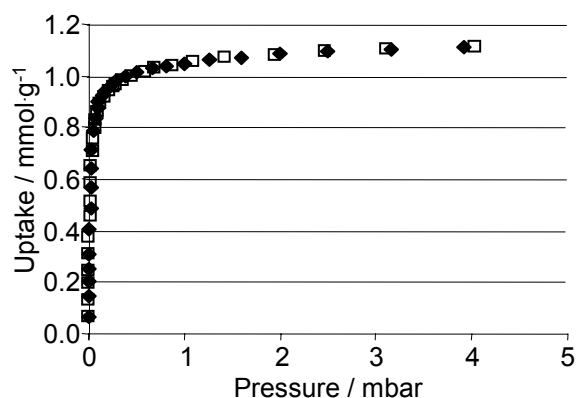


Figure 3.1: Gravimetric adsorption isotherms of n-octane (◆) and 2-methylheptane (□) on H-LaX at 348 K

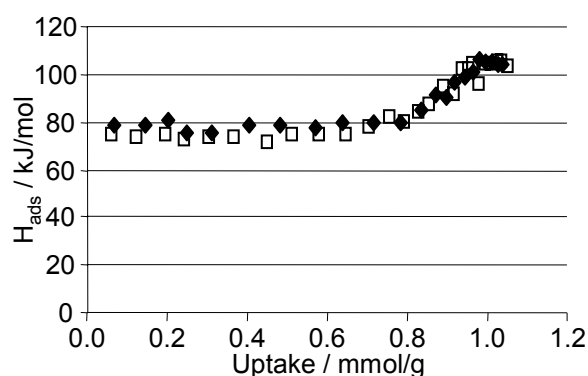


Figure 3.2: Heat of adsorption of n-octane (◆) and 2-methylheptane (□) on H-LaX at 348 K

Table 3.1: Langmuir fitting and adsorption parameters for n-octane and 2-MHp on H-LaX

	n-octane	2-MHp
Initial ΔS_{ads} ($\text{J}(\text{mol}\cdot\text{K})^{-1}$)	-135	-123
Initial ΔH_{ads} ($\text{kJ}\cdot\text{mol}^{-1}$)	-79	-74
K_{ads1}	$8.8 \cdot 10^4$	$8.2 \cdot 10^4$
K_{ads2}	$5.1 \cdot 10^4$	$1.4 \cdot 10^4$
σ_{m1} ($\text{mmol}\cdot\text{g}^{-1}$)	0.81	0.81
σ_{m2} ($\text{mmol}\cdot\text{g}^{-1}$)	0.26	0.27
$\sigma_{\text{m,tot}}$ ($\text{mmol}\cdot\text{g}^{-1}$)	1.07	1.08

3.3.2.2. In situ IR spectroscopy

The spectrum of the activated catalyst is dominated by a broad band between 3780 and 2520 cm^{-1} , which is assigned to the stretching vibrations of water that remained adsorbed on the catalyst activated at 453 K (Figure 3.3a). The four bands, observed on top of this band, are

attributed to LaOH groups (3534 cm^{-1}), bridging hydroxyl groups (3608 and 3652 cm^{-1}) and silanol groups (3730 cm^{-1}) [33].

The IR difference spectra after adsorption of n-octane and 2-MHp on H-LaX are shown in Figure 3.3, curves b and c), respectively. The intensity of the band of the free Brønsted acid sites decreased after each pulse (Figure 3.4). In parallel to this decrease, a new broad band appeared at 3526 cm^{-1} . This band is assigned to Brønsted acid sites, which are hydrogen bonded to adsorbed molecules [11]. The shift of 82 cm^{-1} to lower wavenumbers, however, was somewhat smaller than the values determined by Eder *et al.* for the adsorption of alkanes on H-FAU (Si/Al = 35) [11]. The band at 3534 cm^{-1} characteristic for the LaOH groups hardly varied in intensity, while the band at 1630 cm^{-1} (characteristic for the deformation vibration of molecular water) decreased slowly throughout the experiment.

The Brønsted acid sites were completely covered at 0.013 and 0.028 mbar for n-octane and 2-methylheptane, respectively (Figure 3.4). At these pressures, 0.30 mmol g^{-1} of n-octane and 0.50 mmol g^{-1} of 2-MHp were adsorbed. Note that the heat of adsorption only started to increase at an uptake, which was significantly higher (Figure 2).

The wavenumbers of the CH-stretching bands were nearly identical for both sorbates (Figure 3.3, curves b and c). The bands at 2961 and 2932 cm^{-1} are assigned to the out-of-phase stretching modes of the methyl and methylene groups, respectively [34]. The in-phase stretching vibrations of the same groups were observed at 2871 and 2857 cm^{-1} , respectively. The band at 1465 cm^{-1} is attributed to an overlap of out-of-phase deformation modes of methyl groups and the methylene deformation mode. The stretching vibration band of the tertiary CH group in 2-MHp was not observed, as these vibrations are generally low in intensity [34].

Differences in the spectra were observed in the region between 1400 and 1300 cm^{-1} (Figure 3.3). In the spectrum of adsorbed n-octane a single band was present at 1384 cm^{-1} (in-phase deformation vibration of an isolated methyl group) [34]. The spectrum of adsorbed 2-MHp showed two bands at 1388 and 1372 cm^{-1} , which are assigned to different deformation modes of the isopropyl group. The band of the isolated methyl group is not well resolved, but it is visible in a simulated spectrum (not shown). In comparison with the liquid state IR spectra, the bands of the sorbates on H-LaX were not shifted by more than 2 cm^{-1} .

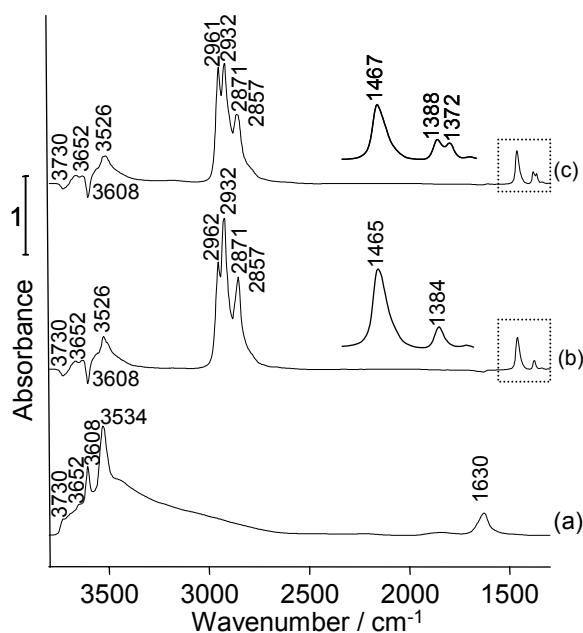


Figure 3.3: IR spectrum of (a) activated H-LaX and difference IR spectra of (b) n-octane (1 mbar) and (c) 2-methylheptane (1 mbar)

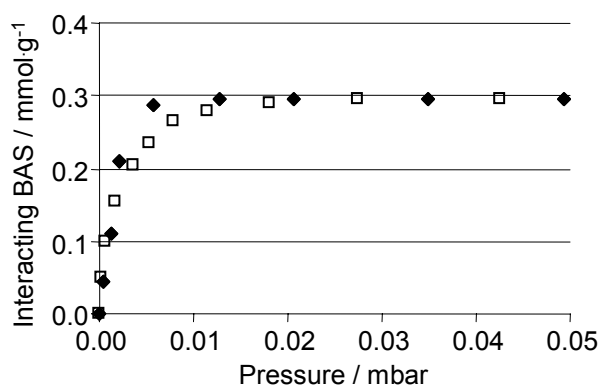


Figure 3.4: Interaction of Brønsted acid sites during the adsorption of n-octane (◆) and 2-methylheptane (□) on H-LaX

Adsorption isotherms of n-octane and 2-MHp were obtained from the IR spectra (Figure 3.5) using the integral of the CH stretching vibrations bands characteristic for the adsorbed alkanes (“IRS-derived isotherms”). The absorbance of a given band does not only depend on the concentration of the corresponding species, but also on the molar extinction coefficient, which may vary due to a different environment of the molecules (*vide infra*). The initial increase of the IRS-derived isotherms was significantly steeper than that of the gravimetric isotherms. At the point of complete saturation of the Brønsted acid sites a kink was observed indicating a sharp transition. The band of the perturbed OH groups increased by less than 10 % after the Brønsted acid sites were saturated, while its position and shape remained unchanged.

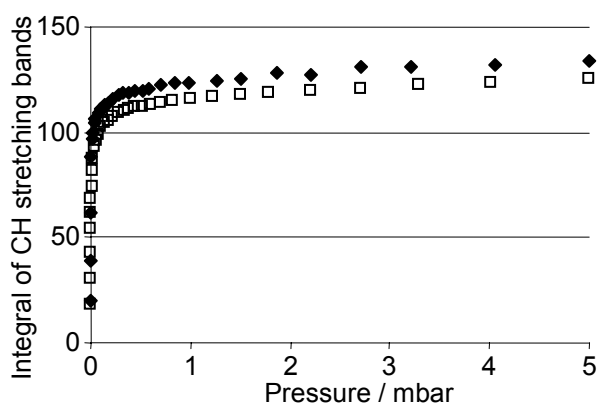


Figure 3.5: IRS derived isotherms: Intensity of the CH stretching vibrations during the adsorption of n-octane (◆) and 2-methylheptane (□) on H-LaX at 348 K

3.3.3. Adsorption and activation of di- and tri-branched alkanes

3.3.3.1. Gravimetric and calorimetric measurements

For all sorbates, the heat of adsorption was $74 \pm 1 \text{ kJ mol}^{-1}$, which is identical to the value observed for 2-MHp indicating that only n-octane is adsorbed more favorably. Once a certain loading of these molecules was reached, they started to react as indicated by a decrease of the sample mass accompanied by a pressure increase and an endothermic calorimetric signal. The loading, at which this process started, is referred to as critical loading. The simultaneous occurrence of all three observations is attributed to cracking of sorbed molecules.

Approximately, the same critical loading was found for all trimethylpentane isomers (Table 3.2). In contrast, 3,4-dimethylhexane began to react at a loading, which was almost four times as high as that of the trimethylpentanes.

Table 3.2: Critical loadings and pressures for different sorbates

Sorbate	Critical loading (mmol g ⁻¹)	Molecules per BAS ^a	Molecules per strong BAS ^a	Initial rate (mmol s ⁻¹)	Initial TOF (s ⁻¹)	Critical pressure (mbar)
2,2,4-TMP	0.20	0.7	2.2	$4.2 \cdot 10^{-7}$	$1.3 \cdot 10^{-4}$	0.002
2,3,3-TMP	0.17	0.6	1.9	$3.7 \cdot 10^{-7}$	$1.1 \cdot 10^{-4}$	0.001
2,3,4-TMP	0.18	0.6	2.1	$2.0 \cdot 10^{-6}$	$6.2 \cdot 10^{-4}$	0.002
3,4-DMH	0.69	2.4	7.9	$3.0 \cdot 10^{-7}$	$1.0 \cdot 10^{-4}$	0.030

^a BAS = Brønsted acid site

The pressure increase during the reaction was used to calculate the rate of the reaction based on the assumption that every cracking step leads to the release of one molecule into the gas phase. As will be shown later, this is only a rough indication, because the rate of desorption depends on a rather complicated reaction network including cracking, hydride transfer, polymerization, desorption of the reactant and adsorption of the products. As a result, the reported values are the lower limit. However, these rates allow the rough comparison between various reactants and temperatures.

The rate decreased throughout the entire reaction time. The initial rates for different isomers are compiled in Table 3.2. The initial turnover frequencies (TOF), normalized to the amount of Brønsted acid sites, allow for a better comparison by considering slight variations in catalyst loading. Approximately the same initial turnover frequency was observed for 2,2,4-TMP and 2,3,3-TMP, while for 2,3,4-TMP the TOF was markedly higher. The reaction of 3,4-DMH only started at a significantly higher pressure, which does not allow to compare the turnover frequencies directly.

With 2,2,4-TMP, as example for the tribranched alkanes, the critical loading increased with decreasing temperature (Figure 3.6), but the reaction was observed even at 323 K. The temperature dependence of the rate of cracking of the branched alkanes is surprisingly low (Table 3.3).

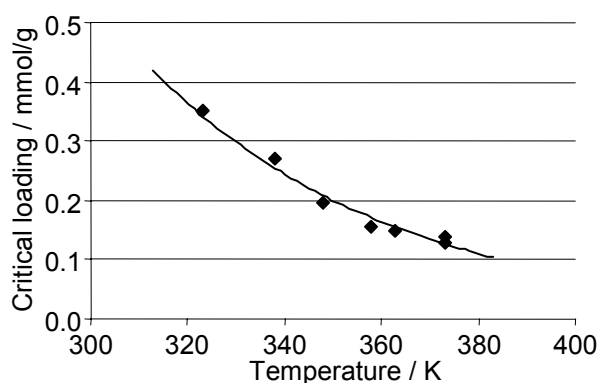


Figure 3.6: Temperature dependence of the critical loading for 2,2,4-TMP

Table 3.3: Initial rates of the reaction of 2,2,4-TMP at different temperatures

Temperature (K)	Critical loading (mmol g ⁻¹)	Initial rate (mmo s ⁻¹)	Initial TOF (s ⁻¹)
323	0.35	$8.2 \cdot 10^{-7}$	$2.0 \cdot 10^{-4}$
338	0.27	$7.6 \cdot 10^{-7}$	$1.8 \cdot 10^{-4}$
348	0.20	$4.2 \cdot 10^{-7}$	$1.3 \cdot 10^{-4}$
373	0.13	$3.5 \cdot 10^{-7}$	$9.1 \cdot 10^{-5}$

In a further experiment the catalyst was first loaded with $0.12 \text{ mmol}\cdot\text{g}^{-1}$ of 2,2,4-TMP at 348 K, which is equivalent to 62% of the critical loading. Then, n-octane was added in pulses. When the total loading reached $0.25 \text{ mmol}\cdot\text{g}^{-1}$, the reaction started. The initial turnover frequency was $9.2\cdot 10^{-5} \text{ s}^{-1}$, which is only slightly lower than that observed when only 2,2,4-TMP was adsorbed.

3.3.3.2. Analysis of the gas phase

Isobutane and isopentane were the most abundant products in the gas phase after all reactions (Table 3.4). However, it has to be noted that the freezing procedure may not allow quantitative collection of the $\text{C}_1\text{-C}_3$ fraction and hydrogen. The concentration of unconverted reactant differed significantly between the isomers. After reaction of 2,2,4-TMP and 2,3,3-TMP, 9.4 and 8.5 wt.% of the reactant were observed in the gas phase, respectively, while after the reaction of 2,3,4-TMP, only 0.4 wt.% of the reactant were found. Apart from the reactant a maximum of 0.6 wt.% of other octane isomers were detected. For all three TMPs, small amounts of branched hexane and heptane isomers were also formed. In addition to alkanes, traces of alkenes (mainly butenes) were also observed. The alkene concentration was, however, significantly higher after the reaction of 2,3,4-TMP.

After the conversion of 3,4-dimethylhexane the sum of the isobutane and isopentane fractions only accounted for 54 % of the product mixture, while considerably higher concentrations of the $\text{C}_6\text{-C}_8$ molecules were observed. The octane fraction consisted mostly of dimethylhexane isomers. Among those, the major contribution was 2,4-DMH with a concentration of 7.8 wt %, which is twice as high as the concentration of the reactant (3.8 wt.%).

Dihydrogen was detected in the gas phase by mass spectroscopy. Due to the complexity of the gas phase composition, the carbon containing fragments were not assigned to particular molecules.

Table 3.4: Product distribution in the gas phase after conversion of different octane isomers (in wt.%)

	2,2,4-TMP	2,3,3-TMP	2,3,4-TMP	3,4-DMH
Alkenes	1.1	0.8	3.4	0.6
Isobutane	79.3	83.6	84.7	33.7
Isopentane	14.1	11.0	8.2	20.4
n-Pentane	0.1	0.1	0.1	0.0
Hexane isomers	3.8	3.1	2.2	15.4
Heptane isomers	0.9	0.7	0.6	13.1
Methylheptanes	0.1	0.0	0.1	2.3
Dimethylhexanes ^a	0.2	0.1	0.3	13.7
Trimethylpentanes ^a	0.2	0.4	0.2	0.1
C ₉₊	0.2	0.2	0.2	0.7

^a The concentrations given in the table do not include the reactant.

3.3.3.3. Analysis of the catalyst after reaction

In the catalyst residue alkanes with 9 to 13 carbon atoms were detected by GC/MS, the most abundant being dodecane and octane isomers (Figure 3.7). Note that alkanes with less than eight carbon atoms could not be separated from the solvent (CH₂Cl₂) used for the extraction. All peaks were assigned to alkanes. The short retention time indicated a high degree of branching.

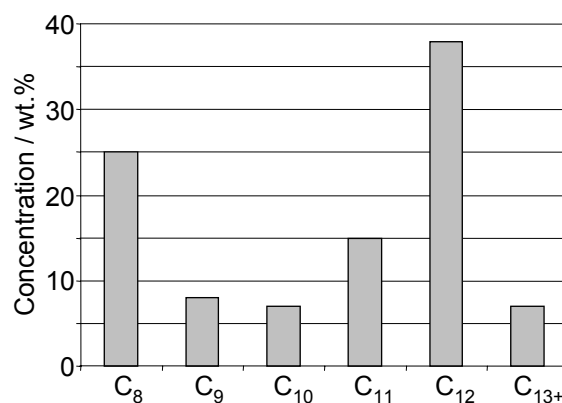


Figure 3.7: Composition of the residue on the catalyst after reaction of 2,2,4-TMP derived from GC/MS

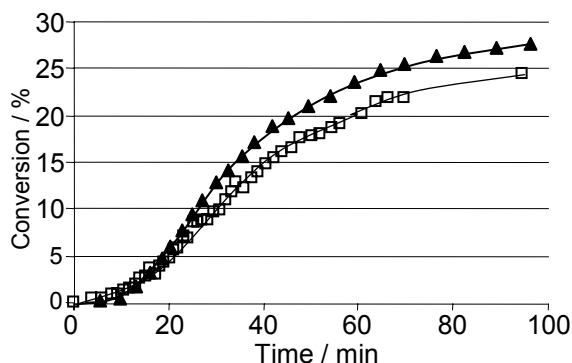


Figure 3.8: Conversion of sorbate molecules (▲) and occupied Brønsted acid sites (□) during the reaction of 2,2,4-TMP

3.3.3.4. *In situ* IR spectroscopy measurements

The interaction of 2,2,4-TMP with H-LaX was also investigated by *in situ* IR spectroscopy. The onset of the reaction was observed by an increase of the pressure. This occurred when 83 % of the Brønsted acid sites interacted with adsorbed molecules. During the reaction, the band at 3609 cm^{-1} increased again indicating that 25 % of the Brønsted acid sites interacting with sorbate molecules when the reaction started became unoccupied during the reaction (Figure 3.8). In parallel, the band of the perturbed Brønsted acid sites decreased. Figure 3.8 also shows that in the beginning of the reaction a Brønsted acid sites was freed for each sorbate molecule converted. The ratio decreased somewhat as the reaction proceeded.

When the reaction started, two new bands were observed at 1628 and 1616 cm^{-1} (Figure 3.9). These IR bands are usually assigned to C=C stretching vibrations [34]. In this particular case, the bands are tentatively attributed to the C=C stretching vibration of isobutene adsorbed on weak and strong Lewis acid sites, respectively. Note that the band at 1616 cm^{-1} , which was the stronger one initially, remained constant after approximately 25 min, while the band at 1628 cm^{-1} continued to increase in intensity. This indicates that adsorption on the strong Lewis acid sites is favored until these sites are saturated. While the reaction proceeded, both bands shifted to slightly higher wavenumbers. The pressure increase, the detection of C=C stretching vibrations and the increase of the acidic OH vibration band occurred within one minute from each other. Note that the intensity of all the bands remained constant after 55 min (Figure 3.10).

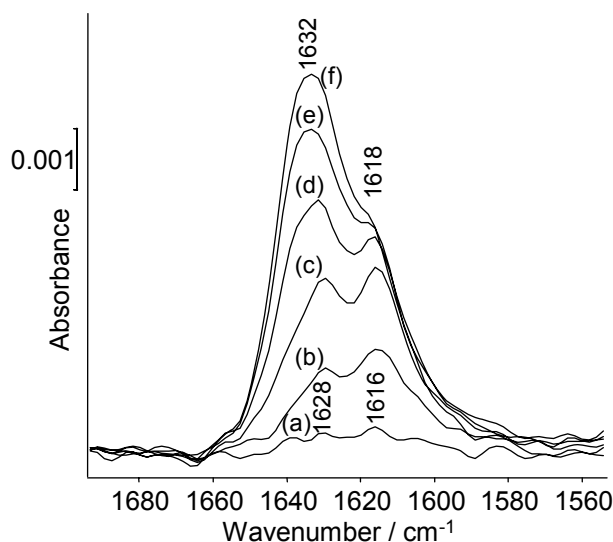


Figure 3.9: Development of C=C stretching vibration bands: (a) 5 min, (b) 10 min, (c) 15 min, (d) 20 min, (e) 25 min, (f) 30 min from the beginning of the reaction of 2,2,4-TMP

Figure 3.11 shows the difference IR spectra during the reaction of 2,2,4-TMP. The CH stretching vibrations decreased continuously, which is in agreement with the mass loss observed in the microbalance. More complex changes were observed for the CH deformation vibrations. The symmetric methyl deformation vibrations consisted of three peaks at 1395 (*tert*-butyl group), 1385 (isopropyl group or gem-dimethyl groups) and 1366 cm^{-1} (*tert*-butyl and isopropyl group) as well as a shoulder at 1354 cm^{-1} [34]. The changes of these bands show that during the reaction the concentration of *tert*-butyl groups decreases, while isopropyl groups or gem-dimethyl groups are formed (Figure 3.10).

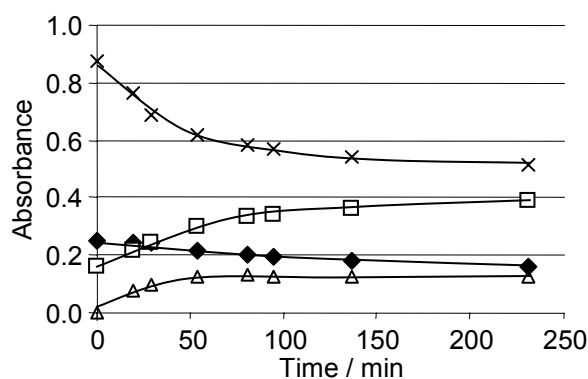


Figure 3.10: Changes of the intensity of the methyl deformation vibrations and C=C stretching vibrations during the reaction of 2,2,4-TMP: (x) band at 1367 cm^{-1} , (□) band at 1385 cm^{-1} , (◆) band at 1395 cm^{-1} , (Δ) bands at 1616 and 1628 cm^{-1}

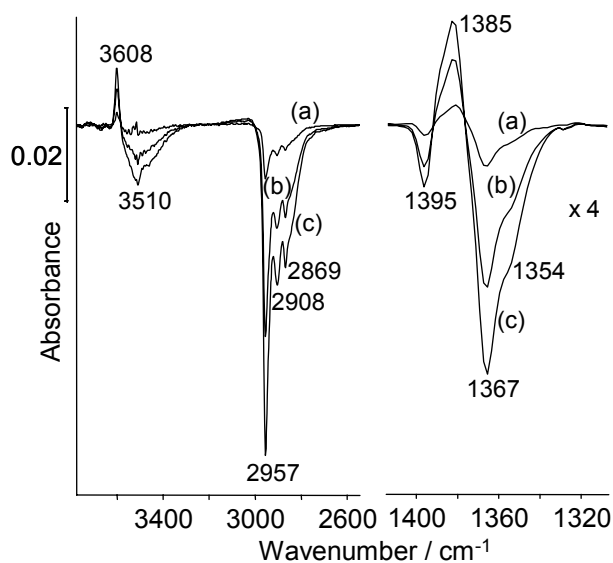


Figure 3.11: Difference IR spectra during the reaction of 2,2,4-TMP: (a) 10 min, (b) 20 min, (c) 30 min from the beginning of the reaction

3.4. Discussion

3.4.1. Adsorption of alkanes

The adsorption of alkanes in zeolites is generally dominated by dispersion forces contributing the more energy per carbon atom the better the steric fit between the molecule and the pore is [9-11]. The initial enthalpy of adsorption of n-octane was approximately 5 $\text{kJ}\cdot\text{mol}^{-1}$ higher than that of all branched isomers. However, it was accompanied by lower entropy of adsorption indicating that the stronger interaction reduces the configurational entropy in the tighter bound alkane. The stronger interaction of n-octane suggests that the presence of tertiary carbon atoms reduces the flexibility to assume a structure optimal for the interactions with the faujasite structure.

Initially, the Brønsted acid sites are the preferred sites of sorption, because the interaction with Brønsted acid sites in a faujasite type zeolite provides additional 6 $\text{kJ}\cdot\text{mol}^{-1}$ to the dominating van der Waals forces [10]. The dipole induced in the alkane by the OH group allows establishing a hydrogen bonding interaction (dipole induced hydrogen bonding). Because of the proximity of Brønsted acid sites in the material studied, every adsorbed molecule of n-octane interacts in average with 1.3 Brønsted acid sites until most sites are covered (see Figure 3.12a). Only close to full coverage, a deviation from this correlation was observed. In contrast to n-octane, 2-methylheptane initially interacts with up to three Brønsted acid sites (Figure 3.12b). This different stoichiometry is explained by the different structure of the two molecules. The linear n-octane can interact with not more than two Brønsted acid

sites, while the branching in 2-methylheptane offers an additional possibility of interacting with a third acid site across a channel or cage, if sufficiently close. Approximately one third of the Brønsted acid sites are located in a suitable environment for this kind of interaction (Figure 3.12b). Once the Brønsted acid sites in this arrangement are saturated, additional sorbate molecules interact either with free Brønsted acid sites or with interacting sites replacing adsorbed molecules, which were previously bound to two or three Brønsted acid sites. Therefore, the stoichiometry for the newly sorbed molecules decreases to 0.6 in average.

The enthalpy of adsorption remains constant until a loading of $0.8 \text{ mmol}\cdot\text{g}^{-1}$, while the concentration of Brønsted acid sites was only $0.29 \text{ mmol}\cdot\text{g}^{-1}$. This suggests either that the stoichiometry of interaction at the Brønsted acid sites must change or that other sorption sites contribute additional interactions similar to that of the Brønsted acid sites. Interaction of more than one alkane molecule with one Brønsted acid site in zeolite H-MFI was reported by Eder *et al.*, who observed by an increased shift of the IR band of the perturbed OH groups to lower wavenumbers [11]. As in our experiments the position of this band remained constant, we conclude that other sorption sites have to exist in H-LaX, which adsorb n-octane with the same adsorption enthalpy as the Brønsted acid sites. One could suggest that the additional

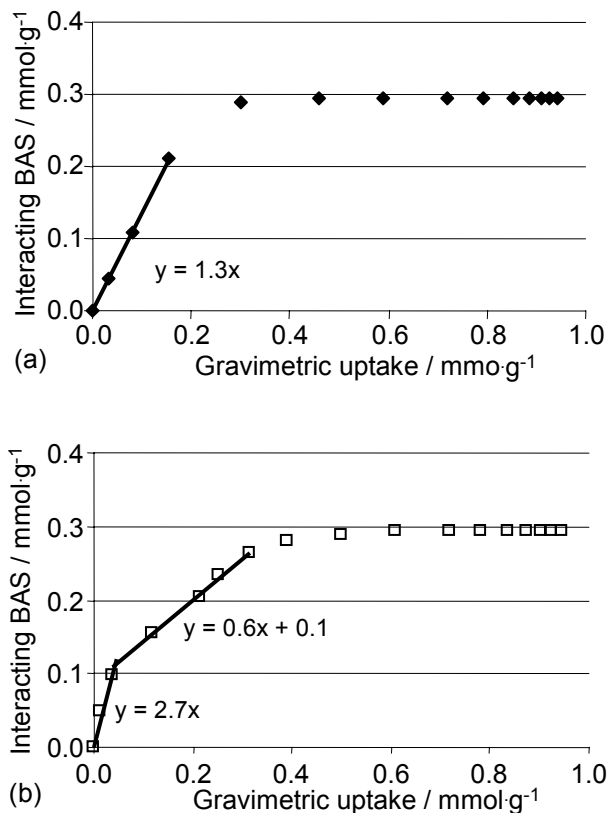


Figure 3.12: Interaction of sorbate molecules with Brønsted acid sites: (a) n-octane, (b) 2-methylheptane

sorption sites are Lewis acid sites or that sorbate-sorbate interaction compensate for the loss of the directed interaction. As the low concentration of Lewis acid sites ($0.10 \text{ mmol}\cdot\text{g}^{-1}$) compared to the concentration of the sorbed molecules ($0.8 \text{ mmol}\cdot\text{g}^{-1}$) makes the first hypothesis improbable, we speculate that the additional contribution to the sorption enthalpy is caused by sorbate-sorbate interactions.

With increasing loading, the steric constraints in the pores increase leading to a larger loss of entropy upon adsorption. This affects not only the new molecules entering the pore, but also those, which are already present. Therefore, adsorption in a unit cell with a low or moderate loading is thermodynamically favorable, although a higher enthalpy would be obtained in a unit cell, which is close to complete filling. Thus, the increase of the adsorption enthalpy only occurred, when the concentration of sorbate molecules reached approximately three times that of the Brønsted acid sites.

Kazansky *et al.* suggested that the extinction coefficient of IR bands is an indicator for the polarization of the adsorbed molecule [35]. Figure 3.13 shows the absorbance of the CH stretching vibrations versus the gravimetric uptake for n-octane and 2-methylheptane. In both cases, the highest extinction coefficients (steepest increases) were observed in the initial part of the isotherm followed by lower extinction coefficients, once the Brønsted acid sites were saturated. At low uptake 2-methylheptane was polarized stronger than n-octane. This may result either from a strong polarization of the additional methyl group in the branched molecule or from a polarization, which is induced indirectly *via* the tertiary CH group. Despite the drastic spectral effect, the contribution of this polarization to the heat of adsorption would amount at best to $2\text{-}3 \text{ kJ}\cdot\text{mol}^{-1}$ [36].

The extinction coefficients of both sorbates decreased drastically after saturation of the Brønsted acid sites. When the loading approached the limit of complete pore filling (above $1.0 \text{ mmol}\cdot\text{g}^{-1}$), the apparent extinction coefficients increased again. It is concluded that sorbate-sorbate interactions also lead to an increased polarization of the adsorbed molecules. It is noteworthy that under these conditions the values for both sorbates are very similar showing that the intermolecular interactions affect the molecules evenly.

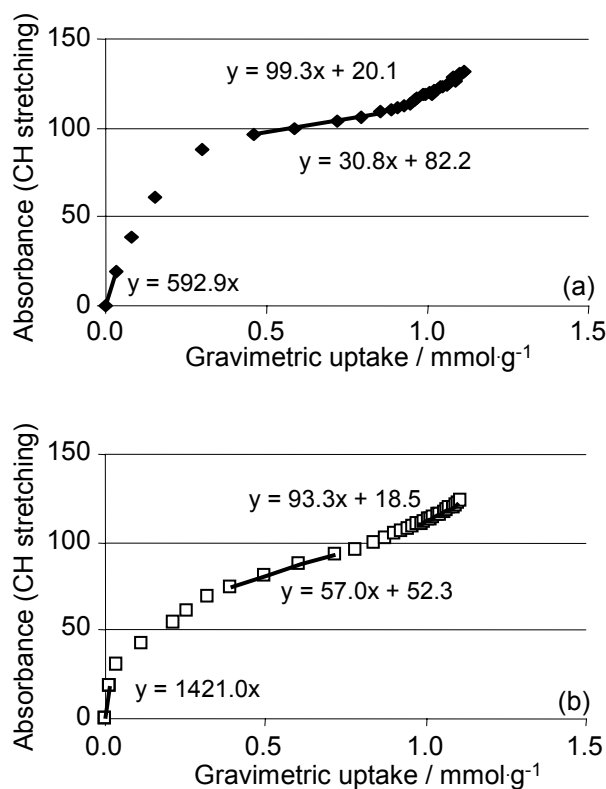


Figure 3.13: Correlation of the CH stretching vibrations with the gravimetric uptake for (a) n-octane and (b) 2-methylheptane on H-LaX

3.4.2. Activation of alkanes

When the critical concentration of sorbate molecules in the zeolite pores is reached, di- and tri-branched isomers are activated. Note that this was not observed during the adsorption of n-octane and 2-methylheptane.

Frequently, olefin impurities in the feed are claimed to be the source of carbenium ions that start the alkane activation processes. However, in the present case the C=C double bond stretching band was only observed, when the reaction already became observable. This is unlikely to occur, if olefins are added with each pulse of sorbate.

Several mechanisms for alkane activation have been suggested in the literature [22,25,27,37,38]. Protolytic cracking over zeolite catalysts is usually observed at temperatures above 700 K, which are much higher than the ones in our study (323-373 K) [22]. As strong Brønsted acid sites are active for this reaction, one would expect that these sites activate the alkanes independently from the surface coverage.

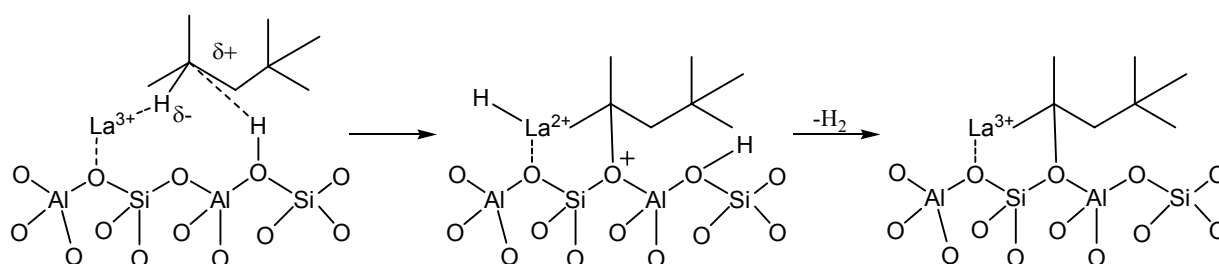
Based on DFT calculations, Fărcașiu *et al.* suggested the insertion of Al^{3+} into a CH bond for the activation of propane [27]. La^{3+} could act in a similar way. However, the calculated activation energy for this reaction ($236 \text{ kJ}\cdot\text{mol}^{-1}$) is comparable to the values published for protolytic cracking and renders this activation pathway unlikely at near ambient conditions.

Activation by hydride abstraction on Lewis acid sites was proposed by Schoofs *et al.* during the H/D exchange of isobutane over deuterated MFI- and FAU-type zeolites at temperatures between 413 and 533 K [25]. They suggested deprotonation of the carbenium ion, but did not provide mechanistic details on this step. It should be also noted that the lifetime of the formed olefin would be limited near a Brønsted acid site.

We suggest, therefore, that the activation of the adsorbed di- or tri-branched octane isomers starts with the abstraction of a hydride ion by a Lewis acid site (Scheme 3.1). Note that in our material 70% of the Lewis acid sites are strong. These strong Lewis acid sites could be related to extra-framework Al^{3+} and/or La^{3+} cations, but their nature is still under dispute [39,40]. The hydride abstraction step leads to a carbenium ion, which interacts with a framework oxygen atom. This leads to a positive charge close to a Brønsted acid site. Consequently, the acidic proton can combine with the hydride ion on the Lewis acid site forming H_2 , which was detected in the gas phase. Such reactions have also been reported by Narbeshuber *et al.* at higher temperatures [37,38]. Note that the mirrored process is also possible, in which the Lewis acid site stabilizes an organic carbenium rest and a proton is chemisorbed to a lattice oxygen. The subsequent elimination reaction would lead to an olefin and dihydrogen, whereby the olefin forms immediately a carbenium ion /alkoxy group with a Brønsted acid site.

Let us address now the question, why the alkane activation is only observed above a certain concentration in the pores. At least three factors could play a role here. First, with increasing loading it becomes more likely that the alkanes are adsorbed close to strong Lewis acid sites. Second, alkanes are necessary to release the alkane by hydride transfer after cracking has occurred. Finally, the high density of molecules increases the polarization and, thus, favors the activation *via* intermolecular interactions.

It is rather unlikely that the last factor plays a major role as strong polarization already occurred after adsorption of the first molecules. As such strong polarization has not been



Scheme 3.1: Activation of 2,2,4-TMP by hydride abstraction on a Lewis acid site and recombination of the hydride ion with a proton forming H_2

observed in La^{3+} free zeolites, we speculate that the strong polarization at very low coverage is induced by La^{3+} ions. The first two factors can also explain the decrease of the critical loading with increasing temperature. On one hand, high temperature may favor the (activated) chemisorption on Lewis acid sites. On the other hand, high temperature increases the mobility of the alkane molecules in the zeolite pores and, therefore, enhances hydride transfer. When non-reactive n-octane was added to a subcritical loading of 2,2,4-TMP, the reaction was also observed. This could be related to the higher statistical presence of mobile branched alkanes. However, blockage of the strongest sorption sites may also lead to adsorption of 2,2,4-TMP close to Lewis acid sites, which again initiates activation of branched alkanes.

3.4.3. Carbon-carbon bond related surface reactions

After generation of carbenium ions by hydride abstraction, the activation of octanes proceeds *via* hydride transfer. Scheme 3.2 shows the reaction mechanism for 2,2,4-TMP. Once *tert*-2,2,4-trimethylpentyl carbenium ions are formed, a β -scission step leads to a *tert*-butyl carbenium ion and isobutene (Reaction a). As the concentration of alkanes in the pores is sufficiently high that an appreciable concentration exists in the mobile state, the *tert*-butyl carbenium ion abstracts a hydride from a 2,2,4-trimethylpentane molecule forming an *tert*-2,2,4-trimethylpentyl carbenium ion and isobutane (Reaction b). The heat of adsorption of isobutane on H-LaX (43 kJ mol^{-1}) is significantly lower than the heat of adsorption of the 2,2,4-trimethylpentane, so that the majority of the isobutane molecules will be in the gas phase leading to the observed pressure increase. Hydride transfer from 2,2,4-trimethylpentane molecules to *tert*-butyl carbenium ions is the most likely reaction to explain the observation that approximately 25% of the interacting Brønsted acid sites were freed during the reaction (Figure 3.8). It has to be mentioned that 2,2,4-TMP, which donates the hydride ion, is present in a mobile phase not interacting with a Brønsted acid site. However, when it undergoes hydride transfer, the sorption equilibrium is shifted and another molecule desorbs from a Brønsted acid site restoring the IR band of the unperturbed bridging hydroxyl group. Although there is the possibility that some sorbate molecules interact with more than one Brønsted acid sites, the concentration of freed Brønsted acid sites indicates how many sorbate molecules participate in the hydride transfer reaction.

Isobutene, which is formed by β -scission, can react *via* at least three routes. The first possibility is adsorption on a strong Brønsted acid site and formation of a *tert*-butyl carbenium ion (Reaction c). However, the increase of the IR band of the free OH groups during the reaction suggests that isobutene is not protonated to a significant extent. The

second possibility is that isobutene adsorbs on Lewis acid sites. The increase of the bands of olefinic C=C double bonds suggests that at least some of the molecules follow that route. The third possible route is the addition of isobutene to an existing carbenium ion, which is the inverse reaction of β -cracking (Reaction d) [41,42]. The relevance of oligomerization is indicated by the considerable concentrations of dodecane isomers found on the zeolite after reaction. Only traces of molecules with more than 8 carbon atoms were found in the gas phase due to their higher adsorption constants. This shows that the bulky structure of the oligomers hinders hydride transfer or, if it occurs, effective desorption of the molecule from the pores. Note that the high abundance of dodecanes on the catalyst proves that butenes must be intermediate products. The formation of n-butene would involve isomerization of the *tert*-2,2,4-trimethylpentyl carbenium ion and β -scission to an energetically unfavorable secondary carbenium ion. Therefore, isobutene is suggested to be the main olefinic intermediate. The high reactivity of olefins in acidic zeolites, however, prevents detection of significant concentrations of isobutene in the gas phase.

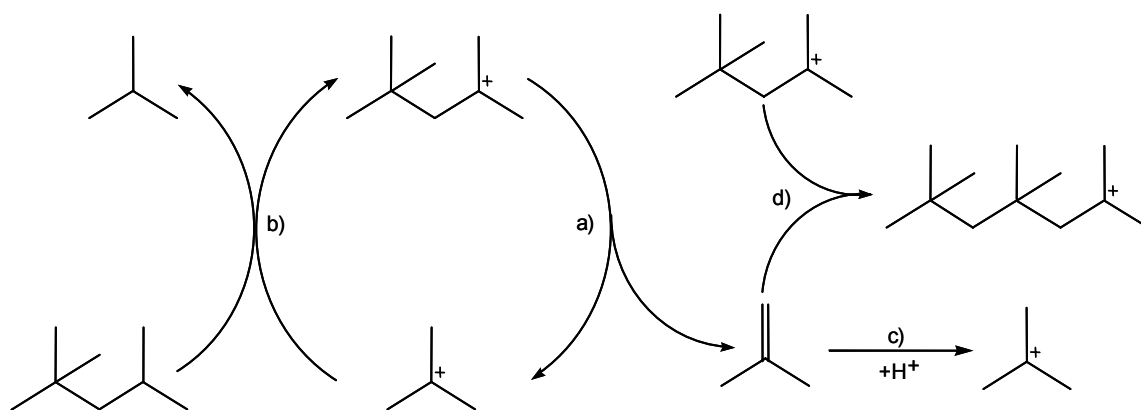
Additional evidence for oligomerization is provided by the changes of the CH deformation vibration in the IR spectra. The decrease of the band of *tert*-butyl groups combined with an increase of *gem*-dimethyl/isopropyl band can be explained by isomerization or oligomerization (Scheme 3.3). It has to be mentioned that the IR spectrum of isobutene also contains a *gem*-dimethyl/isopropyl band and it is likely that it contributes to the increase of the *gem*-dimethyl/isopropyl band in the initial stage of the reaction. However, the integral of the C=C stretching vibration band remained constant after 55 min, while the *gem*-dimethyl/isopropyl band continued increasing (Figure 3.10). This shows that, in particular at the later stage of the reaction, the formation of *gem*-dimethyl/isopropyl groups is due to oligomerization.

Also the presence of different octane isomers in the gas phase shows that isomerization must play an important role in the reaction network. In particular, the reaction of 3,4-DMH led to the formation of various dimethylhexane isomers with a preference towards 2,4-DMH. This isomerization step is necessary for the cracking of 3,4-DMH because direct β -scission of the corresponding carbenium ion would lead to the formation of an unstable primary carbenium ion, while β -scission of a *tert*-2,4-dimethylhexyl carbenium ion yields a secondary carbenium ion. The product distribution suggests that mainly methyl-group shift reactions occur. It is likely that methylheptane isomers are formed *via* oligomerization of cracking products rather than *via* skeletal isomerization.

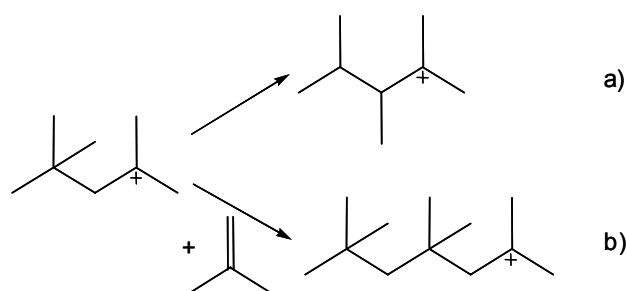
The role of isomerization is also demonstrated by the high concentration of isobutane in the gas phase after the reaction of 2,3,4-TMP and 2,3,3-TMP. Direct β -scission of the corresponding carbenium ions cannot lead to a *tert*-butyl carbenium ion. This suggests that a *tert*-2,2,4-trimethylpentyl carbenium ion is formed by isomerization, which is able undergo β -scission starting from a *tert*-carbenium ion and producing a *tert*-carbenium ion.

In all reactions, isopentane was one of the main products. Based on the elementary steps discussed above, we suggest a sequence of oligomerization, methyl group shift, β -scission and hydride transfer steps as the main route to isopentane. Only the sequence of these steps can explain the formation of isopentane without energetically unfavorable secondary carbenium ions as intermediates and measurable concentrations of C_3 products.

The reaction of 3,4-DMH led to a significantly different distribution of butane and pentane isomers, as well as to high concentrations of hexane and heptane isomers. This distribution cannot be explained by tertiary-tertiary β -scission as the case of the of trimethylpentane isomers.



Scheme 3.2: Mechanism of the reaction of 2,2,4-trimethylpentane: a) β -scission, b) hydride transfer, c) protonation of isobutene and d) oligomerization



Scheme 3.3: Possible reactions explaining the changes of the CH deformation vibrations: a) isomerization, b) oligomerization

3.5. Conclusions

Linear or single branched octane isomers such as n-octane and 2-methylheptane adsorb associatively on H-LaX. As indicated by the higher heat of adsorption for n-octane than for the branched isomers the linear isomer adapts itself more efficiently to the structure of the zeolite. Although the interaction of alkanes with acidic zeolites is mostly due to dispersive forces, strong polarization of the C-H bonds was also observed at low loadings. This effect was stronger for 2-methylheptane than for n-octane indicating that tertiary CH bonds or methyl groups are particularly affected.

When the loading of di- and tri-branched isomers reached a critical value, a chemical reaction was observed even at near ambient temperatures. These reacting alkanes are activated by hydride abstraction on a Lewis acid site. The abstracted hydride ion recombines with a proton from a Brønsted acid site forming H₂.

The onset of the reaction after reaching a critical uptake is explained by two different scenarios. Either some of the adsorbed molecules are forced into an entropically unfavorable position close to a Lewis acid site or a sufficient amount of mobile alkanes is needed to release the activated species from the surface by hydride transfer. Activation of the adsorbed alkanes leads eventually to the formation of carbenium ions, which participate in a complex reaction network including β -cracking, isomerization, alkylation and hydride transfer. While judging from the *in situ* IR spectra a sizable concentration of olefins is adsorbed on the zeolite, nearly only alkanes, in particular isobutane, were observed as reaction products in the gas phase.

The reaction of branched alkanes on H-LaX opens a new route to alkane activation under extremely mild condition. The present results demonstrate also that alkanes react much easier on zeolites with highly charged cations than previously thought. This is especially important to understand the surface chemistry during low temperature acid/base reactions such a zeolite catalyzed alkylation of alkanes with alkenes.

2.6. Acknowledgements

The author thanks Martin Neukam and Xaver Hecht for the AAS and BET measurements and Helmut Krause for the GC-MS analysis, as well as the experimental support by Manuel Stratmann. Partial financial support by the Verband der Chemischen Industrie and the European Union in the framework of NMP3-CT-2005-011730 IDECAT WP5 is gratefully acknowledged.

3.7. References

- [1] A. Corma, A.V. Orchilles, *Micropor. Mesopor. Mater.* 35-36 (2000) 21.
- [2] A.C. Butler, C.P. Nicolaidis, *Catal. Today* 18 (1993) 443.
- [3] J. Weitkamp, Y. Traa, *Catal. Today* 49 (1999) 193.
- [4] A. Feller, I. Zuazo, A. Guzman, J.O. Barth, J.A. Lercher, *J. Catal.* 216 (2003) 313.
- [5] K. Gaare, D. Akporiaye, *J. Phys. Chem. B* 101 (1997) 48.
- [6] J.A. van Bokhoven, A.L. Roest, D.C. Konigsberger, J.T. Miller, G.H. Nachttegaal, A.P.M. Kentgens, *J. Phys. Chem. B* 104 (2000) 6743.
- [7] A.V. Ivanov, G.W. Graham, M. Shelef, *Appl. Catal. B-Environ.* 21 (1999) 243.
- [8] R. Carvajal, P.-J. Chu, J.H. Lunsford, *J. Catal.* 125 (1990) 123.
- [9] F. Eder, J.A. Lercher, *J. Phys. Chem. B* 101 (1997) 1273.
- [10] F. Eder, J.A. Lercher, *Zeolites* 18 (1997) 75.
- [11] F. Eder, M. Stockenhuber, J.A. Lercher, *J. Phys. Chem. B* 101 (1997) 5414.
- [12] J.A.Z. Pieterse, S. Veefkind-Reyes, K. Seshan, J.A. Lercher, *J. Phys. Chem. B* 104 (2000) 5715.
- [13] C.L. Cavalcante, Jr., D.M. Ruthven, *Ind. Eng. Chem. Res.* 34 (1995) 177.
- [14] C.L. Cavalcante, Jr., D.M. Ruthven, *Ind. Eng. Chem. Res.* 34 (1995) 185.
- [15] M.S. Sun, O. Talu, D.B. Shah, *J. Phys. Chem.* 100 (1996) 17276.
- [16] W.J.M. van Well, X. Cottin, J.W. de Haan, B. Smit, G. Nivarthi, J.A. Lercher, J.H.C. van Hoff, R.A. van Santen, *J. Phys. Chem. B* 102 (1998) 3945.
- [17] S. Savitz, F. Siperstein, R.J. Gorte, A.L. Myers, *J. Phys. Chem. B* 102 (1998) 6865.
- [18] J.F. Denayer, G.V. Baron, J.A. Martens, P.A. Jacobs, *J. Phys. Chem. B* 102 (1998) 3077.
- [19] J.F. Denayer, W. Souverijns, P.A. Jacobs, J.A. Martens, G.V. Baron, *J. Phys. Chem. B* 102 (1998) 4588.
- [20] S.P. Bates, W.J.M. van Well, R.A. van Santen, B. Smit, *J. Am. Chem. Soc.* 118 (1996) 6753.
- [21] W.J.M. van Well, X. Cottin, B. Smit, J.H.C. van Hoff, R.A. van Santen, *J. Phys. Chem. B* 102 (1998) 3952.
- [22] W.O. Haag, R.M. Dessau, *Duality of Mechanism for Acid-Catalyzed Paraffin Cracking*; 8th Int. Congress on Catalysis, 1984, Berlin, Vol. 2, p. 305.
- [23] T.F. Narbeshuber, H. Vinek, J.A. Lercher, *J. Catal.* 157 (1995) 388.

-
- [24] S.A. Zygmunt, L.A. Curtiss, P. Zapol, L.E. Iton, *J. Phys. Chem. B* 104 (2000) 1944.
- [25] B. Schoofs, J. Schuermans, R.A. Schoonheydt, *Micropor. Mesopor. Mater.* 35-36 (2000) 99.
- [26] V.B. Kazansky, I.R. Subbotina, N. Rane, R.A. van Santen, E.J.M. Hensen, *Phys. Chem. Chem. Phys.* 7 (2005) 3088.
- [27] D. Fărcașiu, P. Lukinskas, *J. Phys. Chem. A* 106 (2002) 1619.
- [28] B.S. Greensfelder, H.H. Voge, G.M. Good, *Ind. Eng. Chem.* 41 (1949) 2573.
- [29] W.O. Haag, R.M. Dessau, R.M. Lago, *Stud. Surf. Sci. Catal.* 60 (1990).
- [30] G.A. Olah, G. Klopman, Schlosbe.Rh, *J. Am. Chem. Soc.* 91 (1969) 3261.
- [31] C.A. Emeis, *J. Catal.* 141 (1993) 347.
- [32] M. Guisnet, P. Magnoux, *Appl. Catal.* 54 (1989) 1.
- [33] J.W. Ward, *J. Phys. Chem.* 72 (1968) 4211.
- [34] N.B. Colthup, L.H. Daly, S.E. Wiberley, *Introduction to Infrared and Raman spectroscopy*, Academic Press Inc., San Diego, 1990.
- [35] V.B. Kazansky, E.A. Pidko, *J. Phys. Chem. B* 109 (2005) 2103.
- [36] F. Eder, J.A. Lercher, *J. Phys. Chem.* 100 (1996) 16460.
- [37] T.F. Narbeshuber, A. Brait, K. Seshan, J.A. Lercher, *Appl. Catal. A-Gen.* 146 (1996) 119.
- [38] T.F. Narbeshuber, A. Brait, K. Seshan, J.A. Lercher, *J. Catal.* 172 (1997) 127.
- [39] G. Catana, D. Baetens, T. Mommaerts, R.A. Schoonheydt, B.M. Weckhuysen, *J. Phys. Chem. B* 105 (2001) 4904.
- [40] A. Guzman, I. Zuazo, A. Feller, R. Olindo, C. Sievers, J.A. Lercher, *Micropor. Mesopor. Mater.* 83 (2005) 309.
- [41] J.N. Kondo, K. Domen, *J. Mol. Catal. A-Chem.* 199 (2003) 27.
- [42] S. Svelle, S. Kolboe, O. Swang, *J. Phys. Chem. B* 108 (2004) 2953.

Chapter 4

Comparison of zeolites H-LaX and H-LaY as catalysts for isobutane/2-butene alkylation

Lanthanum exchanged faujasite type zeolites were prepared by ion exchange from the sodium form of the zeolites and investigated as catalyst for isobutane/2-butene alkylation. Both zeolites have the same pore structure with a Si/Al ratio of 1.1 for H-LaX and 2.4 for H-LaY. With the reactions performed in a continuously operated stirred tank reactor under industrially relevant conditions ($T = 348 \text{ K}$, $p = 20 \text{ bar}$, paraffin/olefin ratio = 10, olefin space velocity = 0.2 h^{-1}) the catalyst lifetime of H-LaX was nearly twice as long as that of H-LaY. Moreover, a much higher yield of octane isomers was found with H-LaX. The product distributions showed that H-LaX had a high activity for hydride transfer and “self alkylation”. In line with this, the concentration of strong Brønsted acid sites was identified as the key factor for the differences between H-LaX and H-LaY.

Tentatively we conclude that residual sodium cations poison the strongest Brønsted acid sites in H-LaY. Moreover, the incorporation of lanthanum cations into the zeolite leads to an increase of the Si-O-T ($T = \text{Al, Si}$) angle. These changes of the framework geometry weaken the OH bond of bridging hydroxyl groups making them more acidic. This effect was more pronounced in H-LaX, which contains more sites that can accommodate polyvalent cations.

4.1. Introduction

Isobutane/2-butene alkylation is an important petrochemical process for the production of a mixture of branched alkanes with high octane numbers. The concentration of sulfur and aromatic compounds in alkylate is very low making it an ideal blending component for gasoline. The importance of alkylate is expected to increase further as the octane booster methyl-*tert*-butyl-ether is phased out in many industrial countries due to environmental concerns. Currently, industrial alkylation units operate with hydrofluoric or sulfuric acid as catalysts [1]. However, hydrofluoric acid is highly toxic and aerosols are easily formed. Therefore, its industrial application is progressively restricted. For the sulfuric acid based processes, acid consumption can reach 70 – 100 kg·t⁻¹ [2]. The spent catalyst must be regenerated in an expensive process removing water and tarry hydrocarbons.

Consequently, considerable efforts have been made to replace hydrofluoric or sulfuric acid by solid acids, which are easier to handle and more environmentally benign [3,4]. Zeolites received the most attention among the solid acid catalysts tested for this reaction [5-19]. So far, rapid deactivation has prevented industrial application of solid acid catalysts [19-22].

The product distribution in isobutane/2-butene alkylation is determined by the relative rates of three main reaction steps: olefin addition, isomerization and hydride transfer [23]. In particular, a high ratio of hydride transfer to olefin addition is important to prevent the formation of oligomers, which strongly adsorb on the catalyst leading to deactivation (see Chapter 5). Part of this problem may be solved by application of frequent regeneration steps [11,17,21,24,25] and operation of the reaction at low olefin concentrations in a continuously operated stirred tank reactor [6]. However, optimization of the catalytic properties remains the most important task.

Only large pore zeolites are suitable for isobutane/2-butene alkylation as diffusion limitations in medium and small pore zeolites lead to premature deactivation [26,27]. It was shown that zeolites with three dimensional pore networks allow more efficient diffusion of the product, which leads to an increase of the catalyst lifetime [28].

Although it is generally accepted that Brønsted acid sites are the active sites for isobutane/2-butene alkylation, there is an ongoing debate about the extent, to which the concentration and strength of Brønsted acid sites influence the catalytic activity and stability [2,16,29,30]. Feller *et al.* suggested that a high ratio of Brønsted to Lewis acid sites and a large fraction of strong Brønsted acid sites are key parameters for an extended catalytic

stability [8]. Strong Brønsted acid sites are capable of stabilizing the charge separation in the transition state for reactions such as hydride transfer [23]. Strong Lewis acid sites promote the formation of unsaturated deposits, which lead to deactivation of the catalyst [13,30].

Several authors suggested that hydride transfer is favored for zeolites with a low Si/Al ratio [31,32]. In contrast to this, Yoo and Smirniotis found that the catalytic performance for isobutane/2-butene alkylation of zeolite beta hardly changed, when the Si/Al ratio was varied from 6 to 15 [5]. Only for a Si/Al ratio of 30, reduced activity was found.

Lanthanum exchanged faujasites are among the most promising candidates for zeolite catalyzed isobutane/2-butene alkylation [8,9,13,20,21,33,34]. Particularly interesting is H-LaX, in which a high concentration of strong Brønsted acid sites can be achieved [8,9,20,34].

The lanthanum exchange influences the properties of zeolites in a complex way. After calcination most lanthanum cations are located in the sodalite cages [35]. For zeolite Y, the effect of incorporating La^{3+} cations is comparable to the stabilization achieved by mild steaming during the synthesis of H-USY [36]. However, the extent of dealumination is lower, when the stabilization is achieved by ion exchange. Some of the extraframework aluminum species formed during dealumination give rise to Lewis acidity [13,30]. Further, the La^{3+} cations are involved in the formation of Brønsted acid sites by hydrolysis of water [34,37,38]. It has also been reported that incorporation of lanthanum cations leads to an increase in the strength of Brønsted acid sites as the zeolite framework is polarized [36].

In this chapter, lanthanum exchanged zeolites X and Y, which both have a faujasite structure but different Si/Al ratios, were compared as catalysts for isobutane/2-butene alkylation. The differences in the catalytic performance are related to the physicochemical properties of the catalysts, in particular, Brønsted acidity.

4.2. Experimental

4.2.1. Catalyst preparation

La-exchanged zeolite X (LaX) was prepared from NaX (Si/Al = 1.1), which was provided by Chemische Werke Bad Köstritz. NaY from Akzo Nobel (Si/Al = 2.4) was used for the preparation of lanthanum exchanged zeolite Y (LaY). The same ion exchange procedure was applied to both zeolites, in which the parent material was ion exchanged twice in 0.2 M $\text{La}(\text{NO}_3)_3$ for 2h at 353 K using a ratio of solution to zeolite of 11 ml·g⁻¹. The zeolite was thoroughly washed with bi-distilled water and dried at room temperature. Then the sample was calcined in a flow of air with a heating rate of 0.5 K·min⁻¹ up to 723 K. After rehydration

on air, three further ion exchange steps followed by washing, drying, calcination and rehydration were applied.

4.2.2. Alkylation reaction

The alkylation reactions were performed in a CSTR with a volume of 50 ml. Prior to reaction, the catalyst was activated *in situ* at 453 K for 14 h in H₂. Then, the reactor was cooled to 348 K, pressurized with H₂ to 20 bar and filled with pure isobutane (AIR LIQUIDE, 99.95%). The reaction was started by feeding a mixture of isobutane and 2-butene (Messer, 99.4%) with a molar ratio of 10/1. The olefin space velocity was $0.2 \text{ g}_{\text{butene}} \cdot \text{g}_{\text{catalyst}}^{-1} \cdot \text{h}^{-1}$ and the stirring rate 1600 rpm. Samples from the product stream were taken periodically and analyzed with a HP 6830 gas chromatograph equipped with an FID-detector and a 50 m DB-1 column.

4.2.3. Physicochemical characterization

For atomic absorption spectroscopy (AAS), 20-40 mg of the sample was dissolved in 0.5 ml of hydrofluoric acid (48%) and heated to 343 K until the entire liquid had evaporated. The residue was dissolved in water and the solution analyzed with a UNICAM 939 atomic absorption spectrometer.

The lanthanum content was measured by neutron activation analysis (NAA). Aliquots of 40 mg of each sample were closed in PE-bags and co-irradiated with a Al-Au monitor for 5 minutes in position Strang-6 at the FRM-II reactor in Garching, Germany. Five days after irradiation, the samples and Al-Au monitor were counted at positions of 15 cm from calibrated detectors. The k_0 -method [39] implemented in the program MULTINAA [40] was applied to calculate all the elements in the samples. In this work, the nuclide ¹⁹⁸Au of the co-irradiated Al-Au monitor was used as the comparator in the k_0 -method.

The BET surface area and micropore volume were determined by nitrogen physisorption on a PMI Automated BET Sorptometer. Prior to the measurements the samples were heated to 393 K for 2 h in vacuum.

The unit cell size of the samples was determined by XRD. The position of the signals was referenced against silicon powder. A Philips X'Pert Pro System (Cu K α 1-radiation, 0.154056 nm) was used at 40 kV/40 mA. The measurements were performed with a step scan of 0.0047 °/min from 50 to 60° 2 θ .

Acid site concentrations were obtained from IR spectra of adsorbed pyridine. The samples were pressed into self supporting wafers, dried in vacuum at 393 K for 4 h and activated at 453 K for 8 h to remove most of the physisorbed water. The heating rates were $5 \text{ K} \cdot \text{min}^{-1}$. Pyridine was adsorbed at 423 K with a pressure of 0.1 mbar until no changes were observed in the spectrum. The samples were outgassed for 1 h to remove weakly physisorbed pyridine and a spectrum was taken. The strength of the acid sites was probed by increasing the temperature in steps of 50 K. After reaching a new temperature the sample was outgassed for 30 min before the spectrum was measured. For quantification the molar extinction coefficients published by Emeis were used [41].

The acid site concentration and strength were investigated by temperature programmed desorption of ammonia (NH_3 -TPD). The samples were pressed in pellets (0.7-2.0 mm) and approximately 200 mg were activated in He using the same temperature program as for the IR experiments. Then, NH_3 was adsorbed by passing a He/ NH_3 mixture (10% NH_3) over the catalyst for 1 h at 375 K. After outgassing for 2 h in He at 375 K, the TPD was carried out applying a heating rate of $10 \text{ K} \cdot \text{min}^{-1}$. The NH_3 in the effluent was monitored by a Pfeiffer QMS 200 mass spectrometer using the signal for $m/e = 16$. For quantification of the total acidity, the peak area was compared with a standard (ZSM5 SAR: 180 from Süd-Chemie, $0.19 \text{ mmol acid sites} \cdot \text{g}^{-1}$). The spectra were deconvoluted with Gaussian peaks using the least square fit method.

For MAS NMR measurements the samples were packed into a ZrO_2 rotor and spun at 15 kHz. All samples were measured on a Bruker AV500 spectrometer. For ^{27}Al the resonance frequency was 130.3 MHz. The spectra were measured as the sum of 2400 scans with a recycle time of 250 ms. A $\pi/12$ pulse (pulse length = $1.0 \mu\text{s}$) was applied for excitation. The chemical shifts were referenced against an external standard of solid $\text{Al}(\text{NO}_3)_3$ ($\delta = -0.54 \text{ ppm}$). The ^{27}Al MQMAS spectra were recorded using a pulse sequence including a z-filter. The pulse lengths were 3.0, 1.1 und $20.0 \mu\text{s}$. For each row of the spectrum 2400 scans were recorded. The recycle time was 250 ms. The ^{29}Si spectra were recorded as the sum of at least 10000 scans with a recycle time of 5 sec. The excitation pulse had a length of $1.2 \mu\text{s}$. The spectra were referenced against tetrakis(trimethylsilyl)silane ($\delta = -9.843 \text{ ppm}$ for the left peak).

4.3. Results

4.3.1. Physicochemical characterization

The results of the physicochemical characterization of H-LaX and H-LaY are compiled in Table 4.1. The main difference between the two samples is that after the same ion exchange procedure almost quantitative exchange of the sodium cations was achieved for H-LaX, while the ion exchange degree was only 87% for H-LaY.

The same concentration of Brønsted acid sites was measured by IR spectroscopy for both materials (Figure 4.1). However, the strength of the Brønsted acid sites was significantly stronger in H-LaX than in H-LaY. The concentration of Lewis acid sites in H-LaX was three times as high as in H-LaY, but the fraction of strong Lewis acid sites was significantly higher for H-LaY. Acid sites, which retain pyridine at 723 K, are hereafter referred to as strong acid sites.

Additional information on the strength distribution of the acid site was obtained by temperature programmed desorption of ammonia (NH_3 -TPD). The ammonia uptake was significantly higher than the sum of Brønsted and Lewis acid sites as determined by IR spectroscopy (Table 4.1). A possible explanation is that ammonia is adsorbed on sites, which are accessible for pyridine molecules. The TPD profiles and deconvolution for both zeolites are shown in Figure 4.2. In both cases three contributions were identified. The first two peaks were centered at slightly higher temperatures for H-LaY. Note that hardly any strong acid sites were observed in H-LaY.

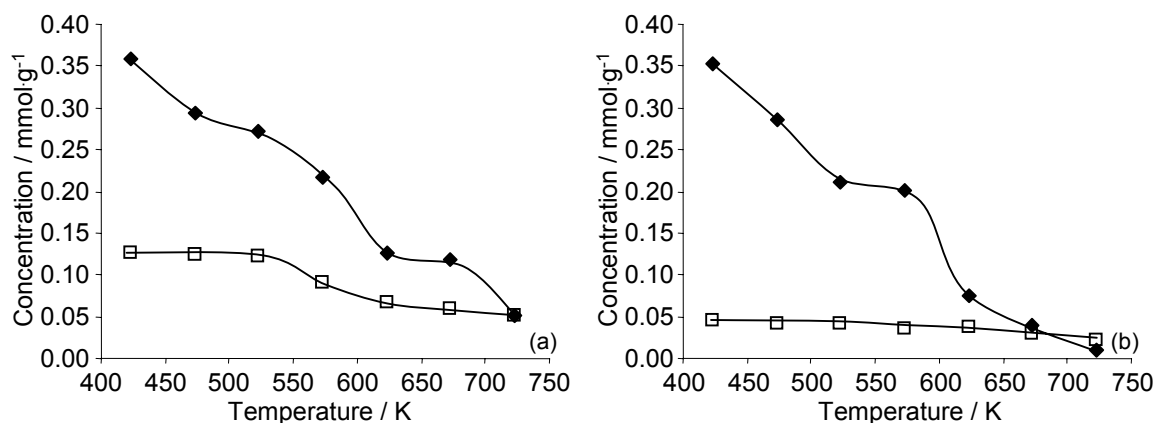
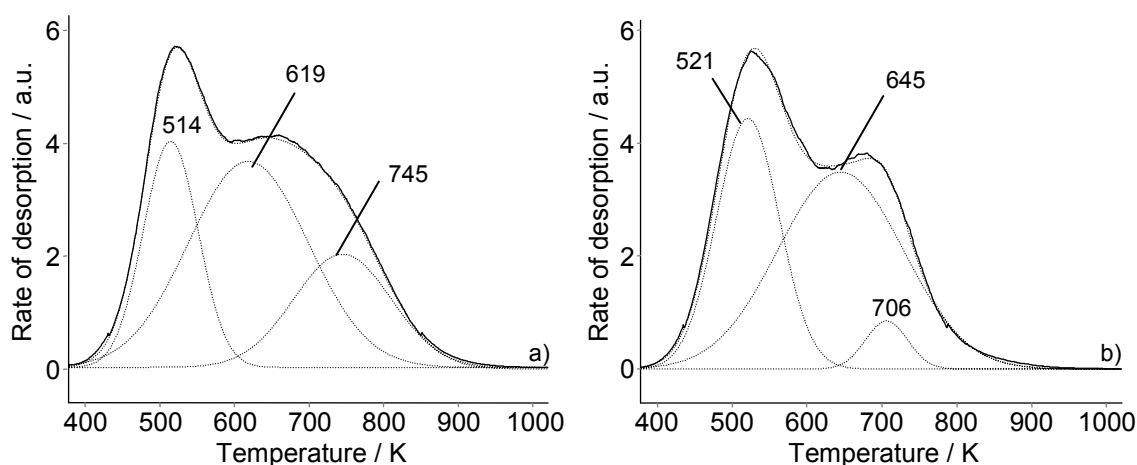


Figure 4.1: Concentrations of Brønsted (◆) and Lewis (□) acid sites, which retain pyridine at different temperatures: (a) H-LaX, (b) H-LaY

Table 4.1: Elemental composition, BET surface area, micropore volume and acid site concentration for H-LaX and H-LaY

	LaX	LaY
<i>Elemental composition (wt.%)</i>		
Si (AAS)	16.4	20.3
Al (AAS)	14.3	8.0
Na (AAS)	0.08	0.87
La (NAA)	22.1	13.8
Si/Al ratio	1.1	2.4
Ion exchange degree / %	99.3	87.2
BET surface area ($\text{m}^2 \cdot \text{g}^{-1}$)	456	545
Micropore volume ($\text{m}^3 \cdot \text{g}^{-1}$)	0.178	0.169
Unit cell size (Å)	25.0	24.8
<i>Acidity (IR) ($\text{mmol} \cdot \text{g}^{-1}$)</i>		
BAS ^a	0.348	0.356
LAS ^b	0.107	0.033
Strong BAS ^a	0.052	0.010
Strong LAS ^b	0.051	0.022
BAS ^a / LAS ^b	3.3	10.8
Strong BAS ^a / total BAS ^a	0.15	0.03
Strong BAS ^a / strong LAS ^b	1.02	0.46
<i>Acidity (TPD) ($\text{mmol} \cdot \text{g}^{-1}$)</i>		
Weak sites	0.24	0.24
Medium sites	0.48	0.38
Strong sites	0.21	0.03
Sum	0.93	0.65

^a – BAS = Brønsted acid sites, ^b – LAS = Lewis acid sites

**Figure 4.2:** Temperature programmed desorption of ammonia from H-LaX a) and H-LaY b): experimental curves (—) and fits (---)

The ^{29}Si MAS NMR spectra of H-LaX and H-LaY (Figure 4.3) each contained five peaks corresponding to Si atoms with 0 to 4 next nearest Al neighbors (Table 4.2). The peak position for Si nuclei in the vicinity of a lanthanum cation is shifted to a higher field by approximately 4 ppm [42]. This shift is caused by an increasing strain of the Si-O-T bonds (T being Al or Si) in the six ring window close to the La^{3+} cation in a sodalite cage [43]. The line width increased with decreasing number of next nearest Al neighbors. This is attributed to the overlap of two contributions corresponding to silicon atoms with and without lanthanum cations located nearby. In case of the latter species, the framework charges in the vicinity are compensated by protons or, in case of H-LaY, also by sodium ions. The preference of lanthanum cations for sites in the vicinity of several aluminum atoms is explained by the fact that it is more likely to find a suitable site for a polyvalent cation in such an environment. Due to its high Si/Al ratio H-LaY contains a significant number of isolated aluminum sites, which cannot accommodate a polyvalent cation.

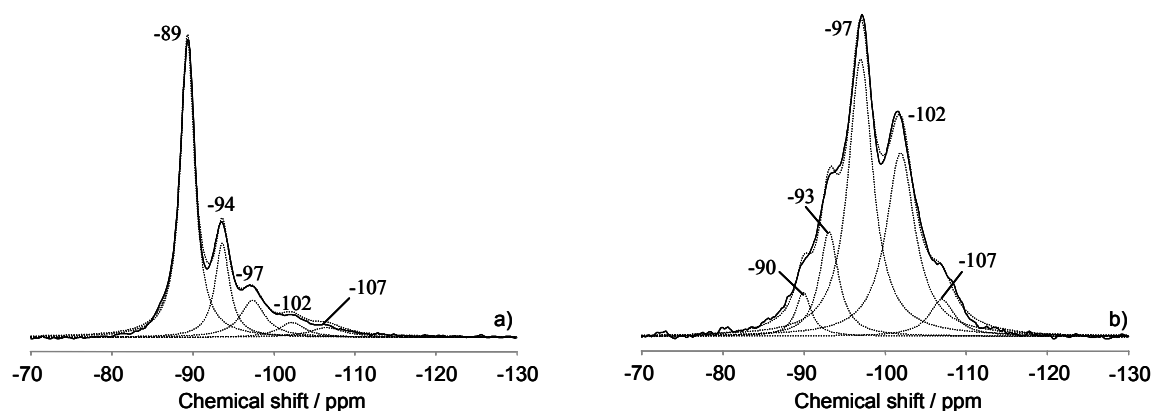


Figure 4.3: ^{29}Si MAS NMR spectra of hydrated H-LaX a) and H-LaY b): experimental spectra (—) and simulation (⋯)

Table 4.2: Fitting parameters of the ^{29}Si MAS NMR spectra of hydrated H-LaX and H-LaY

Si(nAl)	H-LaX			H-LaY		
	Chemical shift (ppm)	Line width (ppm)	Relative area (%)	Chemical shift (ppm)	Line width (ppm)	Relative area (%)
n = 4	-89.4	2.1	59	-90.0	2.3	4
n = 3	-93.6	2.1	19	-93.1	2.8	13
n = 2	-97.4	3.7	13	-97.0	3.5	43
n = 1	-102.2	4.0	5	-101.9	4.3	34
n = 0	-106.6	5.1	4	-107.0	4.1	6

The local environment of the aluminum atoms in H-LaX and H-LaY was investigated by ^{27}Al MAS NMR spectroscopy (Figure 4.4 inserts). In both spectra peaks corresponding to aluminum atoms with tetrahedral (60 - 40 ppm) and octahedral (20 - 0 ppm) coordination were observed. For simulation of the MAS NMR spectra, additional information was obtained from ^{27}Al MQMAS NMR spectra (Figure 4.4). In the tetrahedral region of the ^{27}Al MQMAS NMR spectra of H-LaX two contributions were distinguished. The center of gravity of the first one was located at $\delta_{F1} = 63$ ppm and $\delta_{F2} = 58$ ppm. This sharp peak was located close to the diagonal of the spectrum corresponding to a small average quadrupolar coupling constant of 2.4 MHz. This shows that the corresponding Al atoms experience a rather weak distortion of their local environment. Therefore, this peak is assigned to framework aluminum atoms with protons as charge compensating cations [36]. Note that charge compensation by sodium cations would give rise to a peak in the same position. However, due to the low sodium concentration in H-LaX such an attribution is not feasible.

The second species is located at $\delta_{F1} = 69$ ppm with a large distribution in F_2 dimension. As ^{27}Al is a nucleus with a quadrupolar moment, a charge gradient on the nucleus, which is caused by a distorted environment, causes a quadrupolar induced shift. In the present case, the distortion is caused by an increase in the Si-O-Al angles [36]. The large distribution in F_2 dimension shows that the extent of this effect varies between different atoms and is indicative of a wide distribution of the degree of distortion, which is experienced by the corresponding aluminum species. In the simulation a chemical shift of approximately 55 ppm was found for this species. In consequence, the difference in the isotropic shift in the MQMAS spectrum is explained by the quadrupolar induced shift [44].

The same species were observed in the spectrum of H-LaY. Note that in this case a significant part of the sharp feature in the tetrahedral region is attributed to framework aluminum atoms with Na^+ as charge compensating cations.

The existence of an additional contribution with a similar isotropic shift and $\delta_{F2} = 59$ ppm was observed from the shape of the peak in the MQMAS spectrum. The peak is assigned to framework aluminum species in the vicinity of lanthanum cations, which experience only a weak distortion of their environment. The observation of two different aluminum species with lanthanum as charge compensating cation is in contrast to the work of van Bokhoven *et al.* on LaNaY [36]. However, as a result of multiple ion exchange steps, the La content of the zeolites used in our study was significantly higher than the highest La content of the zeolites used in their work. Therefore, lanthanum cations are also found in sites, which are less favorable for ion exchange. We assume that these sites are isolated or paired Si-O-Al sites.

Marked differences were also observed for aluminum atoms with octahedral coordination. In the spectrum of H-LaY a single sharp peak was observed, while an additional broad peak necessary to reach a reasonable fit of the spectrum of H-LaX. Omega *et al.* demonstrated that octahedral alumina species, which give rise to sharp peaks, can be transformed into tetrahedral framework species by ammonia treatment [45]. Therefore, the sharp peaks are assigned to aluminum species, which are associated to the framework and possess a certain level of flexibility. Note that the concentration of this species was identical to the concentration of Lewis acid sites. The broad peak in the spectrum of H-LaX is assigned to a separate extraframework alumina phase outside of the zeolite pores.

Using the information obtained from the ^{27}Al MQMAS NMR spectra, the ^{27}Al MAS NMR spectra were simulated (Table 4.3). The concentration of aluminum in the vicinity of sodium cations and protons corresponds well with the sum of the sodium concentration as measured by AAS and the concentration of Brønsted acid sites as determined by IR spectroscopy of adsorbed pyridine. In case of H-LaX, the concentration of sodium cations was very low, while in case of H-LaY the concentrations of protons and Brønsted acid sites were approximately equal. However, the charges of most framework aluminum atoms were compensated by lanthanum cations.

By analyzing the spectrum of H-LaX approximately 4.5% of the aluminum atoms were found in octahedral coordination, which shows that during calcination dealumination occurred to a certain extent. Only a very small concentration of octahedral aluminum was observed in

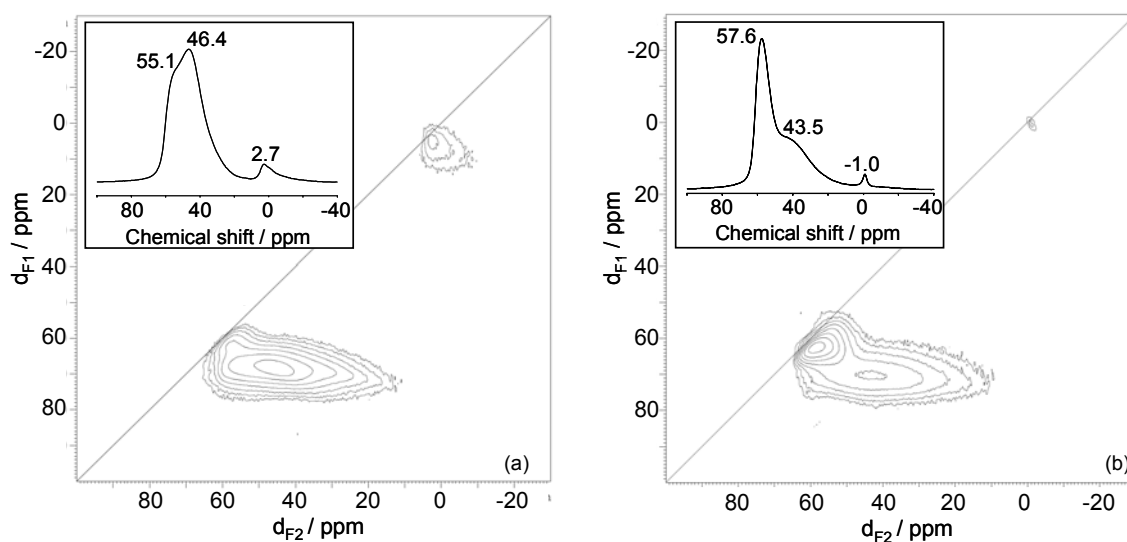


Figure 4.4: ^{27}Al MQMAS NMR and MAS NMR (inserts) spectra of hydrated samples: a) H-LaX and b) H-LaY

Table 4.3: Fitting parameters of the ^{27}Al MAS NMR spectra of hydrated H-LaX and H-LaY

Assignment	H-LaX			H-LaY		
	δ (ppm)	Average QCC (MHz)	Conc. (mmol/g) ^a	δ (ppm)	Average QCC (MHz)	Conc. (mmol/g) ^a
Td Al ³⁺ close to H ⁺ or Na ⁺	59	2.3	0.46	61	2.2	0.81
Td Al ³⁺ weakly distorted by La ³⁺	-	-	0.00	58	2.7	1.06
Td Al ³⁺ strongly distorted by La ³⁺	55	4.3	4.58	51	4.8	1.48
Flexible EFAl	6	2.3	0.10	1	1.6	0.03
Separate EFAl phase	2	3.1	0.13	-	-	0.00

^a - Based on the total Al concentration as determined by AAS

the spectrum of H-LaY indicating a higher thermal stability as a result of the higher Si/Al ratio of this material [46]. Moreover, the absence of a broad feature shows that no separate extraframework alumina phase was formed.

4.3.2. Performance in alkylation

The conversion of 2-butene vs. time on stream (TOS) over H-LaX and H-LaY is shown in Figure 4.5. Initially, the conversion was higher than 99%. Rapid deactivation started after ca. 7.5 and 14.3 h for H-LaY and H-LaX, respectively. This TOS will hereafter be referred to as catalyst lifetime. Note that the conversion with H-LaY decreased significantly faster than that with H-LaX.

Integral yields of different product groups are shown in Figure 4.6. In the beginning of the reaction (up to 7 h TOS) the integral yield of the C₈ fractions increased linearly. Note that at this stage the same yield (2.5 g_{cat}⁻¹) was reached over both catalysts. In the reaction over H-LaX the formation of C₈ products stopped within 2 hours from the end of the catalyst lifetime.

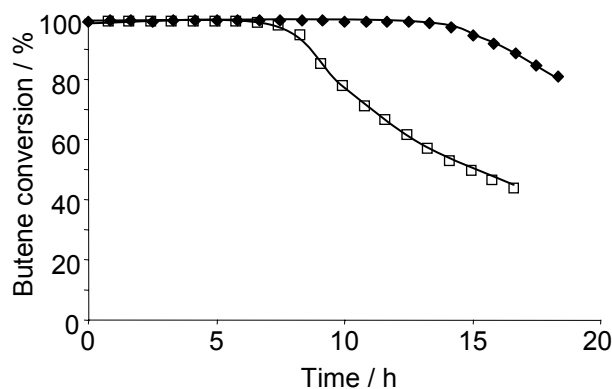


Figure 4.5: Conversion of 2-butene over H-LaX (◆) and H-LaY (□) at T = 348 K, p = 20 bar, P/O ratio = 10, OSV = 0.2 h⁻¹

In case of H-LaY the integral yield of C₈ products even decreased by ca. 15 % after the catalyst lifetime indicating that products are readsorbed and converted into different compounds. In total 6.2 and 2.4 grams of alkylate per gram of catalyst were produced in the reaction over H-LaX and H-LaY, respectively.

The rate of formation of C₅-C₇ products was almost identical for both catalysts before the deactivation of H-LaY started. Then, the same trends as for the C₈ fraction were observed, when deactivation started, namely a stop of C₅-C₇ production over H-LaX and a slight decrease of the yield over H-LaY.

The rate of formation of heavy products with 9 or more carbon atoms (C₉₊) was low in the beginning of the reaction, but increased steadily. During the catalyst lifetime more heavy products were formed over H-LaY. Moreover, the production of C₉₊ products continued for another hour after the yield of the other fractions started to decrease. Then, the yield remained constant until a small increase was observed again after 13 hours. The formation of heavy products was slower over H-LaX. In contrast to H-LaY, it continued when deactivation started.

In the reaction, with H-LaX four times as much n-butane was produced than with H-LaY. Note that the production of n-butane stopped after significantly shorter times on stream than the production of other hydrocarbons.

The distribution of the main compounds of the C₈ fraction is illustrated in Figure 4.7. During the catalyst lifetime an approximately linear increase of the yields with TOS was observed. In the reaction over H-LaX, the production of octane isomers stopped within two hours from the beginning of rapid deactivation. Note that 2,3,3-trimethylpentane and 2,3,4-trimethylpentane were produced for a slightly longer time. Over H-LaY, all octane isomers

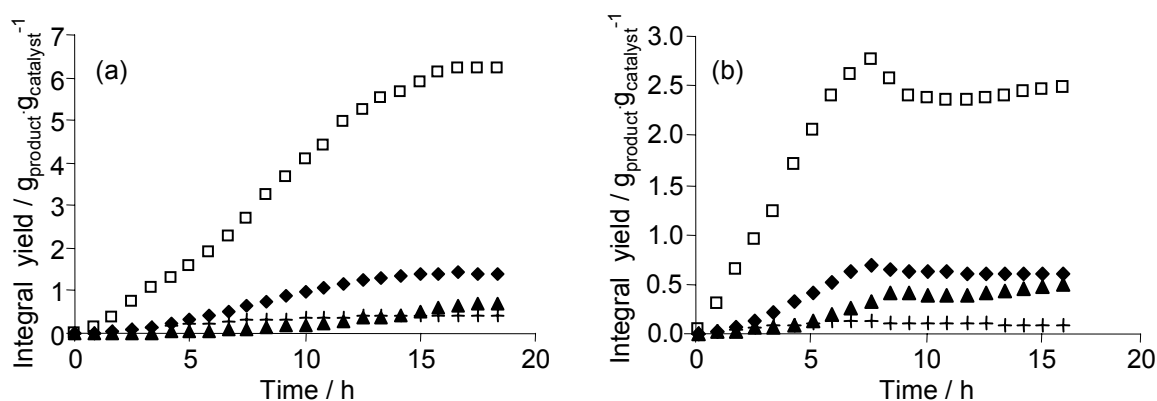


Figure 4.6: Integral product group yields over H-LaX a) and H-LaY b): C₅-C₇ (◆), C₈ (□), C₉₊ (▲) and n-butane (+)

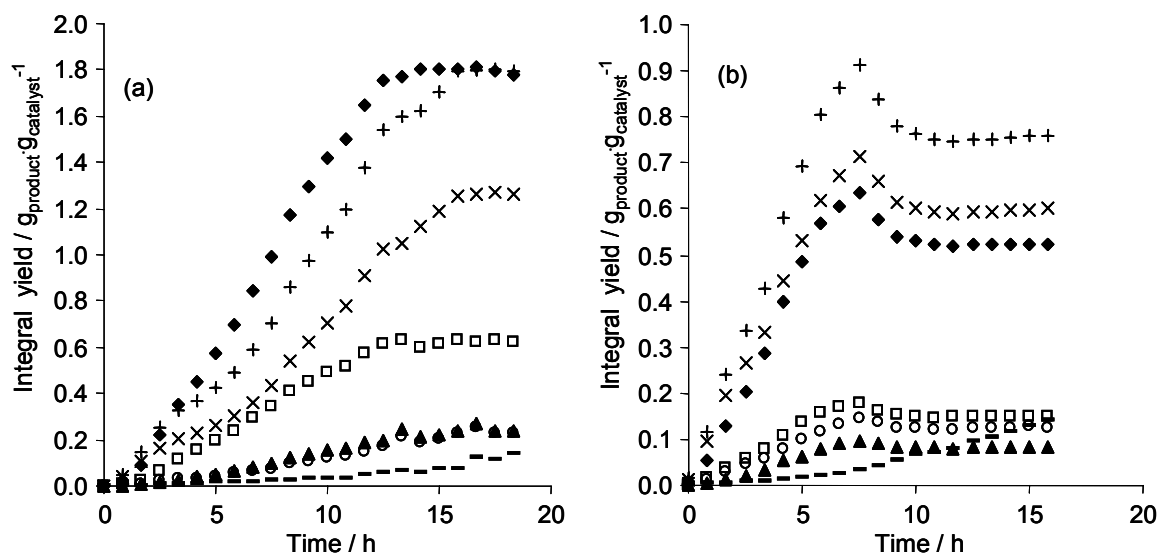


Figure 4.7: Integral yields of individual C₈ products over H-LaX a) and H-LaY b): 2,2,4-TMP (◆), 2,3,3-TMP (+), 2,3,4-TMP (x), 2,5-DMH/2,2,3-TMP (□), 2,3-DMH (○), 2,4-DMH (▲), C₈= (-)

were equally affected by the decrease of the integral yield, which was observed when deactivation started.

The trends for the integral yield towards various octane isomers and octenes are more obvious, when the differential selectivities within the C₈ fraction are considered (see Figure 4.8). The main products were 2,2,4-trimethylpentane (2,2,4-TMP), 2,3,3-trimethylpentane (2,3,3-TMP) and 2,3,4-trimethylpentane (2,3,4-TMP) together amounting to approximately 80% of the C₈ fraction during the catalyst lifetime. As reported by Feller *et al.*, the selectivity towards 2,2,4-TMP in the reaction over H-LaX increased in the beginning of the reaction and went through a maximum after ca. 6h [8]. It was the main product for most of the catalysts lifetime. The opposite trend was observed for the selectivities towards 2,3,3-TMP and 2,3,4-TMP, which went through a minimum after the same time. The peak corresponding to the primary product of isobutane/2-butene alkylation, 2,2,3-trimethylpentane (2,2,3-TMP), could not be separated from 2,5-dimethylhexane (2,5-DMH) but the low concentration of other dimethylhexane isomers led to the assumption that the greater part of the overlapping peaks is to be assigned to 2,2,3-TMP. The selectivity to 2,2,3-TMP (and/or 2,5-DMH) changed in parallel to the selectivity to 2,2,4-TMP. The selectivity towards other dimethylhexane isomers was nearly constants and it did not exceed 5% for any isomer. Only very small amounts of

methylheptane isomers and no n-octane were detected. After the end of the catalyst lifetime the selectivity towards octene isomers increased significantly.

Marked differences were observed between the two catalysts. In the reaction over H-LaY, the selectivities to 2,3,3-TMP and 2,3,4-TMP were significantly higher. The increase of the selectivity to 2,2,4-TMP with time on stream was much less pronounced than in the reaction over H-LaX. The selectivity to 2,2,3-TMP/2,5-DMH was less than half the value obtained over H-LaX. Moreover, the selectivities to less branched isomers were higher. The most important difference, however, was the significantly more pronounced increase of the selectivity to octene isomers after the end of the catalyst lifetime (7.5 h).

The trimethylpentane / dimethylhexane ratio is an indicator for the extent that alkylation is favored over dimerization (Figure 4.9). At the beginning of the reaction over H-LaX the TMP/DMH ratio was 19. It decreased steadily for the first 7 hours and stabilized then at a value of 10. When rapid deactivation started the TMP/DMH ratio decreased again. The TMP/DMH ratio of the reaction over H-LaY was consistently lower than over H-LaX. Moreover, the stabilization after the initial decrease was less pronounced.

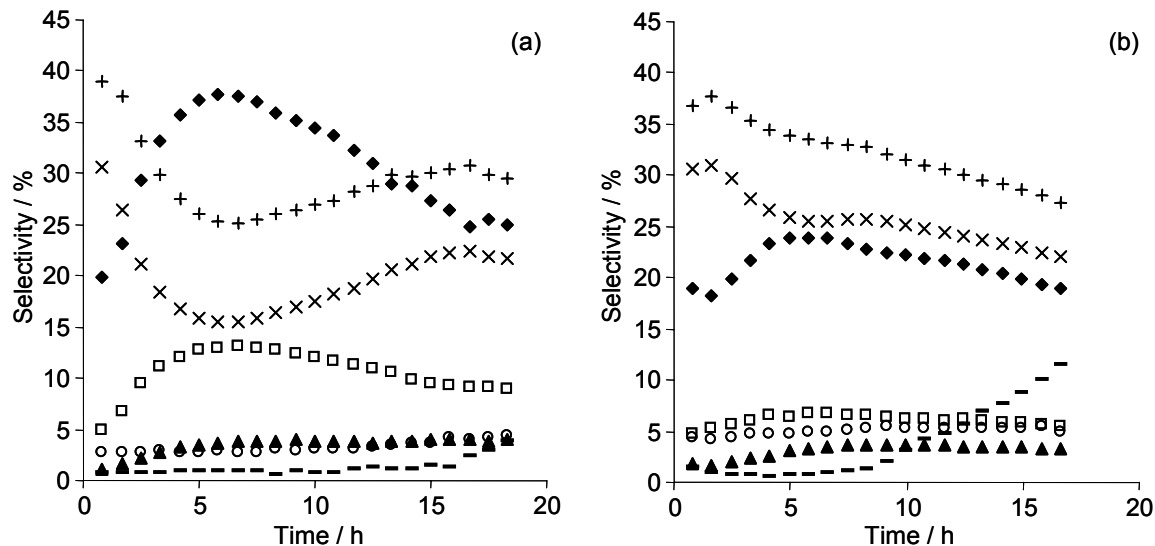


Figure 4.8: Differential Selectivities within the C₈ fraction over H-LaX a) and H-LaY b): 2,2,4-TMP (◆), 2,3,3-TMP (+), 2,3,4-TMP (x), 2,5-DMH/2,2,3-TMP (□), 2,3-DMH (○), 2,4-DMH (▲), C₈= (-)

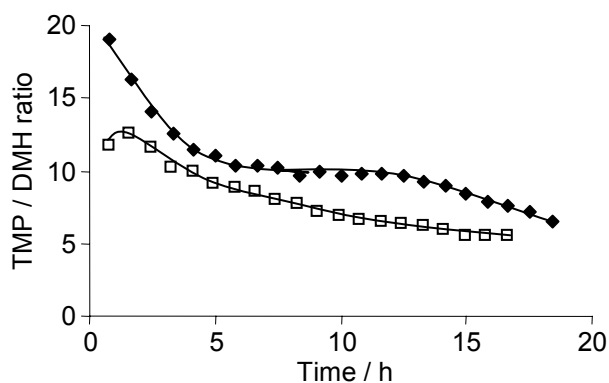
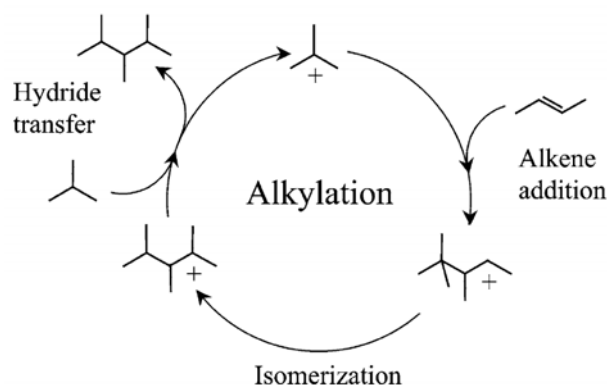


Figure 4.9: Trimethylpentane / dimethylhexane ratio for isobutane/2-butene alkylation over H-LaX (♦) and H-LaY (□)

4.4. Discussion

4.4.1. Catalytic performance

A simplified reaction mechanism for isobutane/2-butene alkylation is shown in Scheme 4.1 [8,47]. The main steps are olefin addition, isomerization and hydride transfer. The selectivity to octane isomers is determined by the relative rates of hydride transfer and olefin addition [23]. A high hydride transfer activity is necessary for obtaining a sufficient number of turnovers per active site. When the rate of olefin addition becomes too high, multiple olefin molecules are added to a carbenium ion before hydride transfer can take place and heavier products are formed, which play a key role in deactivation (see Chapter 5) [19,20]. Therefore, it is advisable to conduct the reaction with a low olefin concentration in the reactor. This is achieved by a high paraffin-to-olefin ratio in the feed and the use of a continuously operated stirred tank reactor (CSTR), which provides a high degree of backmixing [6].



Scheme 4.1: Simplified mechanism of isobutane/2-butene alkylation [8]

Lanthanum exchanged faujasites have previously been used as catalysts for isobutane/2-butene alkylation [8,9,13,20,21,33,34]. However, it is difficult to draw conclusions from a comparison of these studies due to differences in the operating conditions. Consistent data sets, in which the same conditions were applied for both samples, were published by Weitkamp *et al.* [9,21] and Feller *et al.* [8] agreeing on the point that H-LaY deactivates faster than H-LaX. However, the reasons for the differences of the catalytic performance were not discussed in these studies.

Faster deactivation of H-LaY was confirmed in the present study. Marked differences in the product distribution indicate that the relative rates of the reaction steps vary significantly. The distribution within the C₈ fraction is governed by the ratio of the rates of isomerization and hydride transfer to the particular carbenium ion [8]. Fast hydride transfer would lead to a high concentration of the primary product, 2,2,3-TMP, whereas isomerization would lead to a thermodynamic equilibrium of the carbenium ions on the catalyst. However, it has to be kept in mind that this does not necessarily mean that a thermodynamic product mixture is obtained, because the extent, to which steric hindrance affects hydride transfer to different carbenium ions, varies depending on the structure of the carbenium ion [8]. In the reaction over H-LaY the selectivity to the primary product 2,2,3-TMP was less than half as high than in the reaction over H-LaX. This is a strong indication for a higher hydride transfer activity of H-LaX with respect to isomerization.

During most of the catalyst lifetime 2,2,4-TMP was the main product in the reaction over H-LaX, while the selectivity towards 2,2,4-TMP was significantly lower over H-LaY. Under the reaction conditions, which were applied in this study, 2,2,4-TMP is the thermodynamically favored product. Therefore, a high concentration of 2,2,4-TMP can be seen as an indicator for a low hydride transfer/isomerization ratio. However, 2,2,4-TMP can also be formed *via* self alkylation (*vide infra*). In the reaction over H-LaY the highest selectivities were observed for 2,3,3-TMP and 2,3,4-TMP, which are formed by hydride transfer to carbenium ions with much lower steric demand than that of the 2,2,3-trimethyl-3-pentyl carbenium ion, which would give the primary product 2,2,3-TMP.

In the beginning of the reaction, the first carbenium ions are formed by protonation of 2-butene molecules. The resulting secondary carbenium ion may abstract a hydride from an isobutane molecule and be released from the surface as an n-butane molecule. If this was the only mechanism for the formation of n-butane, the total yield of n-butane could not be higher than the concentration of Brønsted acid sites (0.35 mmol g⁻¹) [8]. However, this value was exceeded by a factor of 2.5 for H-LaY and 12 for H-LaX. Therefore, a different possibility for

freeing Brønsted acid sites must exist. Self alkylation has been suggested in literature as an explanation [8,12,18,19,48]. The most important step in this sequence is the deprotonation of a *tert*-butyl carbenium ion, which leads to the formation of isobutene. This frees a Brønsted acid site, on which another *n*-butene molecule will be protonated. The resulting isobutene molecule is added to a *tert*-butyl carbenium ion forming a 2,4,4-trimethyl-2-pentyl carbenium ion. If this carbenium ion abstracts a hydride from another molecule before it isomerizes, it is released as 2,2,4-TMP. The high selectivities towards *n*-butane and 2,2,4-TMP over H-LaX indicate that self alkylation has a significant influence on the product distribution. In consequence, the extent of self alkylation over H-LaY was much lower.

In addition to trimethylpentanes, the C₈ fraction contained dimethylhexane isomers. Under the experimental condition in this study it is likely that skeleton isomerization, which involves a cyclopropyl carbonium ion as transition state, does not play a significant role. Therefore, dimethylhexane isomers are concluded to form by dimerization of 2-butene. The TMP/DMH ratio indicated that this pathway is more relevant in the reaction over H-LaY, but the accumulated selectivity to dimethylhexane isomers remained below 20% at all times. The decrease of the TMP/DMH ratio in the regime of rapid deactivation indicates that the selectivity to dimerization increases at this stage. We conclude that the selectivity to dimerization products is relatively high when the number of available alkylation sites on the catalyst is limited. In general the differences in the selectivity over H-LaX and H-LaY are due to the higher rates of hydride transfer and self alkylation activity in the reaction over H-LaX.

The selectivity towards heavy products with nine or more carbon atoms (C₉₊) was much higher in the reaction over H-LaY. This indicates a lower ratio of hydride transfer to olefin addition. It is interesting to note that over both catalysts, deactivation started when an integral yield of 0.4 g_{C₉₊}·g_{catalyst}⁻¹ had been reached.

Another difference between the two catalysts is the fact that the production of C₉₊ products over H-LaX continued during the rapid deactivation indicating the existence of polymerization sites, which are not blocked in the same way as the alkylation sites (see Chapter 5). Taking the observation of a lattice independent alumina phase in H-LaX by ²⁷Al NMR into account, we suggest that polymerization over H-LaX can be catalyzed by an alumina phase, which is located outside the zeolite lattice (see Chapter 5).

In addition to the C₈ fraction and heavy products (C₉₊), a light fraction with 5 to 7 carbon atoms was found in the product mixture. The formation of these compounds must include a β-scission step of a carbenium ion with more than eight carbon atoms, as the reaction network of olefin addition and hydride transfer can only yield products with carbon numbers that are

multiples of four. It is commonly accepted in literature that only strong zeolitic Brønsted acid sites are capable of catalyzing cracking reactions [8,12]. During the lifetime of H-LaY the integral yield of C₅-C₇ products was identical for both catalysts. The formation of C₅-C₇ products stopped at the same time as the formation of C₈ products when deactivation started indicating that the same active sites are responsible for alkylation and cracking.

After the catalysts lifetime of H-LaY, some of the C₈ and C₅-C₇ products, which were left in the reactor, were consumed. There are two reaction pathways, which can explain this conversion. The first possibility is deprotonation followed by oligomerization. In line with this interpretation, the production of C₉₊ products continued for 1.5 h after the maximum in the C₈ and C₅-C₇ integral yield. However, the amount of C₉₊ products formed in this period only accounts for 20 % of the converted compounds. The remaining oligomers would have to be retained on the catalyst. Accumulation of carbonaceous deposits was indeed observed at this stage of the reaction over H-LaX (see Chapter 5). However, in the present case the deposits would amount to 27 % of the catalyst mass. Note that this number does not include deposits, which were formed during the catalyst lifetime. In contrast, most studies on fully deactivated faujasites reported coke contents of approximately 10 wt.% [19]. Therefore, it is likely that another reaction pathway is operative.

The second pathway for the conversion of C₈ and C₅-C₇ products is cracking. As described in Chapter 3, lanthanum exchanged faujasites are capable of converting alkanes under the reaction conditions, which were applied in this study. As the decrease of the C₈ fraction is paralleled by the C₅-C₇ fraction, the cracking reaction would have to occur with a high selectivity to isobutane. This assumption is reasonable when the high selectivity to isobutane during the conversion of different octane isomers over H-LaX is taken into account (see Chapter 3). Therefore, it is assumed that at least a part of the consumed products is converted in cracking reactions.

4.4.2. Influence of physicochemical properties

Many studies on solid alkylation catalysts have focused on the correlations between the catalytic performance and the acidity of the catalyst. Nivarthi *et al.* found that the lifetime of zeolite H-BEA depends on the concentration of Brønsted acid sites [29]. In later studies various researchers showed that strong Brønsted acid sites are required for hydride transfer [8,14,26,49]. In particular, the ratio of strong Brønsted acid sites to total Brønsted acid sites was proposed as critical property of the catalyst [14,49]. In contrast to this, Diaz-Mendoza *et al.* suggested the medium strong Brønsted acid sites are the active centers for isobutane/2-

butene alkylation [30]. Weak Brønsted acid sites are not capable of catalyzing hydride transfer, but some of them are sufficiently strong to catalyze the polymerization of butene leading to deactivation of the catalyst (see Chapter 5) [50].

Thus, the strength of the Brønsted acid sites determines the conversion of the carbenium ion like species on the catalyst surface. Although the active species in isobutane/2-butene alkylation are commonly referred to as carbenium ions, their ground state is more appropriately described as alkoxy groups [51]. The formation of the transition state involves the heterolytic cleavage of the alkoxy bond. The energy required for this step largely depends on the capability of the zeolite lattice to stabilize the negative charge.

Pronounced differences were found for the acidity of H-LaX and H-LaY. Although both catalysts had the same concentration of Brønsted acid sites, H-LaX had a much higher concentration of strong Brønsted acid sites. Together with the product spectra, this shows that the strong Brønsted acid site in H-LaX give rise to a high hydride transfer and self-alkylation activity. Although weak Brønsted acid sites are not active for these reactions they may still catalyze oligomerization forming heavy products, which adsorb strongly on the zeolite and contribute to deactivation.

Several studies found that Lewis acid sites promote the formation of unsaturated compounds, which play a key role in the deactivation of the catalyst (see Chapter 5) [8,30]. Feller *et al.* suggested a high Brønsted to Lewis acid site ratio as a criterion for a good alkylation catalyst [8]. In contrast to this, a longer catalyst lifetime was found for H-LaX although its Brønsted to Lewis acid site ratio was only a third of the value found for H-LaY. The opposite trend was observed when only the strong acid sites were taken into account. In this case the Brønsted to Lewis acid site ratio was twice as high on H-LaX. Therefore, we conclude that Lewis acid sites must possess a minimum strength in order to catalyze the adverse reactions such as dehydrogenation or oligomerization. The extended lifetime of H-LaX shows that a considerable part of the Lewis acid sites in this material must have strength below this threshold. However, the high fraction of strong Lewis acid sites in H-LaY may play a major role for the decrease of the C₅-C₈ yield after the catalyst lifetime.

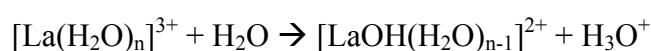
The influence of the Si/Al ratio on the catalytic performance of zeolites in isobutane/2-butene alkylation has been the subject of various studies [2,5,6,12]. In particular, in faujasites with a low Si/Al provides a long catalyst lifetime. This finding is supported by reports on increasing hydride transfer activity with decreasing Si/Al ratio for faujasites used as cracking catalysts [32]. The most straightforward approach would be to assign this observation to a high density of Brønsted acid sites. In metal exchanged zeolites the situation is more complex

because a part of the lattice charges is compensated by different cations. In the present case, the same Brønsted acid site concentration was observed for H-LaX and H-LaY despite the pronounced difference in their aluminum content. Therefore, a more complex correlation must exist between the Si/Al ratio and the catalytic performance (*vide infra*).

It is interesting in this context to note that Platon and Thomson suggested that the butene conversion over solids acids correlates well with the surface area instead of the acid site concentration [52]. In contrast to this, we found that the product yield and catalytic stability of H-LaY was much lower compared to H-LaX although the BET surface area of H-LaY was significantly larger and a comparable micropore volume was observed.

4.4.3. Influence of lanthanum exchange

Ion exchange with rare earth cations is a common procedure in synthesis of faujasite based catalysts. The main purpose of this modification is a stabilization of the zeolite framework [53]. The achieved effect is comparable to the stabilization by steaming in the synthesis of USY zeolites [36]. At temperatures above 333 K lanthanum cations start to migrate into the sodalite cages [34,35]. The preferred locations are the SI' and SII' position, which are located in the center of six membered rings adjacent to hexagonal prisms and supercages, respectively [36,54]. In addition to the stabilizing effect, rare earth cations are involved in the formation of Brønsted acid sites via hydrolysis [34,37,55]:



Cheetham *et al.* found that in calcined H-LaY every La^{3+} cation has an affiliated OH group [56]. Various studies reported that significantly lower ion exchange degrees are reached for NaY than for NaX [8,21]. In agreement with this, almost quantitative substitution of the sodium cations was achieved for H-LaX, while the ion exchange degree of H-LaY was only 87%. One of the reasons for the lower ion exchange degree in H-LaY is the lower concentration of aluminum in the zeolite framework. During ion exchange La^{3+} cations migrate into the pores replacing three sodium cations. In order to accommodate a La^{3+} cation, an environment is needed, in which three framework aluminum atoms are found close to each other.

It was shown by ^{29}Si MAS NMR that in H-LaX most silicon atoms have four aluminum atoms as next nearest neighbors. This results in a high probability of finding a suitable location for a trivalent cation. In H-LaY most silicon atoms only had 1 or 2 next nearest

aluminum neighbors and the Si/Al ratio of 2.4 is equivalent to an average of 1.7 Al atoms per six membered ring. In other words 30 % of the six membered rings in H-LaY only contain a single aluminum atom and, thus, a single lattice charge. Therefore, the number of appropriate sites for La^{3+} and $[\text{LaOH}]^{2+}$ cations is rather limited. In the six membered ring with only one aluminum atom in H-LaY the compensating cation will have the composition $[\text{La}(\text{OH})_2]^+$.

A high ion exchange degree was shown to be essential for a good catalyst lifetime in isobutane/2-butene alkylation [34]. Fritz and Lunsford found that sodium cations decrease the cracking activity of zeolite Y [57]. They showed that sodium cations selectively poison the acid sites, which are strong enough for hexane cracking. H-LaY still contains a number of Brønsted acid sites which are strong enough to catalyze alkylation. However, rate of hydride transfer over these sites is lower than that observed over the stronger Brønsted acid sites in H-LaX (*vide supra*).

An alternative explanation for the observation of stronger Brønsted acid sites in H-LaX is the distortion of the zeolite framework, which is induced upon lanthanum exchange. Van Bokhoven *et al.* assigned this effect to an increase of the bond angles of Si-O-Si and Si-O-Al [36]. The spectrum of H-LaY contained an additional peak for tetrahedrally coordinated framework aluminum atoms. The charge of these atoms is compensated by lanthanum cations, but it only experiences weak distortion. We suggest that the weak distortion is observed for those framework aluminum atoms having the charge compensated by the monovalent $[\text{La}(\text{OH})_2]^+$ cation, whereas strong distortion is induced to aluminum atoms with La^{3+} and $[\text{LaOH}]^{2+}$ as charge compensating cations. A strong effect on the strength of a Brønsted acid site will only be achieved if it is located in the same six ring as the cation, which induces the distortion. Therefore, six rings containing three framework aluminum atoms are required for the formation of a strong Brønsted acid site. Two framework charges will be compensated by a $[\text{La}(\text{OH})_2]^+$ cation, while the proton compensates the remaining one.

Theoretical studies showed that an increase of the Si-O-Al angle leads to an increase of the acidity of a bridging hydroxyl group [58,59]. This is explained by changes of the hybridization on the bridging oxygen atom. An increase of the Si-O-Al angle leads to an increasing s-character of the O-T (T = Si, Al) bonds. Consequently, the p-character of the O-H bond increases so that this bond is weakened and the acidity of the proton is increased.

It has also been suggested that the polyvalent cations withdraw electron density from the zeolite lattice and, hence, increase the polarity of the O-H bond [36,53]. Strictly, the extent of this effect would depend on the polarization power of the charge compensating cation.

However, the cation with the highest polarization power is a proton. Yet the strength of Brønsted acid sites in zeolites with a high concentration of protons is surprisingly low.

4.5. Conclusions

H-LaX and H-LaY having the same pore structure but different Si/Al ratio are compared as catalyst in the isobutane/2-butene alkylation. The same ion exchange procedure resulted in a significantly lower exchange degree in H-LaY than in H-LaX. In the reaction over H-LaX (Si/Al = 1.1) the catalyst lifetime and the integral yield of octane isomers were twice as high as in the reaction over H-LaY (Si/Al = 2.4). The product distribution indicated that hydride transfer and self-alkylation proceed significantly faster over H-LaX. Moreover, in the reaction over H-LaY, C₅-C₈ were converted to undesired side products after the catalyst lifetime, which may be explained by deprotonation followed by oligomerization or by cracking to isobutane. At the end of the lifetime of H-LaX the production of alkylates stopped immediately, but some activity for oligomerization of butene remained.

The differences in the catalytic performance are attributed to a higher concentration of strong Brønsted acid sites in H-LaX. The apparent contradiction to the general accepted decrease of the acid site strength with increasing aluminum concentration is explained by the high concentration of residual sodium cations in H-LaY, which have been shown to selectively poison the strongest Brønsted acid site of this zeolite. Additionally, the strength of Brønsted acid sites in H-LaX is increased by a strong distortion of the zeolite framework by La³⁺ and [La(OH)]²⁺ cations, which weakens the OH bond of bridging hydroxyl groups making them more acidic. The formation of such a site requires a six membered ring, which contains three framework aluminum atoms. The charges of two of these will be compensated by the [La(OH)]²⁺ cation, while the remaining one is compensated by a proton forming a Brønsted acid site. Due to its higher aluminum content H-LaX offers more sites, which can accommodate these cations. Moreover, the incorporation of polyvalent cations proceeds more efficiently on sites, where two or three framework aluminum atoms are found nearby each other.

The present results indicate that high ion exchange degree is crucial in the synthesis of a good alkylation catalyst. It is likely that H-LaY will show a significantly improved performance, if its ion exchange degree can be increased under optimized conditions.

4.6. Acknowledgement

The author thanks Martin Neukam for the AAS and BET measurements. The author thanks Evgeny A. Pidko, Prof. Rutger van Santen for fruitful discussions, which were financially supported by the European Union in the framework of IDECAT work package 5 (Program Nr. NMP3-CT-2005-011730).

4.7. References

- [1] L.F. Albright, *Ind. Eng. Chem. Res.* 42 (2003) 4283.
- [2] J. Weitkamp, Y. Traa, *Catal. Today* 49 (1999) 193.
- [3] A. Corma, A. Martínez, *Catal. Rev.* 35 (1993) 483.
- [4] A. Feller, J.A. Lercher, *Adv. Catal.* 48 (2004) 229.
- [5] K. Yoo, P.G. Smirniotis, *Appl. Catal. A-Gen.* 227 (2002) 171.
- [6] K.P. de Jong, C.M.A.M. Mesters, D.G.R. Peferoen, P.T.M. van Brugge, C. de Groot, *Chem. Eng. Sci.* 51 (1996) 2053.
- [7] A. Corma, A. Martínez, P.A. Arroyo, J.L.F. Monteiro, E.F. Sousa-Aguiar, *Appl. Catal. A-Gen.* 142 (1996) 139.
- [8] A. Feller, A. Guzman, I. Zuazo, J.A. Lercher, *J. Catal.* 224 (2004) 80.
- [9] R. Josl, R. Klingmann, Y. Traa, R. Gläser, J. Weitkamp, *Catal. Commun.* 5 (2004) 239.
- [10] Y. Zhuang, F.T.T. Ng, *Appl. Catal. A-Gen.* 190 (2000) 137.
- [11] C.A. Querini, E. Roa, *Appl. Catal. A-Gen.* 163 (1997) 199.
- [12] A. Corma, A. Martínez, C. Martínez, *J. Catal.* 146 (1994) 185.
- [13] C. Flego, I. Kiricsi, J. Parker, W. O., M.G. Clerici, *Appl. Catal. A-Gen.* 124 (1995) 107.
- [14] M. Stöcker, H. Mostad, T. Rørvik, *Catal. Lett.* 28 (1994) 203.
- [15] T. Rørvik, H. Mostad, O.H. Ellestad, M. Stocker, *Appl. Catal. A-Gen.* 137 (1996) 235.
- [16] K.S. Yoo, P.G. Smirniotis, *Catal. Lett.* 103 (2005) 249.
- [17] D.M. Ginosar, D.N. Thompson, K.C. Burch, *Appl. Catal. A-Gen.* 262 (2004) 223.
- [18] F. Cardona, N.S. Gnep, M. Guisnet, G. Szabo, P. Nascimento, *Appl. Catal. A-Gen.* 128 (1995) 243.
- [19] J. Pater, F. Cardona, C. Canaff, N.S. Gnep, G. Szabo, M. Guisnet, *Ind. Eng. Chem. Res.* 38 (1999) 3822.
- [20] A. Feller, J.-O. Barth, A. Guzman, I. Zuazo, J.A. Lercher, *J. Catal.* 220 (2003) 192.

-
- [21] R. Klingmann, R. Josl, Y. Traa, R. Gläser, J. Weitkamp, *Appl. Catal. A-Gen.* 281 (2005) 215.
- [22] L.M. Petkovic, D.M. Ginosar, *Appl. Catal. A-Gen.* 275 (2004) 235.
- [23] A. Feller, I. Zuazo, A. Guzman, J.O. Barth, J.A. Lercher, *J. Catal.* 216 (2003) 313.
- [24] D.N. Thompson, D.M. Ginosar, K.C. Burch, *Appl. Catal. A-Gen.* 279 (2005) 109.
- [25] D.N. Thompson, D.M. Ginosar, K.C. Burch, D.J. Zalewski, *Ind. Eng. Chem. Res.* 44 (2005) 4534.
- [26] A. Corma, A. Martinez, C. Martinez, *Catal. Lett.* 28 (1994) 187.
- [27] Y.F. Chu, A.W. Chester, *Zeolites* 6 (1986) 195.
- [28] K. Yoo, E. Burckle, P. Smirniotis, *Catal. Lett.* 74 (2001) 85.
- [29] G. Nivarthi, K. Seshan, J.A. Lercher, *Micropor. Mesopor. Mater.* 22 (1998) 379.
- [30] F.A. Diaz-Mendoza, L. Pernet-Bolano, N. Cardona-Martínez, *Thermochim. Acta* 312 (1998) 47.
- [31] A.F.H. Wielers, M. Vaarkamp, M.F.M. Post, *J. Catal.* 127 (1991) 51.
- [32] K.A. Cumming, B.W. Wojciechowski, *Catalysis Reviews - Science and Engineering* 38 (1996) 101.
- [33] J. Weitkamp, S. Maixner, *Zeolites* 7 (1987) 6.
- [34] A. Guzman, I. Zuazo, A. Feller, R. Olindo, C. Sievers, J.A. Lercher, *Micropor. Mesopor. Mater.* 83 (2005) 309.
- [35] E.F.T. Lee, L.V.C. Rees, *Zeolites* 7 (1987) 143.
- [36] J.A. van Bokhoven, A.L. Roest, D.C. Konigsberger, J.T. Miller, G.H. Nachttegaal, A.P.M. Kentgens, *J. Phys. Chem. B* 104 (2000) 6743.
- [37] P.B. Venuto, L.A. Hamilton, P.S. Landis, *J. Catal.* 5 (1966) 484.
- [38] J.W. Ward, *J. Catal.* 14 (1969) 365.
- [39] A. Simonits, F. Decorte, J. Hoste, *J. Radioanal. Nucl. Chem.* 24 (1975) 31.
- [40] X. Lin, F. Baumgärtner, X. Li, *J. Radioanal. Nucl. Chem.* 215 (1997) 179.
- [41] C.A. Emeis, *J. Catal.* 141 (1993) 347.
- [42] K. Gaare, D. Akporiaye, *J. Phys. Chem. B* 101 (1997) 48.
- [43] H. Klein, H. Fuess, M. Hunger, *J. Chem. Soc.-Faraday Trans.* 91 (1995) 1813.
- [44] J.-P. Amoureux, C. Fernandez, *Solid State Nucl. Magn. Reson.* 10 (1998) 211.
- [45] A. Omegna, J.A. van Bokhoven, R. Prins, *J. Phys. Chem. B* 107 (2003) 8854.
- [46] J. Klinowski, *Prog. Nucl. Magn. Reson. Spectrosc.* 16 (1984) 237.
- [47] L. Schmerling, *J. Am. Chem. Soc.* 68 (1946) 275.
- [48] M.F. Simpson, J. Wei, S. Sundaresan, *Ind. Eng. Chem. Res.* 35 (1996) 3861.

-
- [49] T. Rørvik, H.B. Mostad, A. Karlsson, O.H. Ellestad, *Appl. Catal. A-Gen.* 156 (1997) 267.
- [50] H.B. Mostad, M. Stöcker, A. Karlsson, T. Rørvik, *Appl. Catal. A-Gen.* 144 (1996) 305.
- [51] V.B. Kazansky, *Catal. Today* 51 (1999) 419.
- [52] A. Platon, W.J. Thomson, *Appl. Catal. A-Gen.* 282 (2005) 93.
- [53] R. Carvajal, P.-J. Chu, J.H. Lunsford, *J. Catal.* 125 (1990) 123.
- [54] D.H. Olson, G.T. Kokotailo, J.F. Charnell, *J. Colloid Interface Sci.* 28 (1968) 305.
- [55] A.P. Bolton, *J. Catal.* 22 (1971) 9.
- [56] A.K. Cheetham, M.M. Eddy, J.M. Thomas, *J. Chem. Soc.-Chem. Commun.* (1984) 1337.
- [57] P.O. Fritz, J.H. Lunsford, *J. Catal.* 118 (1989) 85.
- [58] J.B. Nicholas, R.E. Winans, R.J. Harrison, L.E. Iton, L.A. Curtiss, A.J. Hopfinger, *J. Phys. Chem.* 96 (1992) 10247.
- [59] I.N. Senchenya, V.B. Kazansky, S. Beran, *J. Phys. Chem.* 90 (1986) 4857.

Chapter 5

Stages of aging and deactivation of zeolite H-LaX in isobutane/2-butene alkylation

The formation of carbonaceous deposits and their effect on ageing and deactivation of H-LaX during isobutane/2-butene alkylation at 348 K were investigated by stopping the reaction at different times on stream. Four stages of the reaction were identified, i.e., (1) stable alkylation, (2) deposit transformation, (3) slow deactivation and (4) rapid deactivation. Deposits mostly consist of bicyclic compounds and branched carbenium ions, which are formed already at the beginning of the reaction and block Brønsted acid sites. During the deposit transformation migration of smaller entities towards the pore mouth occurs. These cyclic compounds are further alkylated and lead subsequently to pore mouth plugging. In the subsequent stage of rapid deactivation the catalyst stopped producing alkylate and butene oligomerization was the main reaction leading to olefin desorption and massive deposit formation at the outside of the zeolite particles.

5.1. Introduction

Isobutane/2-butene alkylation is an important refining process for the production of a complex mixture of branched alkanes, which is an ideal blending component of gasoline. Currently, commercial alkylation processes operate with sulfuric or hydrofluoric acid as catalysts [1]. The acid consumption in the sulfuric acid based process may reach as much as 70-100 kg t⁻¹ [2]. The spent sulfuric acid must be worked up in a rather expensive treatment to remove hydrocarbons and water. Hydrofluoric acid, on the other hand, is highly toxic and forms aerosols so that its handling is rather difficult. Therefore, many countries do no longer allow building alkylation units, which use HF as catalyst. For this reason, considerable efforts have been made to develop novel alkylation catalysts, which are easier to handle and environmentally more friendly [2].

Among the broad variety of solid acids tested as catalysts for isobutane/butene alkylation [3], zeolites received the most attention. In general, the lifetime of zeolites increases with increasing acid site concentration [4]. In addition, Feller *et al.* demonstrated that a high ratio Brønsted/Lewis acid sites extends the lifetime [5]. On the other hand, fast deactivation was also observed for catalysts with very high Brønsted acidity, e.g., sulfated zirconia [6]. This is speculated to be linked to the high cracking activity of such materials. Zeolites with a three dimensional pore structure and large pores show higher time catalytic stability due to a higher diffusivity [7]. The most promising materials so far tested are based on zeolites Beta [4,8,9], X [5,10] and Y [4,11-20].

Despite the potential benefits presented by these catalysts, their industrial application is constrained by rapid deactivation due to the accumulation of carbonaceous deposits. Both poisoning of active sites [14] and pore mouth plugging [12,21] have been proposed as the reason for deactivation.

The main reason for deactivation is that, especially when the alkene concentration is high, the addition of an alkene molecule to a carbenium ion is faster than intermolecular hydride transfer. This problem can be partially solved by performing the reaction in a CSTR so that sufficient backmixing is provided and the olefin concentration is kept at a low level in the entire reactor volume [4]. Nevertheless, frequent regeneration steps are necessary to extend the total lifetime of a given catalyst to an acceptable length. In this respect, the patent literature suggests that as many as several hundred regenerations are needed for processes based on solid catalysts to be competitive with existing processes using H₂SO₄ and HF [22].

Various regeneration procedures, including extraction with supercritical fluids [19,23,24], combustion [12] and hydrogenative regeneration [25], have been published.

In this respect, a detailed knowledge of the product distribution and formation of carbonaceous deposits with time-on-stream (TOS) is mandatory to understand the deactivation mechanism(s) and, therefore, to design stable catalysts and efficient regeneration procedures. Various researchers have investigated the deactivation process using a combination of characterization techniques, such as IR [10,18,26], UV/Vis [7,14,25-27], ^{13}C -NMR [14,15,28], and ^1H -NMR spectroscopy [18,26], as well as temperature programmed oxidation [12] and matrix assisted laser desorption ionization-time of flight mass spectrometry (MALDI-TOF MS) [26]. However, the alkylation reaction was often carried out in fixed bed or batch reactors [7,8,11,12,14,18,19,28-32], in which the catalysts were exposed to high olefin concentrations and thus deactivated within minutes. In addition, only few studies investigated spent catalysts, which had not passed the stage of full olefin conversion [18,25,26]. However, as the number of data points was limited, no detailed time resolved picture was obtained.

In this chapter, the deactivation of zeolite H-LaX in isobutane/2-butene alkylation is investigated by a multi-technique study. In previous studies it was shown that this catalyst has one of the longest lifetimes among the zeolites [5], due to the high Brønsted/Lewis acid site ratio. The alkylation reaction was performed in a CSTR under optimized condition [5]. Deactivation was studied by stopping the reaction after different times on stream providing a time resolved picture of the physicochemical properties of the catalyst in contrast to previous studies, which focused on the investigation of catalysts after extended use.

5.2. Experimental

5.2.1. Catalyst preparation

La-exchanged zeolite X (LaX) was prepared from NaX (Si/Al = 1.2), which was provided by Chemische Werke Bad Köstritz. The parent material was ion exchanged twice in an excess of 0.2 M $\text{La}(\text{NO}_3)_3$ solution for 2h at 353 K. The zeolite was thoroughly washed with bi-distilled water and dried at room temperature. Finally the sample was calcined in air flow with a slow temperature ramp up to 723 K. After rehydration on air, three additional ion exchange steps followed by washing, drying, calcination and rehydration were performed.

5.2.2. Catalytic reactions

The alkylation reactions were performed in a continuously operated stirred tank reactor (CSTR). Prior to reaction, the catalyst was activated *in situ* at 453 K for 14 h in H₂. The reactor was then cooled to 348 K, pressurized to 20 bar and filled with pure isobutane (AIR LIQUIDE, 99.95%). The reaction was started by feeding a mixture isobutane/2-butene (Messer, 99.4%) with molar ratio 10/1. The olefin space velocity was $0.2 \text{ g}_{\text{butene}} \cdot \text{g}_{\text{catalyst}}^{-1} \cdot \text{h}^{-1}$ and the stirring rate 1600 rpm. The products were analyzed with a HP 6830 gas chromatograph equipped with an FID-detector and a 50 m DB-1 column. The products were collected and isobutane was evaporated after reaction. The remaining organic phase was analyzed by ¹H NMR spectroscopy on a Bruker AM 360 spectrometer using CDCl₃ as solvent.

In order to study the deactivation over time on stream, several catalytic experiments were performed and stopped after different times on stream (0.5, 1.9, 3.8, 5.7, 7.6, 9.5, 12.7, 15.8 h). After drying in nitrogen flow for 4 h at 348 K, the catalyst was removed from the reactor and stored under nitrogen.

5.2.3. Catalyst characterization

For atomic adsorption spectroscopy (AAS) 20-40 mg of each sample was dissolved in 0.5 ml of hydrofluoric acid (48%) and heated to 343 K until the entire liquid evaporated. The measurements were performed on a UNICAM 939 atomic absorption spectrometer. The carbon content of spent catalysts was measured by combustion analysis using an Elementar Vario EL analyzer.

The BET surface area and the micropore volume of the catalyst were determined by nitrogen physisorption on a PMI Automated BET Sorptometer. Prior to the measurements the samples were heated to 393 K for 2 h in vacuum.

Acid site concentrations were obtained from IR spectra of adsorbed pyridine. Prior to measurement, the samples were pressed in self supporting wafers and dried in vacuum at 373 K for 2 h to remove water and weakly adsorbed deposits. Such molecules are supposed to have negligible influence on the catalyst deactivation. Pyridine was adsorbed at 373 K with a pressure of 0.1 mbar until no changes were observed in the spectrum. After outgassing for 1 h to remove weakly physisorbed pyridine, a spectrum was recorded. For quantification, the molar extinction coefficients published by Emeis were used [33].

For MAS NMR measurements the samples were packed into a ZrO₂ rotor and spun at 15 kHz. The measurements were performed on a Bruker AV500 spectrometer with a resonance

frequency of 125.8 MHz for ^{13}C and 130.3 MHz for ^{27}Al . For ^{13}C MAS NMR, the sensitivity was enhanced by applying cross polarization [34]. The contact time was 5 ms. At least 40000 scans were recorded for a spectrum. The spectra were calibrated using the methine carbon atoms of adamantane as an external standard ($\delta = 29.47$ ppm). The ^{27}Al spectra were measured as the sum of 2400 scans with a recycle time of 250 ms. A $\pi/12$ pulse was applied for excitation. The ^{27}Al DOR-NMR measurements were performed on a Bruker AV750 with an outer spinning rate of 1300 Hz and an inner spinning rate of approximately 6 kHz. The resonance frequency for ^{27}Al was 195.5 MHz.

UV/Vis spectra were measured on a MCS 320 Zeiss spectrometer in the wavelength region from 190 to 500 nm. The results are reported as difference spectra, obtained by subtracting the spectrum of the fresh H-LaX zeolite.

For matrix-assisted laser desorption/ionization time-of-flight mass spectrometry (MALDI-TOF MS) 10 mg of the deactivated catalyst was suspended in 200 μl of a 1% trifluoro acetic acid solution, which was saturated with 2,5-dihydroxybenzoic acid (DHB). The mixture was placed in an ultrasonic bath for 15 min. From this suspension 2 μl were deposited on a sample holder. The samples were dried over night at room temperature. MALDI-TOF mass spectra were recorded using a Bruker Biflex III MALDI-TOF mass spectrometer equipped with a N_2 laser ($\nu = 337$ nm) operating at a pulse rate of 3 Hz. The ions were accelerated with pulsed ion extraction after delay of 50 ns by a voltage of 28.5 kV. The analyzer was operated in reflection mode, and the ions were detected using a microchannel-plate detector. Prior to measurement the mass spectrometer was calibrated with a polystyrene standard.

For the analysis of carbonaceous deposits the spent catalyst was dissolved in 40% HF solution. Excess HF was evaporated and the residue extracted with CH_2Cl_2 . Carbonaceous deposits formed from reaction at low temperatures were claimed to be completely soluble in organic solvents [18] and to remain unaltered after the treatment with hydrofluoric acid [35,36]. A Finnigan MAT 8200-GC-MS with an unpolar OV1 methylpolysiloxane column was used for the measurements. The detector was a II-MS with energy of 70 eV. 1 μl of the extracted sample was injected into the column at room temperature according to the “on column”-method. The temperature was first increased to 343 K for 3 min and then to 633 K (heating rate 10 $\text{K}\cdot\text{min}^{-1}$) for 15 min. For additional measurements the extracts were hydrogenated over night (10 bar H_2 , 298 K) using 6 mg of PtO_2 . Pater *et al.* demonstrated that 2,3-dimethyl-2-butene is quantitatively hydrogenated under similar conditions [18].

5.3. Results

5.3.1. Characterization of the fresh catalyst

The overall chemical analysis indicated a Si/Al ratio of 1.1. The apparent BET surface was $529 \text{ m}^2\text{g}^{-1}$ and the micropore volume $0.148 \text{ cm}^3\text{g}^{-1}$. The total concentrations of Brønsted and Lewis acid sites were 0.47 and 0.14 mmol g^{-1} , respectively. The concentrations of strong Brønsted and Lewis acid sites (pyridine molecules persisting evacuation at 723 K) were 0.018 and $0.037 \text{ mmol g}^{-1}$, respectively.

The ^{27}Al -MAS NMR spectra are shown in Figure 5.1. The overlapping peaks at 55 and 46 in the MAS spectrum (Figure 5.1a) correspond to aluminum nuclei with tetrahedral coordination. The former peak is assigned to Al with a proton, the latter with La^{3+} as charge compensation cation [37]. The ^{27}Al double rotation (DOR) NMR spectrum (Figure 5.1b) only showed one peak in this region indicating that the upfield shift of the second peak was caused by quadrupolar interactions due to a heavy distortion of the local environment by the lanthanum cation. It is concluded that charge compensation by La^{3+} does not alter the partial charge of the adjacent Al atoms significantly, but changes their local geometry. The signal at 3 ppm is assigned to octahedral Al, which is present in the form of an aluminum oxo-cluster or in a separate phase outside the zeolite pores [37,38]. In this region both spectra have approximately the same line shape indicating that a variety of chemically different octahedral Al species were present in H-LaX. Approximately 11 % of the Al atoms are concluded to be in an octahedral environment indicating that dealumination has occurred to a certain extent during ion exchange and calcination.

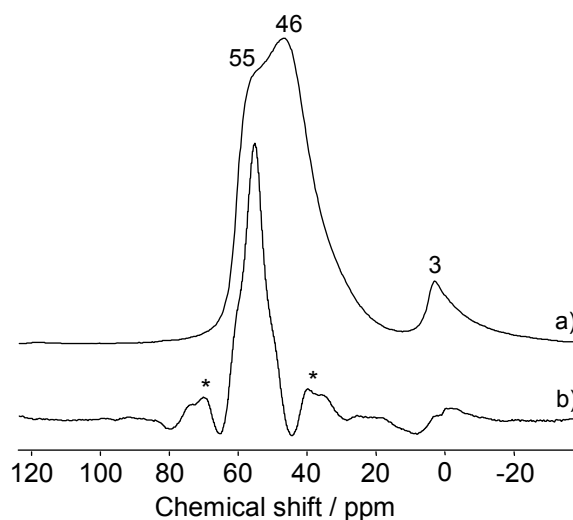


Figure 5.1: ^{27}Al MAS NMR spectra of hydrated H-LaX: a) ^{27}Al MAS NMR, b) ^{27}Al DOR NMR. Spinning side bands are marked with *

5.3.2. Catalytic experiments

In the beginning of the reaction complete conversion of 2-butene was observed (Figure 5.2). After 9.5 h the conversion dropped below 99%, but it only decreased slowly. Rapid deactivation started after 12.9 h. This point will hereafter be referred to as “catalyst lifetime”.

The integral product yield per weight of catalyst is shown in Figure 3. During the catalyst lifetime the product mixture is dominated by the C₈ fraction, which is formed with constant rate as indicated by the linear increase of the yield with time on stream (TOS) (Figure 5.3). The production of octanes stopped within two hours after the end of the catalyst lifetime. The same trend was observed for the C₅-C₇ fraction, which results from cracking of large carbenium ions (C₁₂ or larger) [5]. The production of heavy products (more than 9 carbon atoms) accelerated somewhat after 6 h TOS and continued for at least 3 h after the end of the catalyst lifetime.

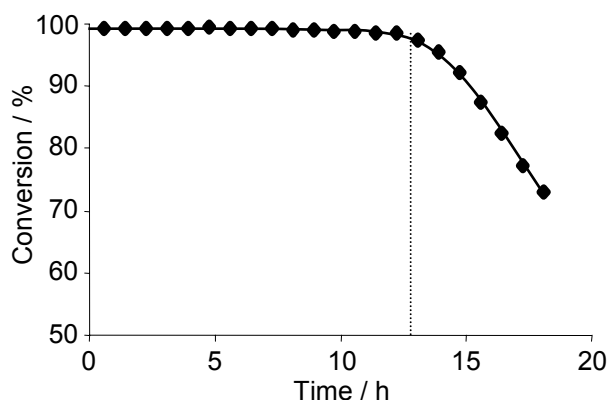


Figure 5.2: Conversion of butene during alkylation over H-LaX at 348K

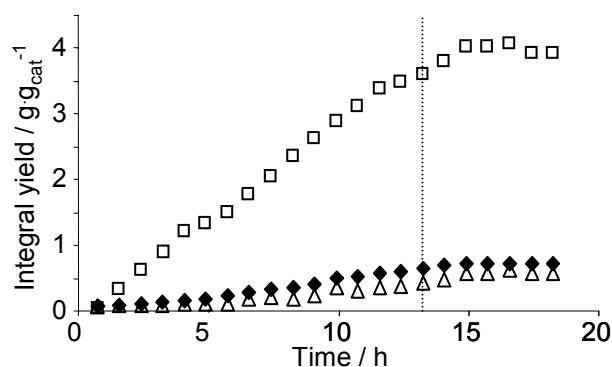


Figure 5.3: Integral product group yield during alkylation over H-LaX at 348K: (◆) C₅-C₇, (□) C₈, (Δ) C₉₊

The C₈ fraction mainly consists of trimethylpentane isomers (Figure 5.4). Note that only small amounts of 2,2,3-trimethylpentane – the primary product of the addition of butene to a *tert*-butyl carbenium ion – were formed. This shows that isomerization by methyl group shift is significantly faster than hydride transfer. Feller *et al.* explained that steric hindrance by the *tert*-butyl group renders hydride transfer to the corresponding carbenium ion unfavorable [5]. Figure 5.4 shows that the production of most C₈ products was constant and stopped within two hours after the end of the lifetime.

A different trend was observed for octene isomers (Figure 5.5). During the catalyst lifetime the C₈ fraction contained at best 0.5 wt.% of olefins. This concentration increased drastically after the end of the catalyst lifetime indicating that at this stage dimerization of butene was the dominant reaction while the alkylation activity of the catalyst had ceased completely. A more detailed study on the product distribution has been published elsewhere [5].

The concentration of aromatics in the product stream was investigated by ¹H NMR (Figure 5.6). For the first 7.6 h on stream the concentration of aromatic protons was constant at approximately 15 ppm. After that a strong increase was observed. Note that these concentrations are integral values. Therefore, the increase of the selectivity towards aromatic products is more pronounced than it appears from Figure 6.

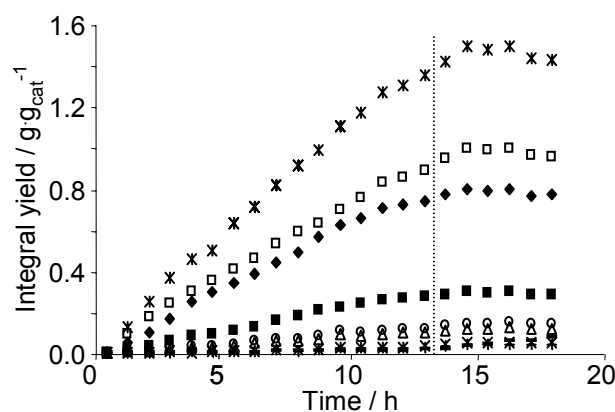


Figure 5.4: Integral yield of octane and octene isomers during alkylation over H-LaX at 348K: (*) 2,3,3-TMP, (□) 2,3,4-TMP, (◆) 2,2,4-TMP, (■) 2,5-DMH/2,2,3-TMP, (○) 2,3-DMH, (△) 2,4-DMH, (x) 3,4-DMH, (-) octene isomers

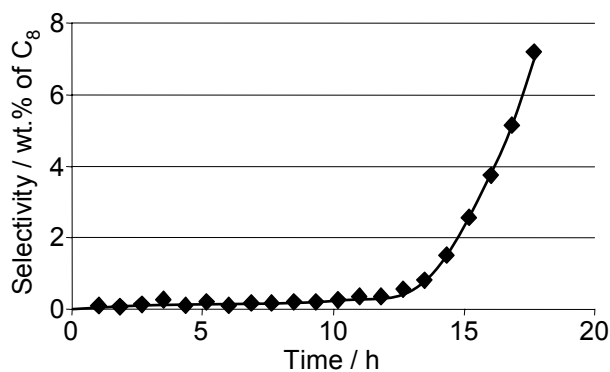


Figure 5.5: Concentration of octene isomers in the C₈ fraction (wt %)

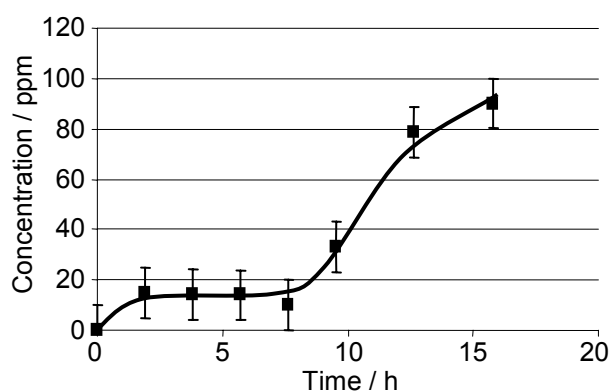


Figure 5.6: Concentration of aromatic protons in the alkylate collected after alkylation over H-LaX at 348K (measured by ¹H NMR)

5.3.3. Characterization of spent catalysts

Figure 5.7 shows the carbon content of the catalyst as a function of TOS. In the first 1.9 h the carbon content increased to a value of approximately 5.5 wt.%. This loading remained constant until 9.5 h on stream. Afterwards it increased again reaching a value of 10.0 wt.% after 15.8 h.

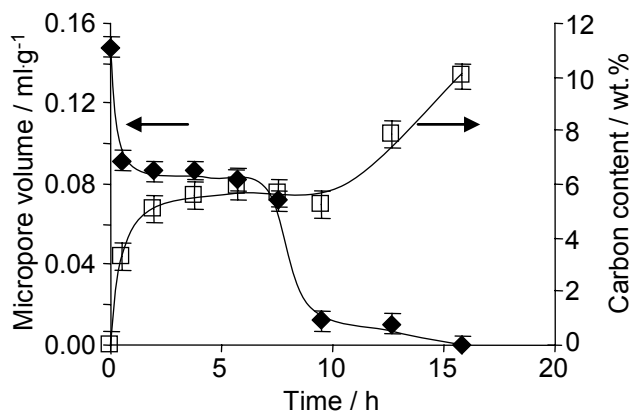


Figure 5.7: Carbon content (□, measured by combustion analysis) and micropore volume (◆, determined by N₂ adsorption) of H-LaX after alkylation

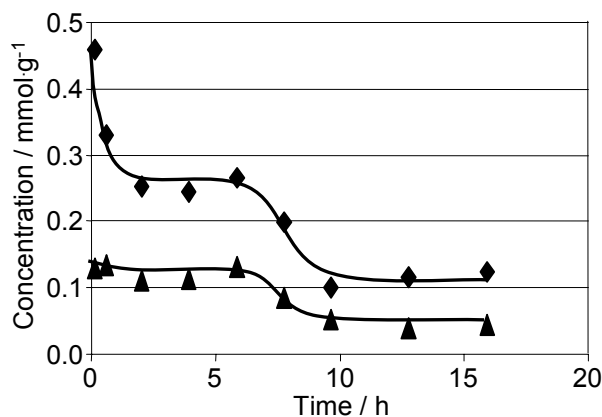


Figure 5.8: Concentration of free acid sites on H-LaX vs. TOS (measured by IR spectroscopy of adsorbed pyridine); (●) Brønsted acid sites, (▲) Lewis acid sites

As shown in Figure 5.7, in the first 1.9 h on stream the micropore volume decreased to slightly more than half of the original value and stabilized at this level. After 7.6 h the micropore volume decreased again until complete blockage of the micropores was observed after 15.8 h.

The concentrations of Brønsted and Lewis acid sites were determined by IR spectroscopy of adsorbed pyridine (Figure 5.8). In the first 1.9 h of the reaction the concentration of Brønsted acid sites available to adsorb pyridine decreased to approximately half of the initial value. However, only a small decrease of the Lewis acid site concentration was observed during this period. Between 1.9 and 5.7 h on stream the concentrations of Brønsted and Lewis acid sites remained unchanged. This period was followed by a decrease of the concentration of accessible Brønsted and Lewis acid sites between 5.7 and 9.5 h on stream. At this point, both concentrations were reduced to approximately half of their previous values. Afterwards they remained constant.

The nature of the deposits was investigated by ¹³C MAS NMR spectroscopy. To obtain spectra with an acceptable signal to noise ratio, cross polarization was used. Although this pulse sequence does not give quantitative results, it can be used to estimate the order of magnitude of a given signal [34,39]. Figure 5.9 shows the ¹³C NMR spectra of H-LaX after various times on stream. In agreement with the trends of the elemental analysis, only a very small increase of the overall intensity was observed between 3.8 and 9.5 h. In all samples the majority of the carbon atoms was found to be aliphatic. The peak position in the spectra between 3.8 and 9.5 h are identical. They are assigned to methyl groups at secondary carbon atoms (9 and 15 ppm), methyl groups at aromatic carbon atoms (18 ppm), methylene groups bound to methyl groups (23 ppm) and methylene groups in different paraffinic environment or methyl groups bound to quaternary carbon atoms (30 ppm) [28]. The relative intensity of the

peak at 18 ppm ($\text{CH}_3\text{-ar}$) increased with time on stream. In addition to these peaks, a shoulder was observed at 21 ppm. It is assigned to methyl groups bound to olefinic carbon atoms.

Between 9.5 and 15.8 h the intensity of the ^{13}C NMR signal increased sharply. In the spectrum corresponding to 15.8 h the peak were shifted by up to 1 ppm. The peak at 9 ppm was only observed as a weak shoulder. In addition to this, the shoulder at 21 ppm became more pronounced and an additional shoulder was observed at 32 ppm, which is assigned to methylene groups in paraffinic environment. The increase of the intensity of the paraffinic bands was mainly due to an increase of the secondary and tertiary carbon species (25-50 ppm), whereas the peaks of the different methyl groups increased more moderately. This is speculatively explained by the formation of naphthenic compounds.

In addition to the paraffinic peaks, a broad peak between 105 and 160 ppm was observed in all spectra. It is assigned to unsaturated carbon atoms of olefinic or aromatic compounds. The maximum of this peak was at approximately 135 ppm. Weitkamp et al. suggested to assign a peak in this position to substituted or bridged aromatics or olefins [28]. Due to the low concentration of aromatics in the products stream, it is more likely that this peak corresponds to olefinic carbon atoms. In the spectrum after 15.8 h on stream an additional peak at 153 ppm was observed. We tentatively assign this peak to highly substituted aromatic ring systems. Alternatively, the signal can be attributed to oxygen containing unsaturated species. In all NMR spectra the area of the peaks corresponding to unsaturated carbon atoms was approximately 8% of the total integral of the individual NMR spectrum.

The unsaturated deposits on the catalyst were further investigated by solid state UV/Vis spectroscopy (Figure 5.10). The band at the lowest wavenumber is assigned to monoenyl carbocations [40]. The position of this band shifted from approximately 300 nm for the first samples to 315 nm for the samples after 12.7 and 15.8 h on stream. The band at 380 nm is assigned to dienyl carbocations. Its position varied only little. At 470 nm a weak band was observed, which is assigned to trienyl carbocations.

In the two spectra recorded at short TOS (0.5 and 1.9 h) only the monoenyl band is well resolved. Between 3.8 and 9.5 h on stream all three bands were observed with some fluctuation of the relative intensities. A strong increase was observed for the monoenyl carbocation peaks after 12.7 h on stream while the trienyl band was not observed anymore. In the last spectrum the bands of monoenyl and dienyl carbocation increased strongly. This indicates that the formation of unsaturated deposits by dehydrogenation becomes a significant reaction pathway only in the end of the catalyst lifetime.

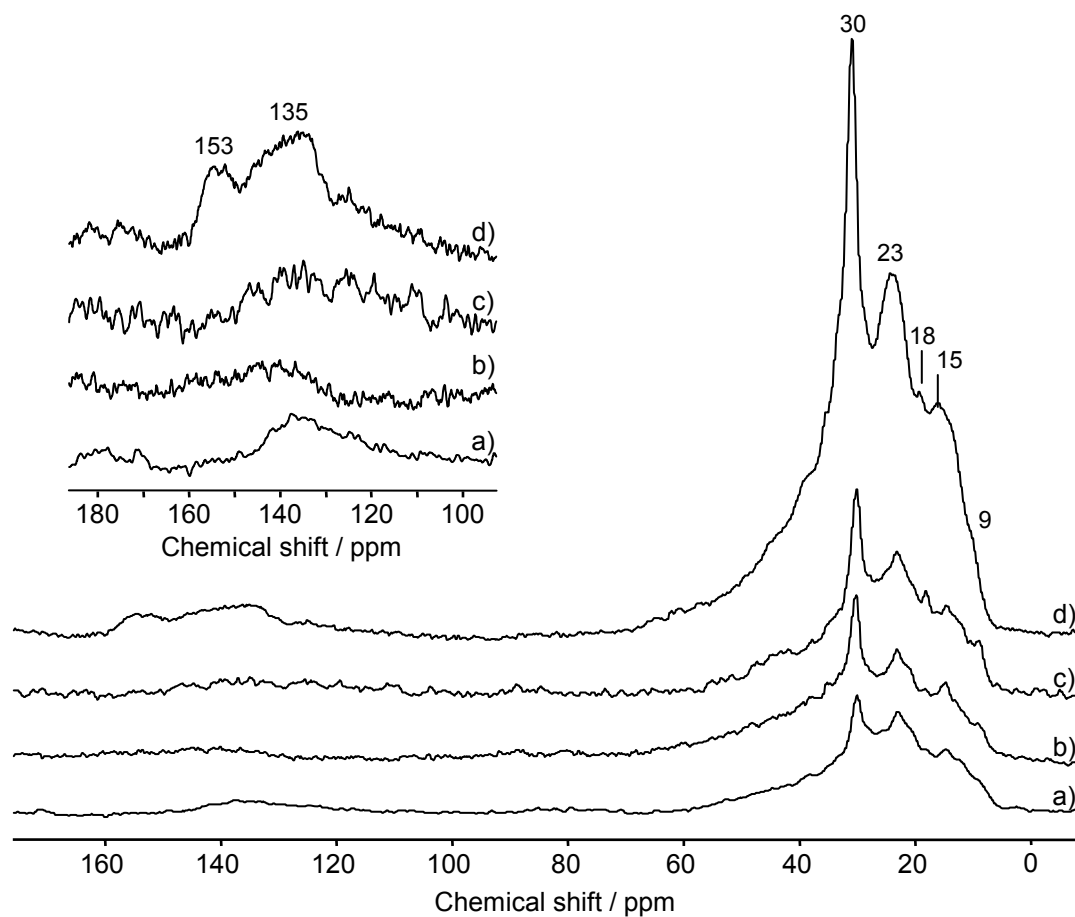


Figure 5.9: ^{13}C CP MAS-NMR spectra of spent H-LaX catalysts after alkylation at 348 K for (a) 3.8 h, (b) 7.6 h, (c) 9.5 h and (d) 15.8 h

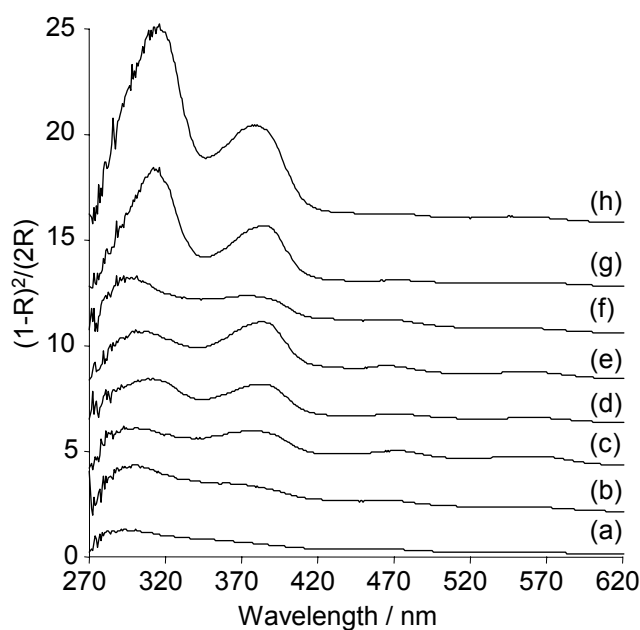


Figure 5.10: Solid state UV-VIS spectra of the spent H-LaX catalysts after alkylation for (a) 0.5 h, (b) 1.9 h, (c) 3.8 h, (d) 5.7 h, (e) 7.6 h, (f) 9.5 h, (g) 12.7 h and (h) 15.8 h

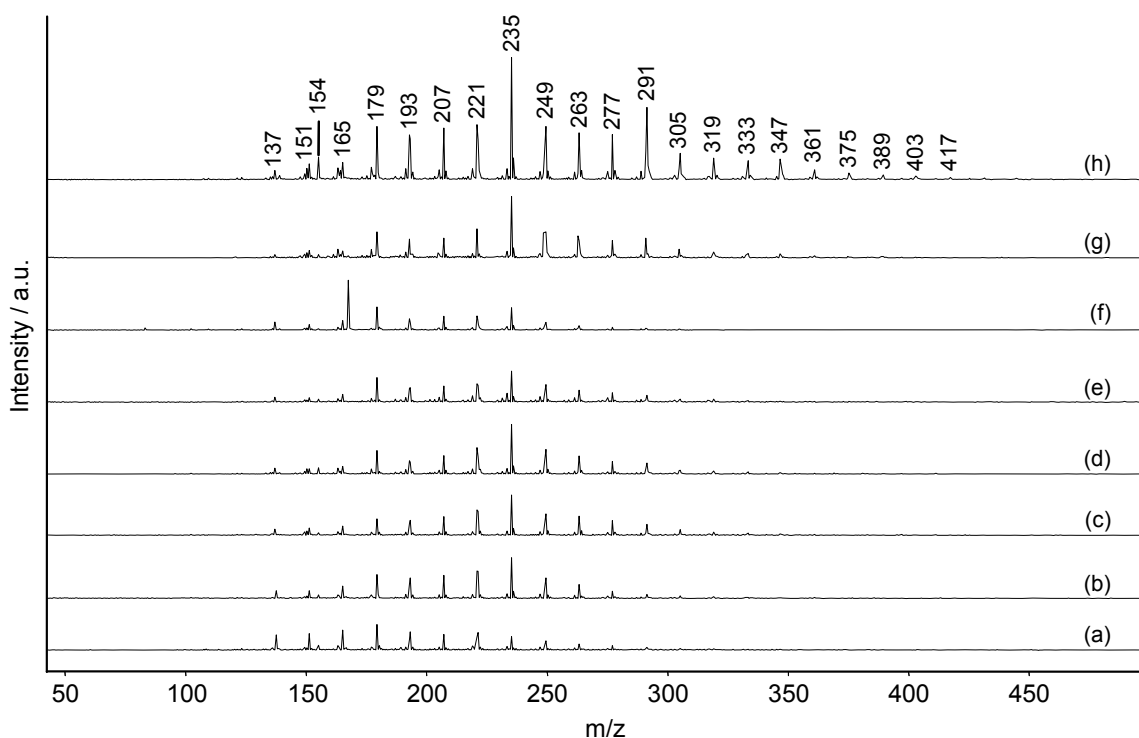


Figure 5.11: MALDI TOF mass spectra of spent H-LaX after (a) 0.5 h, (b) 1.9 h, (c) 3.8 h, (d) 5.7 h, (e) 7.6 h, (f) 9.5 h, (g) 12.7 h and (h) 15.8 h

The spent catalysts were characterized by MALDI-TOF MS, which has previously been applied to spent FCC [41,42] and alkylation [26] catalysts. With this methods protonated or cationized (addition of Na^+ or K^+) species are detected. The main drawback of MALDI TOF MS is that heteronuclear and unsaturated compounds are ionized significantly easier than saturated hydrocarbons [26,43]. Therefore, the spectra may represent minority species.

Figure 5.11 shows the MALDI-TOF mass spectra of the H-LaX catalysts after different times on stream, which were in good agreement with previous results [26]. The spectra are dominated by a sequence of peaks, which differ by 14 m/z. This difference corresponds to the addition of a CH_2 groups, in other words to the extension of an alkyl chain by one carbon atom or the replacement of a proton by a methyl group. Every fourth peak in this series was more pronounced. The smallest mass in this series was 137 m/z. Based on the assumption that protonated species are detected, this peak corresponds to the empirical formula $\text{C}_{10}\text{H}_{16}$ or $\text{C}_9\text{H}_{12}\text{O}$. In addition to the main series, two parallel series were observed, which were shifted by 2 m/z unit to lower masses and by 1 m/z unit to higher masses with respect to the main series. The first series corresponds to compounds with an additional double bond while the second one is tentatively assigned to molecules, which were ionized by losing an electron, thus, having the a mass, which is higher by 2 m/z compared to the main series.

Only a weak matrix peaks (DHB + H⁺) at 155 ppm was observed. Attenuation of this feature is generally associated to readily ionizable heterocompounds [44]. From this observation Feller *et al.* proposed that oxygenated compounds are formed during alkylation at 348 K [26]. However, we cannot exclude their formation during the preparation of the samples for MALDI-TOF MS measurement.

Only few differences were found in the intensities of the spectra up to 9.5 h on stream. Only the peaks corresponding to higher masses in the spectrum after 0.5 h were somewhat smaller than in the following spectra. After 12.7 h a small increase was observed, while the intensities of all peaks strongly increased after 15.8 h. At the same time the highest observed mass increased from 361 m/z after 9.5 h to 501 m/z after 15.8 h.

For further investigation of the deposits the spent catalysts were decomposed in HF. The carbonaceous deposits were extracted from the residue with CH₂Cl₂ and analyzed by GC/MS. In agreement with previous studies on USHY, it was found that the most abundant compounds had a composition of C_nH_{2n-4} indicating that they contain three double bonds or aromatic rings [18,20]. Compounds with the compositions C_nH_{2n-2} and C_nH_{2n-6} were also detected. The majority of the deposits had a carbon number, which was a multiple of 4. In all mass spectra strong peaks were observed for 43 and 57 m/z indicating that the corresponding molecules contained alkyl chains.

A part of the extracted phase was hydrogenated in order to differentiate between double bonds and cycles in the deposit molecules. After hydrogenation, the composition C_nH_{2n-2} was dominant. This indicates that most of the deposits are bicyclic molecules with one double bond [18]. Saturated compounds and molecules with two double bonds were observed in lower concentrations. Compounds with 9 to 40 carbon atoms were detected. The most abundant species had 24 to 32 carbon atoms. Due to the complexity of the mixture a precise quantification of the chromatograms was, however, not possible.

5.4. Discussion

5.4.1. Modification of the catalytic properties

Deactivation of zeolite based catalysts in isobutane/2-butene alkylation has been subject of several studies. However, there is still a dispute about the extent to which poisoning of active sites [14] and pore mouth plugging [12,21] contribute to catalyst deactivation. Several papers suggest that both routes contribute [25,26,45]. In this scenario deposits adsorb irreversibly on Brønsted acid sites, decreasing so the concentration of active sites for

alkylation. Therefore, the olefin concentration per active site increases and polymerization begins to dominate over alkylation. In turn, the formed polymers cause pore mouth plugging. However, these speculations have not been supported by measurements of the concentration of accessible Brønsted acid sites as a function of time on stream.

In most studies, catalysts, which had already passed the stage of full olefin conversion, were investigated [7,10-12,14,45,46]. This approach does not allow differentiating between modifications of the catalyst, which cause the deactivation, and those occurring after the catalyst has lost its alkylation activity. In order to obtain a comprehensive model of the deactivation process the present study focuses on the characterization of the used H-LaX catalyst after different times on stream.

Based on the product distribution and characterization of the spent catalysts, the alkylation of isobutane with 2-butene over H-LaX is divided in four stages, i.e., (1) stable alkylation, (2) deposit modification, (3) slow deactivation and (4) rapid deactivation.

At the beginning of the stage of stable alkylation carbenium ions are formed by protonation of 2-butene molecules. Subsequent olefin addition leads to the formation of octyl, dodecyl and hexadecyl carbenium ions. These reactions result in an increase of the carbon content and to a decrease of the micropore volume and Brønsted acid site concentration. Under the experimental conditions used steady state is reached after 1.9 h on stream. At this point the carbon content amounts to 5.5 wt. %, which would correspond to nearly 50 % micropore filling with isooctane using its liquid phase density. Note that this corresponds qualitatively to the measured decrease of the micropore volume using nitrogen adsorption. This situation remains stable until 5.7 h on stream.

In the second stage between 5.7 h and 9.5 h on stream, changes in the nature of the deposit must take place, while 2-butene is still completely converted. As the concentration of Brønsted and Lewis acid sites decreases, the total carbon content remains unchanged. This suggests that the chemisorbed species are smaller in nature, but distribute better throughout the material. In the last stage of this phase a drastic decrease of the micropore volume from 0.07 to 0.01 ml·g⁻¹ was observed, again without changes in the carbon content (see Figure 5.12). Thus, the deposit transforms further and/or migrates to the pore mouths blocking the entrance for nitrogen. As it will be discussed in detail below, significant modifications of the chemical composition of the deposits are not observed at this stage. Therefore, we conclude that bulky deposits block an increasing part of the pore volume.

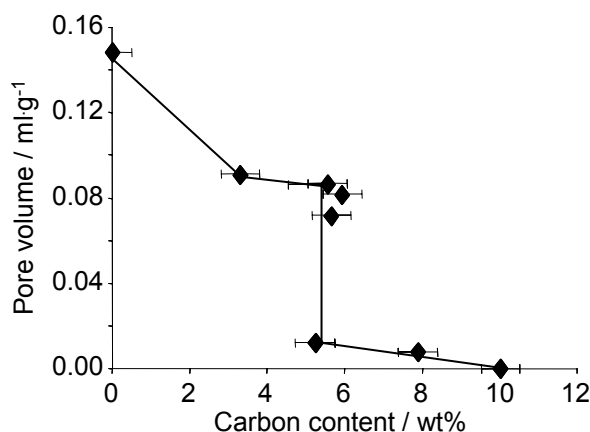


Figure 5.12: Correlation between micropore volume and the carbon content during isobutane/2-butene alkylation over H-LaX

The stage of slow deactivation starts after 9.5 h on stream, when the 2-butene conversion drops below 99% and decreases slowly but steadily. At the same time the carbon content increases strongly. As the pores were already half filled in the first two phases, this increase is attributed mainly to the formation of deposits outside of the pores. The completion of the micropore blocking is slow due to the three dimensional nature of the faujasite lattice. Despite the drastic decrease of the pore volume in this stage, most of the 2-butene entering the reactor was still converted and the product stream was still dominated by alkylation products. Therefore, the reaction is speculated to occur at a limited number of active sites close to the pore mouths.

After 12.9 h, the stage of rapid deactivation starts. Polymerization at the outside of the zeolite particles leads to a drastic increase of the carbon content. This is also shown by the increase of the concentration of octene isomers in the product stream, which result from the dimerization of 2-butene. The formation of deposits outside the zeolite pores completes the pore mouth plugging. In agreement with previous results, the micropores of H-LaX are completely blocked at this stage, but some of the deposits can still be replaced by pyridine [26]. Note in this context that a key role of pore mouth plugging was also suggested in a modeling study by Sahebdehfar *et al.* [21] indicating that pore mouth plugging is essential to explain the changes of the conversion over time.

5.4.2. Nature of the deposits

In agreement with previous studies we observed that the majority of the carbon atoms are aliphatic [14,15,18,28]. However, it has to be kept in mind that cross polarization (CP) NMR underestimates carbon atoms, which are not bound to hydrogen atoms [34]. The peak of

unsaturated carbon atoms amounted to 8% of the total intensity. This value is equivalent to one double bond per 25 carbon atoms. Note that this ratio remained constant over time on stream. The total intensity of the spectrum was in good agreement with the combustion analysis increasing very slightly between 3.8 and 9.5 h on stream and more strongly when the reaction proceeded further.

Despite the high concentration of saturated carbon atoms, it has been suggested that unsaturated compounds play a key role in the deactivation process [14,25]. This may be the case if a minority species irreversibly blocks the active sites of the catalyst. Various studies investigated deactivated zeolitic alkylation catalysts by UV-Vis spectroscopy [14,25,26]. In all studies enylic carbocations were observed on the used catalysts strongly adsorbed on Brønsted acid sites. Here, the bands of enylic cations modestly increased during the initial stage of the reaction, but their accumulation increased after the end of the catalyst lifetime. This indicates that enylic cations are already formed in the beginning of the reaction. It is interesting to note that the band of monoenylic cations remained constant after 1.9 h while the band of bienylic cations still increased and only remained constant after 3.8 h. Afterwards, the UV-Vis bands did not change dramatically until 12.7 h on stream. The initial increase of the concentration of enylic cations coincides with the decrease of strong acid sites. It appears however, through the further transformation that this may be at least in part a parallel process. We speculate that the zeolite catalyzes a slow dehydrogenation of the surface species through direct dehydrogenation [14] as well as through repeated hydride transfer steps [26].

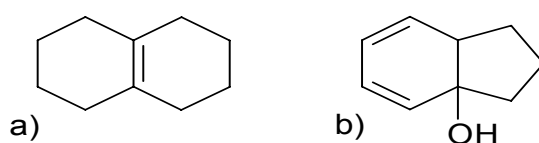
Only few studies suggested specific molecular structures for these deposits [7,18]. Yoo *et al.* identified various saturated and unsaturated cyclic structures for different zeolites [7]. Pater *et al.* investigated extracted deposits after alkylation over USHY by GC-MS and found bicyclic systems with one double bond as the dominant species [18]. Using the same approach we detected bicyclic compounds with 0, 1 or 2 double bonds. When a bicyclic molecule is protonated on a Brønsted acid site a tertiary carbenium ion will be the preferred product. Hydride transfer from an isobutane molecule to this carbenium ion will experience severe steric hindrance, in particular, when alkyl side chains are attached to the bicyclic system. Therefore, bicyclic compounds can efficiently block Brønsted acid sites. We assume that spontaneous desorption/deprotonation may be the more probable pathway to remove a bicyclic carbenium ion from a Brønsted acid site allowing migration of a different site.

The smallest masses found by GC mass analysis corresponds to compounds with 9 carbon atoms. However, compounds with a retention time similar to the solvent (CH_2Cl_2) may not be detected using this approach. This drawback was avoided with the MALDI-TOF-MS

measurements, in which the spent catalyst is only mixed with the matrix and deposited on the target. The smallest molecules detected by MALDI-TOF-MS had the sum formula $C_{10}H_{16}$ or $C_9H_{12}O$. Possible molecular structures are shown in Scheme 1. The sensitivity of bicyclic decene (Scheme 5.1a) is expected to be rather low as this molecule will lose its only π -system by protonation. Bicyclo-nona-dienol (Scheme 5.1b), on the other hand, maintains a double bond when protonated and contains an oxygen atom, which further enhances its sensitivity in the MALDI TOF MS experiment. Moreover, the suppression of the matrix peak is an indication for molecules containing hetero atoms [26,44]. Therefore, it is reasonable to assume that $C_9H_{12}O$ is the correct empirical formula for the lowest mass peak in the MALDI TOF mass spectra. This is confirmed by the observations from the GC/MS measurements where bicyclic compounds with 9 carbon atoms were also observed as the smallest molecules. The presence of oxygen in the deposit molecule, however, is attributed to an artifact resulting from a chemical process during dissolution of the spent zeolite with aqueous HF solution. The absence of alkenes in the MALDI TOF MS is attributed to the selectivity of the ionization process [43].

The periodicity in the MALDI TOF mass spectra indicates that most deposit molecules contain alkyl side chains, which are attached to the bicyclic ring system. These molecules are in consequence so bulky that they must be located at the pore mouth or at the outer surface of the zeolite so that at least parts of them are outside the microporous network of the zeolite.

The preference towards compounds with carbon number that are multiples of 4 shows that a considerable amount of the deposits is formed by oligomerization of butene without being affected by cracking. This observation is in apparent contrast to the fact that concentration of C_5 - C_7 products was 8-15 wt.% indicating that cracking of carbenium ions is an important reaction pathway. However, in case of these large deposit molecules cracking would need to occur far away from the site of being chemisorbed in order to contribute to the C_5 - C_7 products. Thus for such a reaction pathway, overall a di-cation needs to be formed, which is unlikely even in the environment with a high concentration of Brønsted acid sites. This in turn shows that cracking leading to C_5 - C_7 products preferentially would occur on smaller carbenium ions.



Scheme 5.1: Possible deposit molecules with a molecular mass of 136 m/z: a) $C_{10}H_{16}$, b) $C_9H_{12}O$

The largest detected masses correspond to molecules with 40 carbon atoms. These molecules contain long and bulky alkyl side chains. As MALDI-TOF MS measurements indicate that such molecules are located preferentially near or on the outer surface of the catalyst, we speculate that during the phase (2) bicyclic molecules migrate to the pore mouths, where the side chains are added. As all characterization methods suggest the absence of major changes in their nature in the deposits while the catalyst was still active, we conclude that migration of the deposits must play a key role for the deactivation by inducing pore mouth plugging.

These results suggest that the modification of the catalysts, which ultimately lead to deactivation, start after approximately 5.7 h on stream (under the current experimental conditions). For a long term stable operation of such solid catalysts regeneration has to set in at this point. This regeneration has to be very mild, because otherwise the cyclic compounds may rapidly dehydrogenation and may be very hard to remove.

5.5. Conclusions

The stages of the deactivation of H-LaX during isobutene/2-butene alkylation are described by characterization of the used catalyst after different times on stream. Four stages of the catalyst life have been identified, i.e., initiation and stable alkylation, deposit modification, slow deactivation and rapid deactivation.

During the induction period octyl, dodecyl and hexadecyl carbenium ions are formed by sorption of n-butene on Brønsted acid sites and subsequent alkylation or hydride transfer to isobutane and alkylation with n-butene. After this short period, the carbon content remains constant at 5.5 wt.% with approximately 50 % loading of the total pore capacity until 9.5 h on stream. With time the deposit transforms and redistributes into smaller entities, which eventually block nearly all Brønsted acid sites. At this stage, some molecules migrate towards the pore mouth leading to a significant reduction of the micropore volume by blocking. While this process continues these molecules are being alkylated forming larger deposits at the outer surface and pore mouth, which block the access to the micropores more affectively. For a limited time alkylation is observed on the acid sites, which are still accessible. Olefin addition at the outside of the zeolite increases in importance and leads to a rapid accumulation of deposits after the sites for alkylation are not accessible. Most of the deposit molecules are bicyclic systems with one or two double bonds and alkyl side chains. The nature of the deposits did not change significantly during the catalyst lifetime. Significant

amounts of aromatic compounds are only observed, when deactivation is apparent. This suggests that in addition to these processes dehydrogenation can take place either via hydrogen elimination from chemisorbed molecules or via multiple hydride transfer steps. To maintain long catalyst life zeolite catalysts should be regenerated before redistribution of the hydrocarbon sets in.

5.6. Acknowledgements

The author thanks Prof. Freude and Mr. Schneider for the ^{27}Al DOR-NMR measurements, and Mr. Krause for the GC-MS measurements and support for MALDI-TOF-MS measurements. I thank Patrick Magnoux for GC-MS reference measurements. Financial support from Süd-Chemie AG and Lurgi GmbH is gratefully acknowledged. The author thanks Dr. G. Burgfels and Dr. H. Buchold for fruitful discussions. Partial financial support by the European Union in the framework of NMP3-CT-2005-011730 IDECAT WP5 is gratefully acknowledged.

5.7. References

- [1] L.F. Albright, *Ind. Eng. Chem. Res.* 42 (2003) 4283.
- [2] J. Weitkamp, Y. Traa, *Catal. Today* 49 (1999) 193.
- [3] A. Feller, J.A. Lercher, *Adv. Catal.* 48 (2004) 229.
- [4] K.P. de Jong, C.M.A.M. Mesters, D.G.R. Peferoen, P.T.M. van Brugge, C. de Groot, *Chem. Eng. Sci.* 51 (1996) 2053.
- [5] A. Feller, A. Guzman, I. Zuazo, J.A. Lercher, *J. Catal.* 224 (2004) 80.
- [6] A. Corma, M.I. Juan-Rajadell, J.M. López-Nieto, A. Martínez, C. Martínez, *Appl. Catal. A-Gen.* 111 (1994) 175.
- [7] K. Yoo, E. Burckle, P. Smirniotis, *Catal. Lett.* 74 (2001) 85.
- [8] K. Yoo, P.G. Smirniotis, *Appl. Catal. A-Gen.* 227 (2002) 171.
- [9] A. Corma, A. Martínez, P.A. Arroyo, J.L.F. Monteiro, E.F. Sousa-Aguiar, *Appl. Catal. A-Gen.* 142 (1996) 139.
- [10] R. Josl, R. Klingmann, Y. Traa, R. Gläser, J. Weitkamp, *Catal. Commun.* 5 (2004) 239.
- [11] Y. Zhuang, F.T.T. Ng, *Appl. Catal. A-Gen.* 190 (2000) 137.
- [12] C.A. Querini, E. Roa, *Appl. Catal. A-Gen.* 163 (1997) 199.
- [13] A. Corma, A. Martínez, C. Martínez, *J. Catal.* 146 (1994) 185.

-
- [14] C. Flego, I. Kiricsi, J. Parker, W. O., M.G. Clerici, *Appl. Catal. A-Gen.* 124 (1995) 107.
- [15] M. Stöcker, H. Mostad, T. Rørvik, *Catal. Lett.* 28 (1994) 203.
- [16] T. Rørvik, H. Mostad, O.H. Ellestad, M. Stocker, *Appl. Catal. A-Gen.* 137 (1996) 235.
- [17] K.S. Yoo, P.G. Smirniotis, *Catal. Lett.* 103 (2005) 249.
- [18] J. Pater, F. Cardona, C. Canaff, N.S. Gnep, G. Szabo, M. Guisnet, *Ind. Eng. Chem. Res.* 38 (1999) 3822.
- [19] D.M. Ginosar, D.N. Thompson, K.C. Burch, *Appl. Catal. A-Gen.* 262 (2004) 223.
- [20] F. Cardona, N.S. Gnep, M. Guisnet, G. Szabo, P. Nascimento, *Appl. Catal. A-Gen.* 128 (1995) 243.
- [21] S. Sahebdehfar, M. Kazemeini, F. Khorasheh, A. Badakhshan, *Chem. Eng. Sci.* 57 (2002) 3611.
- [22] J. Weitkamp, Y. Traa, in: G. Ertl, H. Knözinger, J. Weitkamp (Eds.), *Handbook of Heterogenous Catalysis*, Wiley-VCH, Weinheim, 1997, Vol. 4, p. 2039.
- [23] D.N. Thompson, D.M. Ginosar, K.C. Burch, *Appl. Catal. A-Gen.* 279 (2005) 109.
- [24] D.N. Thompson, D.M. Ginosar, K.C. Burch, D.J. Zalewski, *Ind. Eng. Chem. Res.* 44 (2005) 4534.
- [25] R. Klingmann, R. Josl, Y. Traa, R. Gläser, J. Weitkamp, *Appl. Catal. A-Gen.* 281 (2005) 215.
- [26] A. Feller, J.-O. Barth, A. Guzman, I. Zuazo, J.A. Lercher, *J. Catal.* 220 (2003) 192.
- [27] I. Kiricsi, C. Flego, G. Bellussi, *Appl. Catal. A-Gen.* 126 (1995) 401.
- [28] J. Weitkamp, S. Maixner, *Zeolites* 7 (1987) 6.
- [29] K. Yoo, P.G. Smirniotis, *Appl. Catal. A-Gen.* 246 (2003) 243.
- [30] A. Platon, W.J. Thomson, *Appl. Catal. A-Gen.* 282 (2005) 93.
- [31] L.M. Petkovic, D.M. Ginosar, *Appl. Catal. A-Gen.* 275 (2004) 235.
- [32] K. Yoo, E.C. Burckle, P.G. Smirniotis, *J. Catal.* 211 (2002) 6.
- [33] C.A. Emeis, *J. Catal.* 141 (1993) 347.
- [34] C.E. Snape, B.J. McGhee, J.M. Andresen, R. Hughes, C.L. Koon, G. Hutchings, *Appl. Catal. A-Gen.* 129 (1995) 125.
- [35] P. Magnoux, P. Roger, C. Canaff, V. Fouche, N.S. Gnep, M. Guisnet, *Stud. Surf. Sci. Catal.* 34 (1987) 317.
- [36] M. Guisnet, P. Magnoux, *Appl. Catal. A-Gen.* 212 (2001) 83.
- [37] J.A. van Bokhoven, A.L. Roest, D.C. Konigsberger, J.T. Miller, G.H. Nachttegaal, A.P.M. Kentgens, *J. Phys. Chem. B* 104 (2000) 6743.

-
- [38] S.M.C. Menezes, V.L. Camorim, Y.L. Lam, R.A.S. San Gil, A. Bailly, J.P. Amoureux, *Appl. Catal. A-Gen.* 207 (2001) 367.
- [39] C.E. Snape, B.J. McGhee, S.C. Martin, J.M. Andresen, *Catal. Today* 37 (1997) 285.
- [40] H. Förster, J. Seebode, P. Fejes, I. Kiricsi, *J. Chem. Soc.-Faraday Trans.* 83 (1987) 1109.
- [41] J.O. Barth, A. Jentys, J.A. Lercher, *Ind. Eng. Chem. Res.* 43 (2004) 2368.
- [42] H.S. Cerqueira, C. Sievers, G. Joly, P. Magnoux, J.A. Lercher, *Ind. Eng. Chem. Res.* 44 (2005) 2069.
- [43] A.W. Ehlers, C.G. de Koster, R.J. Meier, K. Lammertsma, *J. Phys. Chem. A* 105 (2001) 8691.
- [44] R. Knochenmuss, F. Dubois, M.J. Dale, R. Zenobi, *Rapid Commun. Mass Spectrom.* 10 (1996) 871.
- [45] F.A. Diaz-Mendoza, L. Pernet-Bolano, N. Cardona-Martínez, *Thermochim. Acta* 312 (1998) 47.
- [46] C.A. Querini, *Catal. Today* 62 (2000) 135.

Chapter 6

Summary

6.1. Summary

Isobutane/2-butene alkylation is an important refining process for the production of high-octane fuels from light hydrocarbons. In recent literature, it was shown that lanthanum exchanged faujasites with a high aluminum content (H-LaX) have great potential for replacing hydrofluoric and sulfuric acid as catalysts in commercial isobutane/n-butene alkylation units. For this reason, there is a great interest in understanding the interaction of hydrocarbons with these materials. This will help to tailor future generations of refining catalysts with improved properties. However, premature catalyst deactivation by formation of carbonaceous deposits is a major problem of zeolites in isobutane/n-butene alkylation, which has prevented their industrial implementation so far. Therefore, detailed knowledge of the processes leading to deactivation is necessary to define appropriate process conditions for industrial plants and improve existing catalysts.

The aim of this thesis was to gain detailed insight in the interaction and conversion of hydrocarbons with lanthanum exchanged faujasites. The first part was focused on fundamental aspects of the interaction of alkanes with H-LaX. In the second part, lanthanum exchanged faujasite type zeolites were investigated as catalysts for isobutane/2-butene alkylation.

In Chapter 2, alkane isomers from butane to heptane were adsorbed on H-LaX and the interaction was investigated. The conditions were chosen close to the conditions, under which optimum catalytic performance for isobutane/2-butene alkylation was obtained in previous studies ($T = 348$ K). A mild activation procedure was applied, which left small amounts of physisorbed water on the catalyst. As in other zeolites, the interaction of the alkanes with the zeolite was dominated by van-der-Waals forces. The presence of La^{3+} cations increased the heat of adsorption markedly compared to HY zeolites. At high uptake, sorbate-sorbate interactions led to a further increase of the heat of adsorption. Due to a high loss of entropy these interactions were only observed, when complete pore filling was approached. The strongest interaction was found for n-alkanes, which obtained the best fit with the zeolite lattice. Molecules with quaternary carbon atoms showed the weakest interaction.

At low uptake, strong polarization of alkanes with at least 6 carbon atoms was indicated by an unusually high extinction coefficient of the C-H vibrations in the IR spectrum. This was mostly due to interaction of the sorbed molecules with Lewis acid sites. The polarization was particularly strong for molecules, which were branched in the 2 position. The investigation of the specific interaction of different parts of the sorbate molecule by ^{13}C MAS NMR

spectroscopy showed that a partial positive charge is induced on secondary and tertiary carbon atoms, which may be seen as intermediate to hydride abstraction. Moreover, it was shown that the coordination sphere of framework aluminum atoms associated with Brønsted acid sites was distorted upon interaction with sorbed alkanes. The presence of molecular water led to a blockage of the strongest adsorption sites, but it also contributed to the heat of adsorption of alkanes and surprisingly enhanced their polarization.

Chapter 3 describes the adsorption and surface chemistry of octane isomers on H-LaX under the same conditions as in Chapter 2. The polarization of the sorbed molecules was even stronger than that of the smaller molecules. When the coverage of bi- and tri-branched alkanes reached a critical value, chemical reactions were observed. Note that this occurred at a temperature of 348 K, which is surprisingly low for alkane activation. The reactivity increased with the degree of branching. The activation proceeded *on* Lewis acid sites *via* hydride abstraction forming carbenium ions/alkoxy groups. The abstracted hydride recombined with a proton from a Brønsted acid site to form dihydrogen. Two possible explanations are proposed for the existence of a critical uptake. Either it is necessary that adsorbed alkane molecules are forced into an entropically unfavorable position close to a Lewis acid site or a sufficient amount of mobile alkanes is needed to release the activated species from the surface by hydride transfer.

The surface chemistry and alkanes produced showed that adsorption, desorption, cracking, alkylation as well as hydride transfer reactions already occur at near ambient conditions.

In Chapter 4, H-LaX and H-LaY were compared as catalysts for isobutane/2-butene alkylation. Both zeolites had a faujasite type pore structure, but the Si/Al ratio was 1.1 for H-LaX and 2.4 for H-LaY. The catalysts were prepared from the sodium forms using the same ion exchange procedure. While almost complete ion exchange was observed for H-LaX, the ion exchange degree of H-LaY was only 87%. The reactions were performed in a continuously stirred tank reactor under industrially relevant conditions ($T = 348 \text{ K}$, $p = 20 \text{ bar}$, parafin/olefin ratio = 10, olefin space velocity = 0.2 h^{-1}). The lifetime and the integral yield of octane isomers in the reaction over H-LaX were approximately twice as high as the corresponding values over H-LaY. The product distributions indicated that H-LaX had a higher activity for hydride transfer and self alkylation. In the reaction over H-LaY, a part of the C_8 and C_5 - C_7 products was consumed after the catalyst lifetime, which can be explained by deprotonation followed by oligomerization or by cracking to isobutane. At the end of the lifetime of H-LaX, the production of alkylates stopped, but some activity for oligomerization of butene remained.

The higher concentration of strong Brønsted acid sites in H-LaX was identified as the key factor for the differences between H-LaX and H-LaY. The differences in the acidity are explained by the fact that H-LaY contained a considerable amount of residual sodium cations, which selectively poisoned strong Brønsted acid sites. The incorporation of lanthanum cations enhanced to the formation of strong Brønsted acid sites by increasing the Si-O-T (T = Al, Si) bond angles near their location. This change of the framework geometry led to weakening of the OH bond of bridging hydroxyl groups making them more acidic. In H-LaX, all framework aluminum atoms with lanthanum as charge compensating cation were affected by strong distortion, whereas in H-LaY, strong distortion was only experienced by 58% of the framework aluminum atoms, whose charges were compensated by lanthanum cations. The environment of the remaining aluminum atoms was only weakly distorted. It is suggested that $[\text{La}(\text{OH})_2]^+$ clusters are the charge compensating entities, which induce mild distortion, whereas strong distortion was caused by charge compensation with La^{3+} or $[\text{LaOH}]^{2+}$ clusters. Consequently, it was concluded that the formation of a strong Brønsted acid site requires an environment with at least three framework aluminum atoms. Due to the lower aluminum concentration in H-LaY, the probability of finding a suitable environment is much lower than in H-LaX.

In Chapter 5, the formation of carbonaceous deposits and their effect on ageing and deactivation of H-LaX during isobutane/2-butene alkylation at 348 K was investigated by stopping the reaction at different times on stream. Deposits consisted mostly of bicyclic compounds with one or two double bonds and alkyl side chains as well as branched carbenium ions. These deposits were formed already at the beginning of the reaction and their nature did not change during the catalyst lifetime.

Four stages of the reaction were identified, i.e., (1) stable alkylation, (2) deposit transformation, (3) slow deactivation and (4) rapid deactivation. During the stage of stable alkylation, carbenium ions were formed by protonation of 2-butene and subsequent olefin addition. During the deposit transformation stage, Brønsted acid sites were blocked and migration of smaller entities towards the pore mouth occurred. These cyclic compounds were further alkylated, which results in pore mouth plugging. During the subsequent phase of slow deactivation, the conversion of 2-butene decreased but alkylation still proceeded on a small number of acid sites, which were located on or near the outer surface of the catalyst. During the final stage of rapid deactivation, the catalyst stopped producing alkylate. Butene oligomerization was the main reaction leading to olefin desorption and massive deposit formation at the outside of the zeolite particles.

The present results show that lanthanum exchanged faujasite-type zeolites are interesting media for novel routes of low temperature acid / base chemistry. An improved understanding of the formation of strong Brønsted acid site in H-LaX and La-Y and the reactions leading to deactivation during isobutane/2-butene alkylation will provide guidance for the development of improved catalysts and appropriate process conditions for industrial isobutane/2-butane alkylation.

6.2. Zusammenfassung

Isobutan/2-Buten Alkylierung ist ein wichtiger Raffinerieprozess für die Produktion hochoktaniger Kraftstoffe aus leichten Kohlenwasserstoffen. In den letzten Jahren wurde gezeigt, dass Lanthan getauschte Faujasite mit hohem Aluminiumgehalt (H-LaX) das Potential haben, Flußsäure und Schwefelsäure als kommerzielle Katalysatoren für Isobutan/2-Buten Alkylierung zu ersetzen. Aus diesem Grund besteht ein großes Interesse an den Wechselwirkungen von Kohlenwasserstoffen mit diesen Materialien. Die gewonnenen Erkenntnisse bilden die Grundlage für die Entwicklung neuartiger Raffineriekatalysatoren mit verbesserten Eigenschaften. Derzeit ist die schnelle Deaktivierung durch die Bildung kohlenstoffhaltiger Ablagerungen ein großes Problem von Zeolithkatalysatoren in der Isobutan/2-Buten Alkylierung. Dies hat eine industrielle Anwendung bis jetzt verhindert. Die Erforschung der Prozesse, die zur Deaktivierung führen, ist daher notwendig, um geeignete Prozessbedingungen zu definieren und vorhandene Katalysatoren zu verbessern.

Das Ziel dieser Arbeit war es, ein detailliertes Verständnis der Wechselwirkungen und Reaktionen von Kohlenwasserstoffen mit Lanthan getauschtem Faujasiten zu erzielen. Der erste Teil der Arbeit konzentriert sich auf fundamentale Aspekte der Wechselwirkung von Alkanen mit H-LaX. Der zweite Teil behandelt die Untersuchung von Lanthan getauschten Faujasiten als Katalysatoren für Isobutan/2-Buten Alkylierung.

In Kapitel 2 wurden die Wechselwirkungen von Alkanisomeren von Butan bis Heptan mit H-LaX untersucht. Die Versuchsbedingungen wurden entsprechend dem Optimum der Katalysatorstabilität für Isobutan/2-Buten Alkylierung in früheren Studien gewählt ($T = 348$ K). Eine sanfte Aktivierungsmethode wurde gewählt, bei der geringe Mengen von physisorbiertem Wasser auf dem Katalysator verbleiben. Die Wechselwirkungen von Alkanen mit dem Zeolithgitter werden von van-der-Waals-Kräften dominiert. Darüber hinaus führte die Anwesenheit von La^{3+} -Kationen zu einer deutlichen Erhöhung der Adsorptionswärme im Vergleich zu HY Zeolithen. Bei hohen Beladungen erhöhte sich die Adsorptionswärme durch Sorbat-Sorbat Wechselwirkungen. Aufgrund des damit verbundenen Verlusts an Entropie werden diese Wechselwirkungen nur beobachtet, wenn die Poren des Zeoliths fast vollständig gefüllt sind. Die stärksten Wechselwirkungen wurden für n-Alkane beobachtet, welche sich am besten an das Zeolithgitter anpassen können. Moleküle mit quartären Kohlenstoffatomen zeigten schwächere Wechselwirkungen als andere Isomere.

Bei niedrigen Beladungen deuteten ungewöhnlich hohe Absorptionskoeffizienten der CH-Schwingungen im IR-Spektrum auf eine starke Polarisierung von Alkanen mit mindestens 6

Kohlenstoffatomen hin, welche primär durch die Wechselwirkung mit Lewissäurezentren hervorgerufen wird. Eine besonders starke Polarisierung wurde für Moleküle mit einer Verzweigung in der 2-Position beobachtet. Die Untersuchung der spezifischen Wechselwirkungen verschiedener Teile der Sorbatmoleküle mit ^{13}C MAS NMR Spektroskopie zeigte, dass bei der Adsorption positive Partialladungen an sekundären und tertiären Kohlenstoffatomen entstehen. Diese Polarisierung kann als Zwischenstufe zu einer Hydridabstraktion verstanden werden. Außerdem wurde gezeigt, dass die Koordinationssphäre von Gitteraluminiumatomen in der Nähe von Brønstedsäurezentren bei der Wechselwirkung mit sorbierten Alkanen verzerrt wird. Kleine Mengen an molekularem Wasser blockierten die stärksten Adsorptionszentren in H-LaX. Sie erhöhten aber auch die Adsorptionswärme adsorbierter Alkane und trugen überraschenderweise zu deren Polarisierung bei.

Das dritte Kapitel beschreibt die Adsorption und Oberflächenchemie von Oktanisomeren auf H-LaX unter den gleichen Bedingungen wie im zweiten Kapitel. Die Polarisierung der adsorbierten Oktanisomere war noch stärker als die von kleineren Molekülen. Wurde mit der Beladung mit zwei- und dreifach verzweigten Alkanen ein kritischer Wert erreicht, kam es zu chemischen Reaktionen. Dies passierte bei einer Temperatur von 348 K, welche für die Aktivierung von Alkanen ungewöhnlich niedrig ist. Eine erhöhte Reaktivität wurde für stärker verzweigte Moleküle beobachtet. Als Aktivierungsschritt wurde eine Hydridabstraktion durch Lewissäurezentren identifiziert. Dabei wird ein Carbeniumion bzw. eine Oberflächen-Alkoxygruppe gebildet. Das abstrahierte Hydrid verbindet sich mit dem Proton eines Brønstedsäurezentrums zu einem Wasserstoffmolekül. Es gibt zwei Erklärungsansätze für die Beobachtung einer kritischen Beladung. Entweder müssen adsorbierte Alkane in entropisch ungünstige Positionen in der Nähe von Lewissäurezentren gezwungen werden, oder eine bestimmte Menge an mobilen Alkanmolekülen ist nötig, um die aktivierten Oberflächenspezies durch Hydridtransfer freizusetzen. Die Oberflächenchemie und Produktverteilung zeigen, dass Reaktionsschritte wie Adsorption, Desorption, Cracking, Alkylierung und Hydridtransfer in Zeolithen schon bei außerordentlich milden Reaktionsbedingungen stattfinden.

Im vierten Kapitel wurden H-LaX und H-LaY als Katalysatoren für Isobutan/2-Buten Alkylierung verglichen. Beide Zeolithe haben eine Faujasitstruktur aber unterscheiden sich in ihrem Si/Al-Verhältnis, welches bei H-LaX 1.1 und bei H-LaY 2.4 war. Die Katalysatoren wurden unter den gleichen Bedingungen durch Ionenaustausch aus der jeweiligen Natriumform der Zeolithe hergestellt. Während dies bei H-LaX zu fast vollständigem

Austausch führte, wurde bei H-LaY nur ein Ionenaustauschgrad von 87% erreicht. Die Reaktionen wurden in einem kontinuierlich betriebenen Rührkesselreaktor unter industriell relevanten Versuchsbedingungen durchgeführt ($T = 348 \text{ K}$, $p = 20 \text{ bar}$, Isobutane/2-Buten Verhältnis = 10, Raumgeschwindigkeit von 2-Buten = 0.2 h^{-1}). Die Lebenszeit und die integrale Oktanausbeute der Reaktion mit H-LaX waren etwa doppelt so hoch wie die entsprechenden Parameter in der mit H-LaY katalysierten Reaktion. Die Produktverteilungen deuteten auf höhere Aktivitäten für Hydridtransfer und Selbstalkylierung bei H-LaX hin. Nach dem Ende der Lebenszeit von H-LaY wurde ein Teil der C_8 und C_5 - C_7 Produkte durch Nebenreaktionen abgebaut. Dabei könnte es sich um eine Kombination aus Deprotonierung und Oligomerisierung oder Cracking zu Isobutan handeln. Nach dem Ende der Lebenszeit von H-LaX blieb die Ausbeute an Alkylierungsprodukten unverändert. Es wurde aber noch eine Restaktivität für die Oligomerisierung von Buten beobachtet.

Die höhere Konzentration von starken Brønstedsäurezentren in H-LaX wurde als der entscheidende Faktor für die Unterschiede in der Reaktivität von H-LaX und H-LaY identifiziert. Der Grund für die unterschiedliche Säurestärke war, dass in H-LaY noch eine beträchtliche Menge Natriumkationen vorhanden ist, die selektiv die stärksten Brønstedsäurezentren vergiften. Außerdem führt der Einbau von Lanthankationen in die Zeolithe zu einer Erhöhung der Stärke von Brønstedsäurezentren, indem die Si-O-T ($T = \text{Al, Si}$) Winkel in der Nähe des Kations vergrößert werden. Diese Veränderung der Gittergeometrie schwächt die OH Bindung in verbrückenden Hydroxylgruppen und erhöht so deren Säurestärke. In H-LaX waren alle Gitteraluminiumatome mit Lanthan als ladungskompensierendem Kation von einer starken Verzerrung betroffen. Dagegen kam es in H-LaY nur bei 58% der Gitteraluminiumatome mit Lanthan als ladungskompensierendem Kation zu einer starken Verzerrung der Koordinationssphäre, während bei den übrigen nur eine schwache Verzerrung beobachtet wurde. Es wird angenommen, dass $[\text{La}(\text{OH})_2]^+$ Cluster die Einheiten sind, welche nur eine schwache Verzerrung hervorrufen, während eine starke Verzerrung durch Ladungskompensation mit La^{3+} oder $[\text{LaOH}]^{2+}$ Clustern entsteht. Folglich erfordert die Bildung eines starken Brønstedsäurezentrums eine Umgebung mit mindestens drei Gitteraluminiumatomen. Aufgrund der niedrigeren Aluminiumkonzentration ist die Wahrscheinlichkeit, eine solche Umgebung in H-LaY zu finden, deutlich geringer.

Im fünften Kapitel wurde die Bildung von kohlenstoffhaltigen Ablagerungen und deren Einfluss auf die Alterung und Deaktivierung von H-LaX als Katalysator von Isobutan/2-Buten Alkylierung bei 348 K untersucht, indem die Reaktion nach verschiedenen Zeiten abgebrochen wurde. Die Ablagerungen bestanden hauptsächlich aus bizyklischen

Verbindungen mit ein oder zwei Doppelbindungen und Alkylseitenketten sowie verzweigten Carbeniumionen. Die Ablagerungen wurden bereits zu Beginn der Reaktion gebildet, und ihr Aufbau veränderte sich während der Lebenszeit des Katalysators nicht.

Vier Phasen der Reaktion wurden identifiziert, nämlich (1) stabile Alkylierung, (2) Veränderung der Ablagerungen, (3) langsame Deaktivierung und (4) schnelle Deaktivierung. In der Phase der stabilen Alkylierung entstehen Carbeniumionen durch Protonierung von 2-Buten und Addition von weiteren Alkenmolekülen. In der Phase der Veränderung der Ablagerungen werden Brønstedsäurezentren blockiert und kleinere Einheiten wandern zu den Porenöffnungen. Dort werden sie weiter alkyliert, wodurch es zur Verstopfung der Poren kommt. In der Phase der langsamen Deaktivierung kommt es zu einem Rückgang des 2-Buten-Umsatzes. Alkylierung findet noch an einer begrenzten Zahl von Reaktionszentren statt, welche sich auf oder nahe der äußeren Oberfläche befinden. In der abschließenden Phase der schnellen Deaktivierung wird kein Alkylat mehr produziert, und die Oligomerisierung von Buten ist die Hauptreaktion. Dies führt zu einer steigenden Konzentration von Olefinen im Produktgemisch und zu einer deutlichen Zunahme der Ablagerungen auf den Zeolithpartikeln.

Die Ergebnisse dieser Arbeit zeigen, dass Lanthan getauschte Zeolithe mit Faujasitstruktur interessante Reaktionsmedien für neuartige Wege der Säure-/ Base-Chemie bei tiefen Temperaturen sind. Ein verbessertes Verständnis der Bildung starker Brønstedsäurezentren in H-LaX und H-LaY und der Reaktionen, die bei der Isobutan/2-Buten Alkylierung zur Deaktivierung führen, wird eine wichtige Grundlage für die Entwicklung verbesserter Katalysatoren und geeigneter Prozessbindungen für industrielle Isobutan/2-Buten Alkylierung sein.

Curriculum vitae

Carsten Sievers was born on July, 5th of 1977 in Hildesheim, Germany. He attended the Gymnasium Andreanum in Hildesheim from 1988 to 1997, from which with graduated with the Abitur degree. After his military service he started studying chemistry at the Technische Universität München in 1998. During his studies, he participated in two exchange programs working at Wacker do Brasil in São Paulo, Brazil and the National University of Singapore. In 2003 C.S. joint Prof. Johannes A. Lercher's group at the Technische Universität München for his Diplomarbeit (master thesis) on "Aromatic Hydrogenation in the Presence of Dibenzothiophene and Quinoline", which included a stay at Prof. Roul Prins' at the ETH Zürich, Switzerland. After graduation as "Diplom-Chemiker" (master degree) in September 2003 he started to work as a PhD student in Prof. Johannes A. Lercher's group. His work was focused on the chemistry of alkanes on lanthanum exchanged zeolites and included a stay at Prof. Rutger A. van Santen's group at the TU Eindhoven, Netherlands.

List of publications

1. Sievers, C., Zuazo, I., Guzman, A., Olindo, R., Lercher, J. A.; "Stages of aging and deactivation of zeolite LaX in isobutane/2-butene alkylation" *J. Catal.*, submitted for publication.
2. Fow, K. L., Jaenicke, S., Müller, T. E., Sievers, C. "Enhanced Enantioselectivity of Chiral Hydrogenation Catalysts after Immobilisation in Thin Films of Ionic Liquid" *J. Mol. Catal. A-Chem.*, submitted for publication.
3. Sievers, C., Onda, A., Guzman, A., Otillinger, K. S., Olindo, R., and Lercher, J. A. "Low temperature activation of branched octane isomers over lanthanum exchanged zeolite X catalysts" *J. Phys. Chem. B*, accepted for publication.
4. Xu, B., Sievers, C., Hong, S. B., Prins, R., van Bokhoven, J. A.; "Catalytic Activity of Brønsted Acid Sites in Zeolites: Intrinsic Activity, Rate-Limiting Step, and Influence of the Local Structure of the Acid Sites" *J. Catal.*, available online, DOI: 10.1016/j.jcat.2006.08.022.
5. Guzman, A.; Zuazo, I.; Feller, A.; Olindo, R.; Sievers, C.; Lercher, J. A.; "Influence of the Activation Temperature on the Physicochemical Properties and Catalytic Activity of La-X Zeolites for Isobutane/cis-2-Butene Alkylation" *Micropor. Mesopor. Mater.*, available online, DOI: 10.1016/j.micromeso.2006.08.006.
6. Sievers, C., Jimenez, O., Müller, T. E., Steuernagel, S., Lercher J. A.; "Formation of solvent cages around organometallic complexes in thin films of supported ionic liquid" *J. Am. Chem. Soc.*, 128 (2006) 13990.
7. Jimenez, O., Müller, T. E., Sievers, C., Spirkel, A., Lercher J. A.; "Markownikoff and Anti-Markownikoff Hydroamination with Palladium Catalysts Immobilized in Thin Films of Silica Supported Ionic Liquids" *Chem. Comm.* (2006) 2974.
8. Guzman, A.; Zuazo, I.; Feller, A.; Olindo, R.; Sievers, C.; Lercher, J. A. "On the formation of the acid sites in lanthanum exchanged X zeolites used for isobutane/cis-2-butene alkylation" *Micropor. Mesopor. Mater.* 83 (2005) 309-318.
9. Halbach, T. S.; Mix, S.; Fischer, D.; Maechling, S.; Krause, J. O.; Sievers, C.; Blechert, S.; Nuyken, O.; Buchmeiser, M. R. J. "Novel Supported and Unsupported Ru-Based Metathesis Catalysts: Synthesis and Reactivity" *Org. Chem.* 70 (2005) 4687-4694.
10. Cerqueira, H. S.; Sievers, C.; Joly, G.; Magnoux, P.; Lercher, J. A. "Multitechnique Characterization of Coke Produced during Commercial Resid FCC Operation" *Ind. Eng. Chem. Res.* 44 (2005) 2069-2077.
11. Penzien, J.; Abraham, A.; van Bokhoven, J. A.; Jentys, A.; Müller, T. E.; Sievers, C.; Lercher, J. A. "Generation and Characterization of Well-Defined Zn²⁺ Lewis Acid Sites in Ion Exchanged Zeolite BEA" *J. Phys. Chem. B* 108 (2004) 4116-4126.